JUSTUS-LIEBIG-
UNIVERSITÄT
GIESSEN

Photoluminescent Properties and Antimycobacterial Activity of Imidazo[1,5-*α*]quinolines

Kumulative Dissertation zur Erlangung des Grades „Doktor der Naturwissenschaften“ am Fachbereich Biologie und Chemie der Justus-Liebig-Universität Gießen

vorgelegt von

Niclas Kulhanek

Erstgutachter: Prof. Dr. Richard Göttlich

Zweitgutachter: Prof. Dr. Siegfried Schindler

Eidesstaatliche Erklärung

„Ich erkläre: Ich habe die vorgelegte Dissertation selbstständig und ohne unerlaubte fremde Hilfe und nur mit den Hilfen angefertigt, die ich in der Dissertation angegeben habe. Alle Textstellen, die wörtlich oder sinngemäß aus veröffentlichten Schriften entnommen sind, und alle Angaben, die auf mündlichen Auskünften beruhen, sind als solche kenntlich gemacht. Ich stimme einer evtl. Überprüfung meiner Dissertation durch eine Antiplagiat-Software zu. Bei den von mir durchgeführten und in der Dissertation erwähnten Untersuchungen habe ich die Grundsätze guter wissenschaftlicher Praxis, wie sie in der „Satzung der Justus-Liebig-Universität Gießen zur Sicherung guter wissenschaftlicher Praxis“ niedergelegt sind, eingehalten.“

_____ _____

Ort, Datum Unterschrift

„Let there be light"

Genesis 1:3 Torah

Kurzzusammenfassung

Ein Faktor der unsere moderne Welt auszeichnet, ist die Allgegenwertigkeit von elektrischen Geräten und Licht. Diese Leuchtmittel hängen immer mehr mit der Einbindung von organischen Leuchtdiodenmaterialien (*organic light-emitting diode* (OLED)) zusammen und werden aufgrund ihrer Farbreinheit, ihres Farbvolumens und Kontrastes weiter an Bedeutung gewinnen. Eine Herausforderung dieser Emittermaterialien ist dabei oftmals die Lebensdauer und Beständigkeit. Hauptgrund dafür sind die eingesetzten blauen Emitter, die die Lebenszeit-limitierende Komponente der OLED darstellen. Die benötigte weite Bandlücke für eine blaue Emission führen zu ebenso starker Energieaufnahme und sogenannten heißen angeregten Energiezuständen. Dies führt zu einer Degeneration des blauen Emittermaterials aber auch anderer Bauteile. Eine Klasse von blauen organischen Emittermolekülen sind die Imidazo[1,5-*a*]quinoline, die sich durch oxidative Stabilität und struktureller Simplizität auszeichnen.

Ein zentrales Ziel jedes Emittermaterials ist eine möglichst hohe Quanteneffizienz zu erreichen. In den Publikationen dieser Arbeit konnte gezeigt werden, dass eine starke Abhängigkeit der Quantenausbeute (QY) von dem Substitutionsmuster am Imidazolring besteht. Die Kombination eines sterisch anspruchsvollen elektronenschiebenden Rest in Position 1 des Imidazolringes und eines elektronenarmen 2-*N*-Heteroaromaten in Position 3 zeigte größte QY. Andere physikalische Eigenschaften wie Extinktionsmaxima, Emissionsmaxima, HOMO und LUMO-Energien hingegen zeigen eine untergeordnete Abhängigkeit von den Substituenten. Weiterführende Untersuchungen befassten sich mit der Transferierbarkeit der QY in Lösung in die Festphase. Hierbei konnte eine erhebliche Verringerung festgestellt werden, sobald in kristalliner Form gemessen wurde. Dennoch konnten Moleküle identifiziert werden, die eine vergleichbare QY in Festphase aufweisen, wie bereits technisch eingesetzten Emittermaterialien.

Zudem konnte durch weiterführende Untersuchungen festgestellt werden, dass Imidazo[1,5-*a*]quinoline eine biologische Aktivität gegen *Myobacterium tuberculosis (Mtb)* aufzeigen. Der Haupterreger der bakteriellen Infektionserkrankung Tuberkulose ist ein wichtiges medizinisches Ziel, da immer mehr resistente Stämme aufkommen. Erreger die nicht nur resistent gegen zwei, sondern drei der Standardpräperate immun sind, werden immer häufiger nachgewiesen. Chelatisierende Imidazo[1,5-*a*]quinoline konnten ein gute Aktivität zeigen, die durch Einbindung in einen Zinkkomplex erheblich gesteigert werden konnte. Besonders Moleküle mit einem sterisch anspruchsvollen Rest in erster Position und einem 2-Pyridylrest in dritter Position der Imidazolringes zeigten eine hohe Aktivität. Ein weiterer Vorteil dieser Verbindungsklasse ist eine mangelnde Toxizität gegenüber Lungen und Leberzelllinien, was sie zu möglichen Therapeutika qualifizieren könnte.

Abstract

One factor that characterizes our modern world is the ubiquity of electrical devices and light. These light sources are increasingly linked to the integration of organic light-emitting diode (OLED) materials and will continue to gain in importance due to their color purity, color volume and contrast. One challenge of these emitter materials is often their service life and durability. The main reason for this is the blue emitters used, which represent the lifetime-limiting component of the OLED. The wide band gap required for blue emission leads to equally high energy absorption and so-called hot excited energy states. This results in degeneration of the blue emitter material as well as other components. One class of blue organic emitter molecules are imidazo[1,5-*a*]quinolines, which are also characterized by oxidative stability and structural simplicity.

A central objective of every emitter material is to achieve the highest possible quantum efficiency. The publications in this work have demonstrated that a strong dependence of the quantum yield (QY) on the substitution pattern on the imidazole ring can be observed. The combination of a sterically demanding electron-donating moiety in position 1 of the imidazole ring and an electron-poor 2-*N*-heteroaromatic in position 3 showed the highest QY. However, other physical properties such as extinction maxima, emission maxima, HOMO and LUMO energies showed minimal dependence on the substituents. Further investigations focused on the transferability of QY in solution to the solid phase. A considerable reduction was observed as soon as measurements were made in crystalline form. Nevertheless, molecules were identified that exhibit a comparable QY in the solid phase to the emitter materials already in technical use.

In addition, further investigations revealed that imidazo[1,5-*a*]quinoline showed biological activity against *Myobacterium tuberculosis (Mtb)*. Tuberculosis, the main bacterial infectious disease agent, is an important medical target because of the emergence of resistant strains. Pathogens that are not only resistant to two, but three of the standard preparations are being detected more frequently. Chelating imidazo[1,5-*a*]quinolines have shown good activity, which could be significantly increased by incorporation into a zinc complex. Molecules with a sterically demanding residue in the first position and a 2-pyridinyl moiety in the third position of the imidazole ring were particularly active. Another advantage of this class of compounds is a lack of toxicity towards lung and liver cell lines, which could qualify them as potential therapeutics.

Preface

This scientific work was written in the style of a cumulative dissertation and includes the scientific publications in the field of organic chemistry that I was able to obtain during my doctoral work in the working group Göttlich at the Justus-Liebig-University Gießen. The first part of this work will set out the theoretical background and clarify the thesis and challenges. This is intended to show the connection between the state of research and the personal contributions to this field. These contributions are briefly discussed in the second part of this work in relation to leading scientific publications. In the last part, all peer-reviewed publications are reprinted with the permission of the publisher. Additional material on the individual publications (SI and crystal structures) can be found online on the publisher's website.

Table of Contents

1. Introduction

The most stunning aspect of organic chemistry is the near infinite number of possible molecules. Moreover, each of these molecules has its own unique and often unexpected properties. It must have been exciting to discover, for example, that diazo dyes are not only versatile pigments, but can also be employed as antibiotics in the form of sulfamidochrysoidine.[1] The focus of this work was on the class of organic molecules known as aromatics, specifically the combination of two heteroaromatics, imidazole and quinoline (**scheme 1**). These two building blocks can be fused along different bonds of quinoline, eight of which are particularly stable and well-known in the literature. These eight classes extended the properties of the basic bodies, due to the alteration of the electronic environment. A wide range of biological and physicochemical properties are achieved by these molecules, including antibacterial[2], antifungal[3], antiparasitic[4], antiviral[5], antitumoral[6], agonistic[7], flourescent[8] and others. The large variety of attributes and relatively simple preparation makes them a good starting point for the design of molecules with specific properties. In the following, we will focus in particular on the properties of the least researched imidazo[1,5-*a*]quinoline class.

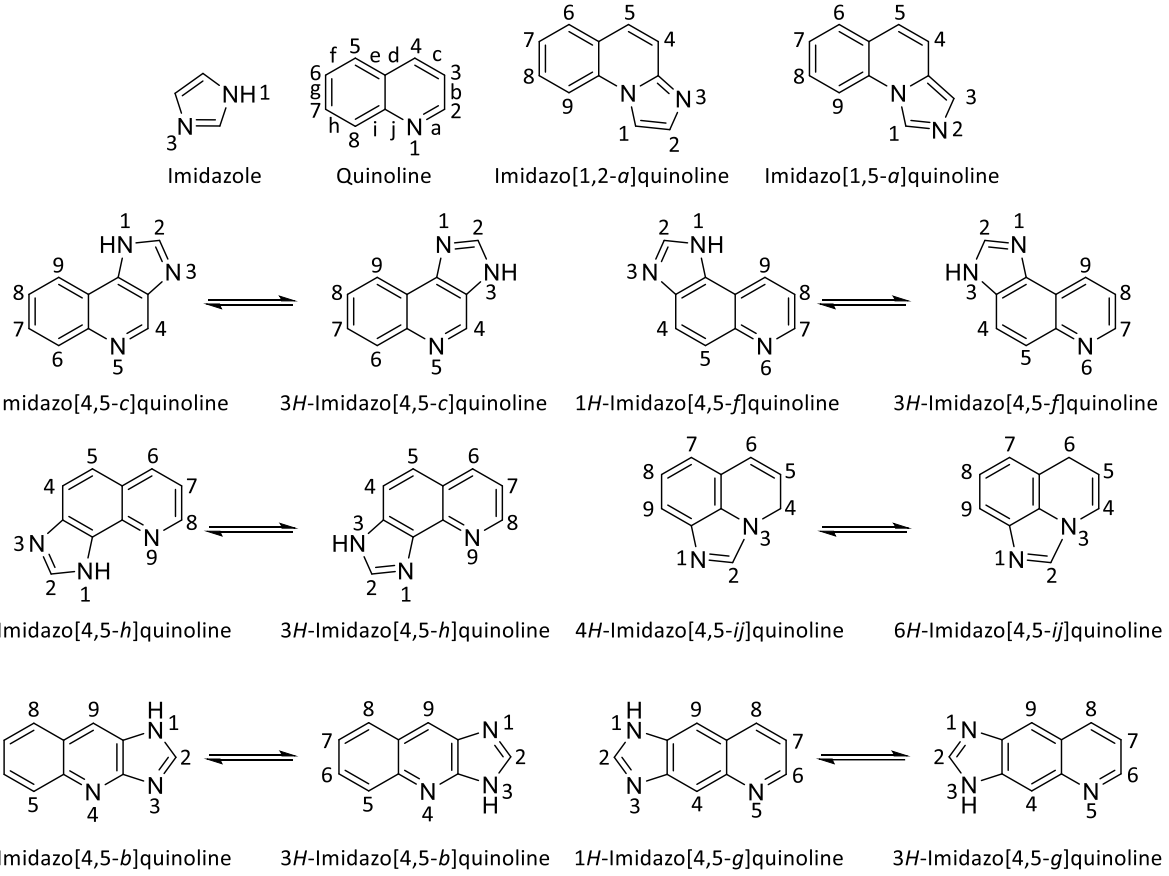

Scheme 1. All possible ring fusions between imidazole and quinoline.

1.1 Synthesis of imidazo[1,5-*a*]quinolines

Since the first preparation of an imidazo[1,5-*a*]quinoline derivative by *v. Bidder* and *Rupe* in 1939, many more modern strategies have been developed to synthesize the fused ring system of imidazo[1,5-*a*]quinolines.[9] Two different approaches are conceivable for the formation of the rings. Either an imidazole ring can be utilized to construct the fused quinoline ring, or the quinoline ring can be employed as a starting point and the imidazole ring can be formed. The first strategy is less popular because it is usually easier to specifically substitute a quinoline than an imidazole ring. Nevertheless, *Cei et al.* were able to react 2-(1H-imidazol-5-yl)acetonitrile **I1** with two 2-halogenbenzaldehyde **I2**, in the presence of copper iodide as catalyst, L-proline as a ligand and an inorganic base to form 4-carbonitrile imidazo[1,5-*a*]quinoline **I3** (**scheme 2 (1)**).[10] In a less limited procedure, *Chen et al.* were able to utilize a rhodium(III) catalyzed C-5 oxidative annulation to prepare various 1-substituted 4,5-diphenylimidazo[1,5-*a*]quinoline derivatives **I6** in up to very good yields (**scheme 2 (2)**).[11] However, both processes are severely limited by their substrates, especially in the substitution of the imidazole ring.

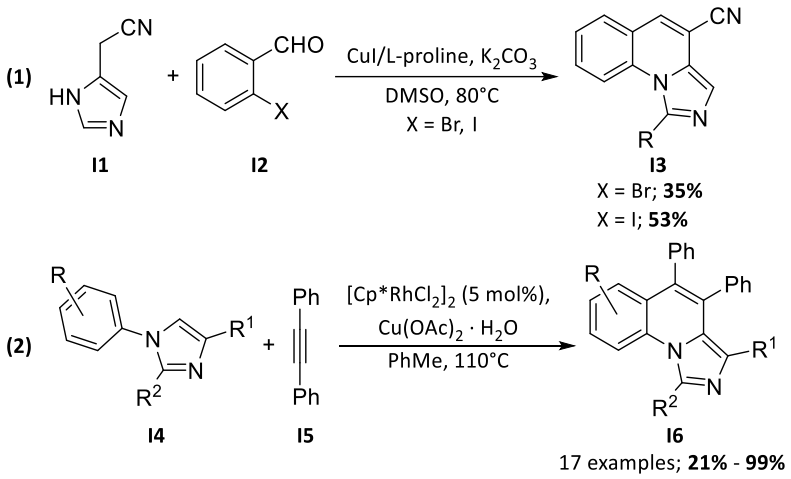

Scheme 2. Imidazo[1,5-*a*]quinoline synthesis strategies starting from the imidazole ring.

Quinoline, on the other hand, is more commonly the starting point. This approach offers more flexibility and has therefore led to significantly more diverse procedures for the formation of the imidazole ring.[12,13,14] The two most frequent among these reactions are *Vilsmeier*-type reactions and C(sp^3)-H amination methods. The *Vilsmeier*-type reactions are usually performed with the assistance of phosphorus oxychloride, with triflic anhydride representing a milder variant (**scheme 3**).[15,16] However, this approach is one of the more complex, since **I7** has to be synthesized from 2-cyanoquinoline in two additional steps.

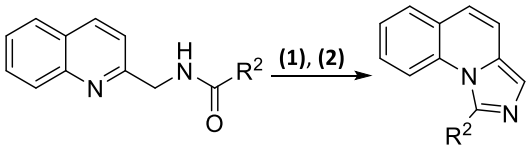

I7 **I8**

(1): $POCl_3$, TEA, DCM, rt, 4 min, R^2 = H **(1)**: **80%**

(2): Tf_2O, 2-MeO-pyridine, DCM, 35°C, 16h R^2 = Ph **(2)**: **77%**

Scheme 3. Different Vilsmeier-type reactions with 2-methylcarbonyl quinolines.

A simpler process is the reaction of 2-methylquinoline derivatives with benzylamines under the influence of copper salts and an oxidant (**scheme 4**).[17,18] The imidazo[1,5-*a*]quinolines are formed directly over sequential double oxidative C-H amination and aromatization. This reaction has the added benefit of also having direct access to a large selection of 3-bromo-imidazo[1,5-*a*]quinolines (**scheme 4 (2)**), which could be further functionalized in the following steps.

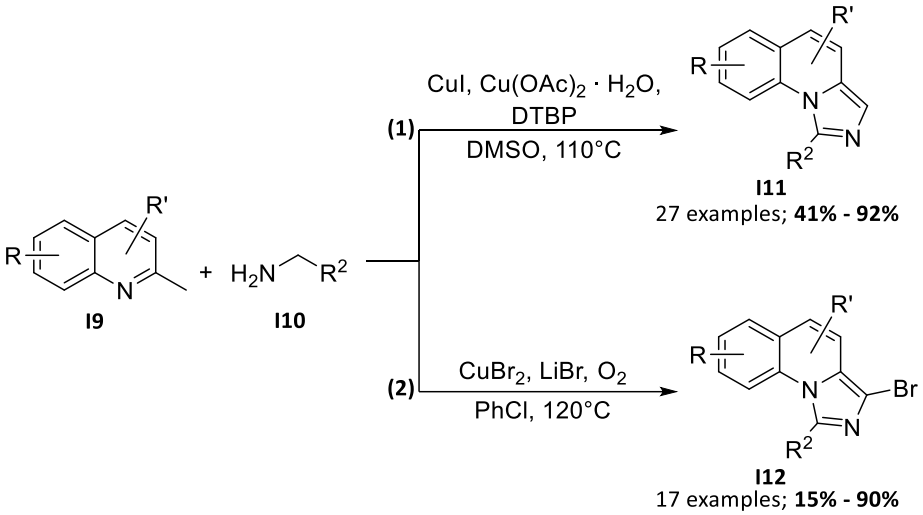

Scheme 4. Double oxidative C-H amination for direct excess to imidazo[1,5-*a*]quinolines.

Another direct approach is the copper-catalyzed oxidative C(sp^3)-H amination. This reaction can involve an aldehyde or ketone in combination with benzylamine (**scheme 5 (1)** and **(2)**).[19,20] However, it is also possible to use an α-amino acid as reaction partner (**scheme 5 (3)**).[21] Only imidazo[1,5-*a*]pyridine have been described in detail in this reaction and only a few imidazo[1,5-*a*]quinolines are known.

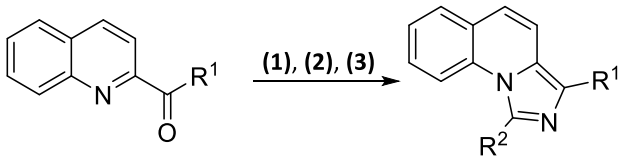

I13 **I14**

(1): CuBr (20 mol%), $BnNH_2$, O_2, MeCN, 80°C, 24h, R^1 = H **(1)**: **87%**
(2): $Cu(OAc)_2 \cdot H_2O$, $BnNH_2$, O_2, DMF, 110°C, 8h, R^1 = Ph **(2)**: **65%**
(3): $Cu(OTf)_2$, $PhC(CO_2H)NH_2$, I_2, DTPB, PhMe, 120°C, 10h, R^1 = Ph **(2)**: **84%**

Scheme 5. Direct copper-catalyzed oxidative C(sp3)-H amination of 2-methylcarbonyl quinoline **I13**. (DTPB = Di-*tert*-butylperoxide)

1.2 Applications of imidazo[1,5-*a*]quinolines

Compounds containing the imidazo[1,5-*a*]quinolines fused ring system show a wide range of physical and biological properties. Cappelli *et al*. was able to functionalise **I15** into an Neurokinin-1 (NK_1) receptor antagonist, for the possible treatment of chemotherapy-induced nausea and vomiting (CINV) (**scheme 6**).[22] His group was also successful in utilizing the structural similarity of imidazo[1,5-*a*]quinolines to benzodiazepines.[12] They synthesized a wide range of different compounds **I16** that displayed high affinity to the *gamma*-aminobutyric acid (GABA) receptor. These compounds displayed pain-relieving properties comparable to benzodiazepines. Another important application utilizes the structure of imidazo[1,5-*a*]quinolines, in particular the formation of an *Arduengo* carbene after deprotonation on the imidazole ring. The application as carbene ligands in palladium complexes demonstrated an increase in catalytic performance.[23] For example, complex **I17** was a suitable catalyst for the ethylene and propylene copolymerization.[24] But there is a wide range of other complexes with such imidazo[1,5-*a*]quinolines ligands for this type of reaction.[25] In addition, some imidazo[1,5-*a*]quinolines derivatives have strong fluorescence and remarkable thermal and oxidative stability, which renders them suitable materials for optoelectrical components.[18,26] However, it is also evident that all these different properties are rather unexplored. The aim of this work was therefore the synthesis and investigation of novel imidazo[1,5-*a*]quinolines to evaluate their optical and medical properties.

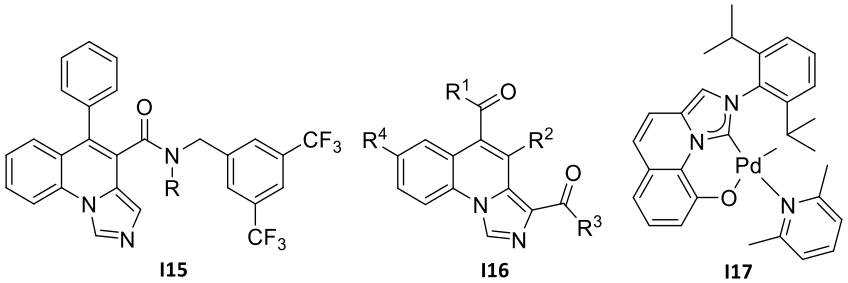

I15 **I16** **I17**

Scheme 6. Examples of imidazo[1,5-*a*]quinolines with versatile biological and physical properties.

1.3 Organic Emitter Materials

Electronic lighting sources and devices have changed the world so much that a future without them is no longer imaginable or desirable. Recently, more and more electronic devices have been utilizing organic light-emitting diodes (OLEDs) for their electroluminescent capabilities. These have grown to a market size of USD 56.37 billion since they were first described by *Tang* and *VanSlyke* in 1987.[27] It is expected that the market value of OLEDs will rise to over USD 344.58 billion by 2034.[28] The main focus for these materials is on increasing the efficiency, with OLEDs already offering better color authenticity, cheaper production and better contrast than other materials.[29]

Luminescence in organic materials is induced by the relaxation of excited states to the ground state through photon emission. These excited states are formed by a bound electron-hole pair, also known as an excitons, which can be generated through various strategies.[30] Two of which are particularly important for this work. On the one hand, the absorption of light can split charge carriers, which forms excitons after association with each other (**figure 1 left**).[31] This, also called photoluminescence, is the basis for all photophysical measurements and results in this work. In OLEDs, on the other hand, the formation of excitons is achieved directly by electroluminescence. Whereby the applied electrical voltage results in a merging of the charge carriers in the emitter layer (**figure 1 right**).[32] Independently of the formation mechanism of the excitons, they can adopt four different excited states. One singlet state in which the spins are exactly opposite or one of three triplet states in which the spins are parallel.[33] This formation of 25% singlet and 75% triplet states limits the efficiency of luminescent materials, depending on which excitons can be utilized for photoemission relaxation.

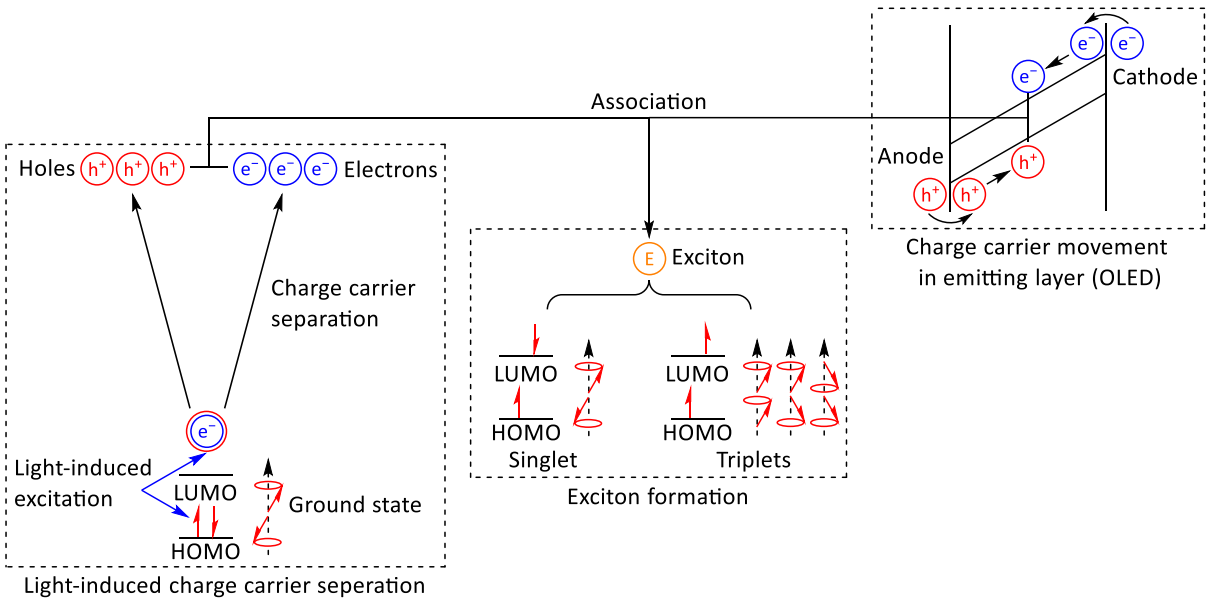

Figure 1. Exciton formation after light-induced charge carrier separation and in the emitting layer of OLEDs.

The first generation of OLED materials primarily relied on the allowed singlet relaxation (fluorescence) (**figure 2 left**).[34] Because the triplet relaxation (phosphorescence) is spin-forbidden due to the same orientation of the spins. As a result, earlier pure fluorescent OLEDs of the first generation have only a theoretical internal quantum efficiency (IQE) of 25%. The enhancement of this efficiency can only be achieved if more of the spin-forbidden triplet states are utilized. Different strategies were pursued to include these in the emission process. On the one hand, triplet fusion (TF) or triplet–triplet annihilation (TTA) can convert two T_1 into one S_1, which increases the IQE to 62.5%.[35] The requirement for this is a high molecular packing density between host and dopant, because TF is a bi-molecular process.[36] Another strategy is to enable the forbidden phosphorescence process by providing additional energy levels for a radiative relaxation from T_1 to S_0 through the introduction of heavy metals. This could bring the IQE to 100%, but it usually requires the use of precious metals such as iridium and platinum.[37] However, newer materials pursue the targeted reversal of the intersystem crossing (ISC) by raising T_1 (**figure 2 right**). The target is a difference between T_1 and S_1 of less than 0.1 eV. This allows the reversed intersystem crossing (RISC) to be performed using thermal energy and reaching an IQE of 100%, a process also known as thermally activated delayed fluorescence (TADF). To obtain such a TADF emitter, electron donor and acceptor moieties are chosen so that their HOMO/LUMO wave functions create an small overlap.[38]

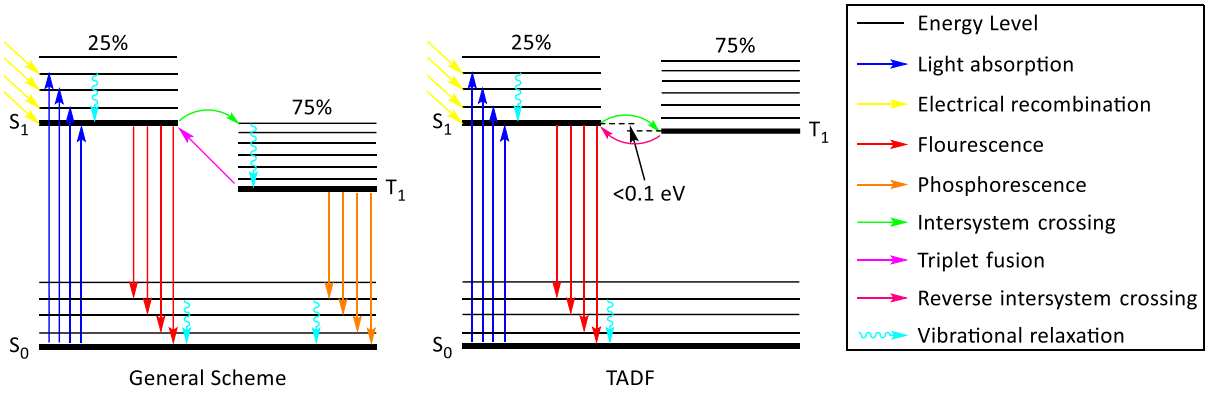

Figure 2. Jablonski diagram for optical excitation of organic molecules.

Using these strategies, many red and green organic emitter materials with good IQEs and stabilities have been developed.[39] However, blue emitters are a challenge regardless of the strategy pursued. Their wide bandgap (~ 3 eV) needed for blue emission is a major impairment for the material. As a result, exciton lifetime is much longer (~ µs). This leads to the formation of hot excited states (~ 6 eV), which degrade the material and limit the lifetime of the material.[40] This is why new materials with blue emission are becoming increasingly important and sought after.

2. Investigation of photoluminescent properties of imidazo[1,5-*a*]quinolines

The properties of imidazo[1,5-*a*]quinolines are not the focus of many scientific studies and therefore this class is quite unknown. However, one known property stands out directly and that is a strong blue emission under UV excitation. In our working group, we found out that imidazo[1,5-*a*]quinolines have a stronger blue emission and higher quantum yield (QY) than imidazo[1,5-*a*]pyridines.[41] In addition, they possessed high stability under oxidative conditions. Since this class of molecules is also quite simple in structure, it would be an excellent emitter material. The integration into an OLED was also successfully carried out and it was observed that the increased melting point compared to imidazo[1,5-*a*]pyridines is a further advantage.[42] This makes it easier to apply the materials via vapor deposition. However, it was also shown in this preceding work that substitution on the imidazole ring has a strong influence on the QY, with the highest being only 40%.[43] To further investigate the influence of the substitution pattern, we developed a new synthetic strategy and studied the effects of the substituents on QY in detail.[44] With these findings, we were able to further optimize the QY and investigate how the emission of these new molecules perform in the solid phase,[45] with an overarching goal to develop an efficient OLED. This paper will first discuss the synthesis strategy developed and then examine the photoluminescent properties of these molecules in more detail.

2.1 Developed synthetic route

A flexible synthetic strategy was required to investigate the influence of substituents on emissions. The substitution at the imidazole ring in position 1 and 3 was our primary goal. This means that we required a synthesis that allowed easy access to these two positions and additionally a wide spectrum of substrates. Among the strategies already discussed in Chapter 1.1 are some very simple and efficient approaches, but not all of these strategies suit our requirements. Using the imidazole ring as a starting material always leads to a substituted quinoline nucleus, since this is not a requirement, the quinoline ring must be used as the starting material.[10,11] However, the C(sp^3)-H amination of 2-methylcarbonyl quinoline[14,19–21] or 2-methyl quinoline[17,46] with benzylamines or benzylamino acids is limited to substituted aryl moieties and simple alkyl chains. For this reason, only the *Vilsmeier* approach can be considered, as a wide substrate range is possible here.[16,47] A C-C coupling would be suitable for the separate introduction of groups in position 3, this allows the synthesis to be branched in contrast to sequential approaches.

In order to prepare the desired 2-aminomethyl quinoline **3** as efficiently as possible and in large quantities, *N*-oxide **1** was selected as a relatively cheap starting material (**scheme 7**). Cyanation with trimethylsilyl cyanide and triethylamine as the base was considered, but rejected as it did only provide

a low yield and was not economically advantageous.[48] More beneficial was the selective cyanation at position 2 by means of a classic *Reissert-Henze* reaction with potassium cyanide and benzoyl chloride.[49] The subsequent reduction of nitrile **2** with sodium borohydride led to a large number of by-products in which the aromatic ring was also reduced.[50] Therefore, nitrile **2** was reduced with Pd/C and hydrogen to the primary amine **3** and precipitated as a hydrochloride salt to increase the stability.[15,51] The first moiety group R^2 was introduced by an *Einhorn* acylation in very good yields for a large variety of compounds.[52] The formation of the imidazole ring from this amid **4** via a classic *Vilsmeier* intermediate showed only a poor tolerance to many moieties and low yields.[15,53] In contrast, the utilization of milder triflic anhydride and 2-methoxypyridine yielded the cyclized imidazo[1,5-*a*]quinoline **5** in up to very good yields.[16] For the preparation of bromide **6**, two different strategies were already known for comparable compounds that could selectively substitute in position 3 of the imidazole ring. As described by *Tan et al,* first attempts with lithium bromide and copper dibromide could not be replicated, and bromine, as reported by *Shibahara et al.*, also produced only a low yield.[18,54] The use of *N*-bromosuccinimide (NBS) instead of bromine and an additional reduction of the reaction temperature suppressed the double bromination overreaction and led to excellent yields.[44] In addition, a high tolerance for a wide range of moieties was observed, which could not be achieved with bromine. This route for the first coupling component **6** yielded good to excellent yields for 10 different R^2.[44,45,55]

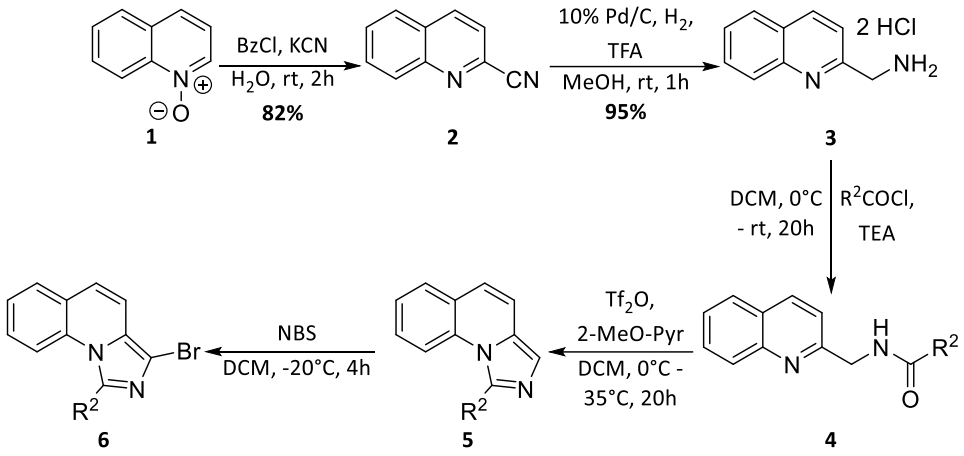

Scheme 7. Introduction of the first selectable moiety R^2 using an *Einhorn* acylation. Subsequent bromination of the cyclized imidazo[1,5-*a*]quinoline **5** with NBS to obtain the first coupling component.

A *Negishi* coupling was selected for the final coupling reaction (**scheme 8 (a)**). The reason for this is that possible 2-boronic acids of *N*-heteroaromatics are unstable.[56,57] Employing a *Suzuki* coupling would therefore unnecessarily limit the possible combinations of substrates. Especially with a class of molecules that have already shown a positive influence on the QY.[41] Due to its stannyl *N*-heteroaromatics, the *Stille* coupling offers a more stable but also toxic coupling component.[56,58] This

disadvantage is overcome by utilizing organozinc components. However, the stability of the desired coupling components was also found to be limited and it was decided to transform **6** into the organozinc component. This strategy led to much more consistent yields for a large variety of coupling combinations performed.[44,45,55] A limitation of the applied transmetallation with lithiated **6** was found, when an *N*-heteroaromatic is present as R^2. In these cases, alkylation of the nitrogen present in R^2 is observed. We eliminated the presence of alkyl bromide in solution by using 2 equivalents of *t*-BuLi.[59] Nevertheless, the yields in these cases could only be increased to an acceptable level.[55] A special case was the coupling with *s*-triazine, because none of the mono halogens of this *N*-heteroaromatic compound could be acquired commercially or were ever synthesized (**scheme 8 (b)**).[60] Instead of coupling, the s-triazine was directly combined with lithiated **6** in an addition reaction and the resulting 1,4-dihydrotriazine compound was oxidized to **8** with 2,3-dichloro-5,6-dicyano-1,4-benzoquinone (DDQ).[61,62] This is possible because in some cases the *s*-triazine behaves like an HCN synthon.[62,63]

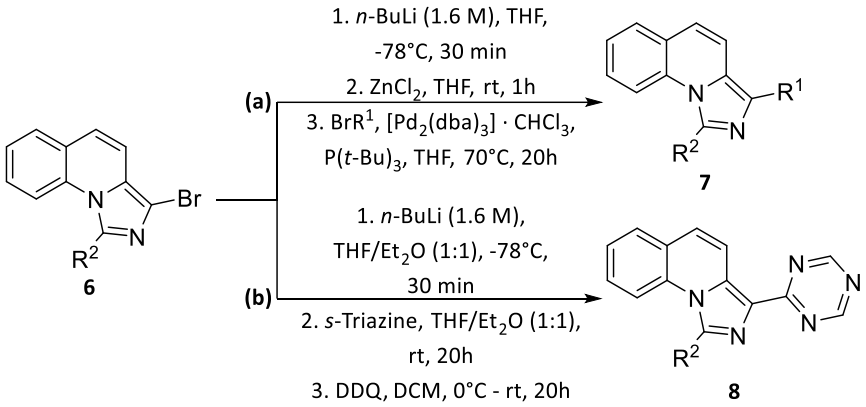

Scheme 8. General coupling strategies for the final products.

For the investigation of their biological properties, some of the synthesized imidazo[1,5-*a*]quinolines were inserted as ligands in zinc, copper and iron complexes by simple reaction of the metal salt in refluxing THF.[55] It is worth noting that this also occurs in the coupling step. The complexes formed are usually only slightly soluble in organic solvents and crystallize out. The separation of this precipitate by simple filtration led in many cases to pure products after reaction with concentrated ammonia solution and represents an advantage.[44,45,55]

A large number of products were synthesized via this six-step procedure, with some special exceptions mentioned above. The obtained **i**midazo[1,5-*a*]quinolines were then analyzed for their photoluminescent activity in solution and in solid state. This will be the subject of the following two chapters.

2.2 Physical properties of imidazo[1,5-*a*]quinolines

The main focus of this work was on optimizing the QY. In order to gain a better understanding of the influence of imidazole ring substitution on QY, different moieties R^1 were first combined with substituted Ph as R^2. The knowledge gained from this was then followed up by an extension of the moieties in R^2. For rapid evaluation, the initial focus was on investigating the photoluminescence properties in solution, but was later expanded to the measurement in solid phase and of the cyclic voltammetry (CV) data. The QY was calculated as described in the literature, using 0.1 µM quinine sulfate in 0.5 M H_2SO_4 as a reference.[64]

Measurements of the extinction showed no great dependence on the residues in R^2 for many combinations, as a similar extinction was measured for the respective substituents in R^1 in most combinations (**figure 3**). An exception here are all combinations of F_3C-Ph in R^2 and electron-deficient substituents as R^1, which showed a shorter extinction wavelength. A reverse effect was observed for PhO and electron-deficient substituents as R^1, as all combinations required significantly higher extinction wavelengths. The specific combination with a nitro substituent showed the highest extinction of all measured systems, while the compound of 2-Me_2N-Ph and 4-MeO-Ph oxidized slowly in air and an accurate measurement was not possible.

The low dispersion of the measured values became even clearer with the emission (**figure 4**). Most of the measured values were in the range of 440 - 480 nm and increased on average only slightly for electron-rich substituents in R^1, while 2-propen-1-yl resulted in lower emissions in this position. This range is the characteristic spectrum of blue and therefore almost all compounds hit our target area. Individually, a greater separation of the emission can be recognized for 2-pyrimidinyl, as very different emissions were measured here depending on R^2. An exception here is again the nitro substituent with the highest emission of all measured values. However, it can be recognized that almost independently of the substituents on the imidazole ring, the imidazo[1,5-*a*]quinolines consistently show a blue emission. This is a great advantage for the development of a blue emitter material on their basis, as a substitution on the imidazole ring of an imidazo[1,5-*a*]pyridine results in a wide spectrum of emission wavelengths.[54] The reason for this independence could be that most physical properties such as emission or HOMO/LUMO of aromatic molecules are only dependent on the longest linear conjugated segment.[65–67] In the case of imidazo[1,5-*a*]quinolines, this is probably the quinoline core, which is not directly substituted and therefore not directly influenced. Whereas in the case of imidazo[1,5-*a*]pyridine, the longest linear segment is the imidazo[1,5-*a*]pyridine core itself.

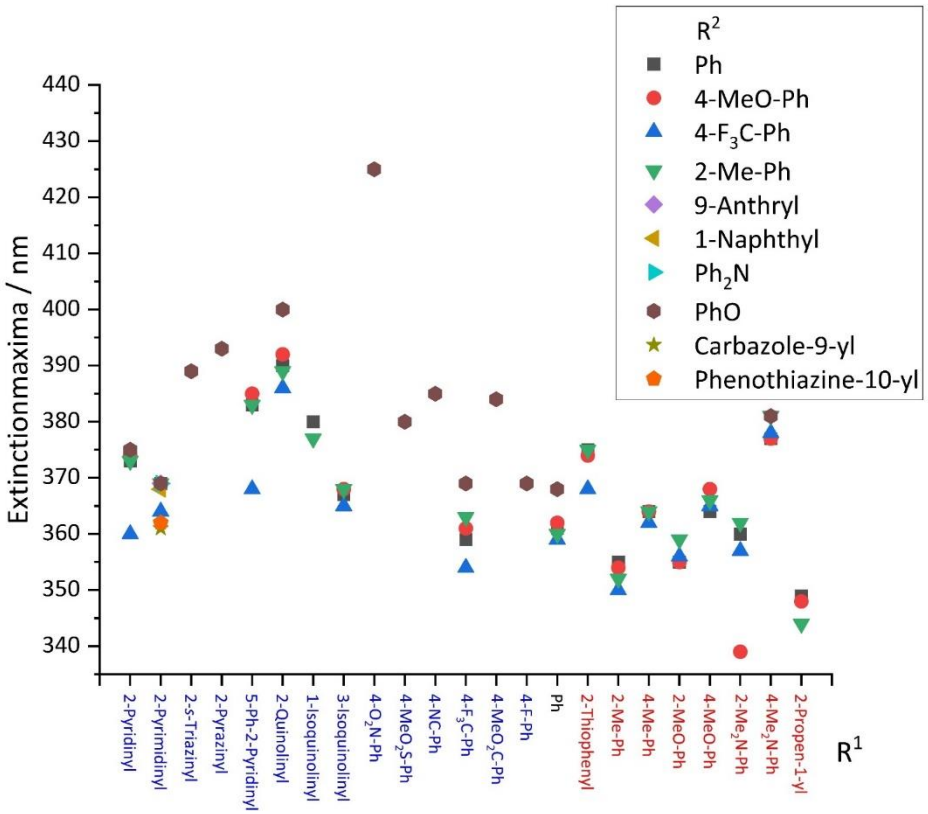

Figure 3. Extinction maxima for different moiety combinations. Measured at 25°C, under air, 0.1 µM solution in $CHCl_3$.

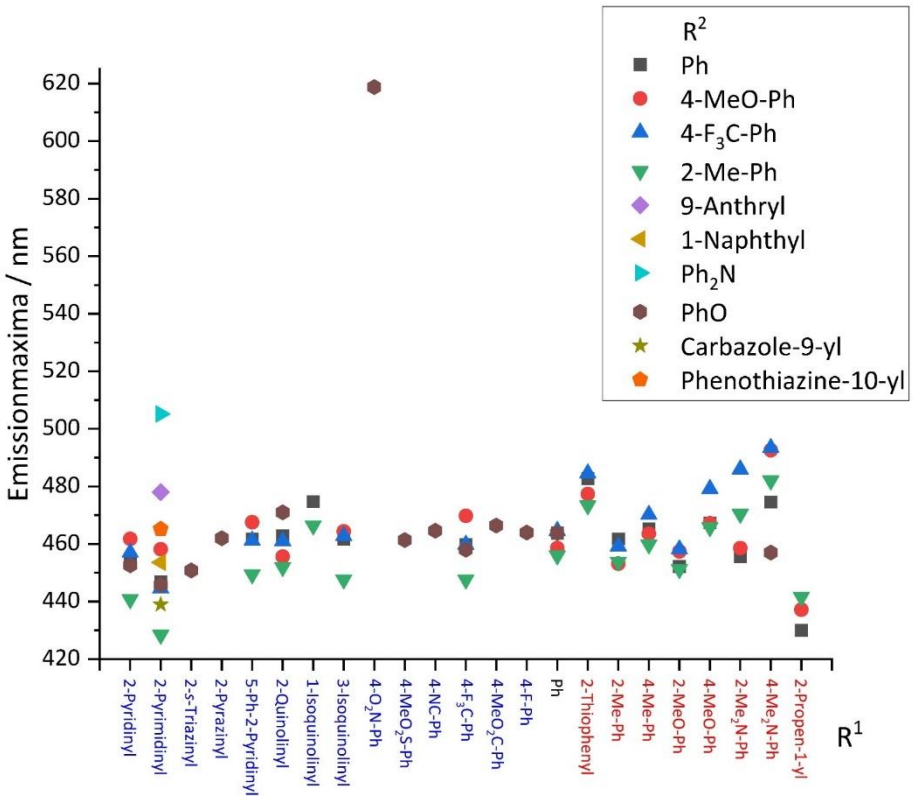

Figure 4. Emission maxima for different moiety combinations. Measured at 25°C, under air, 0.1 µM solution in $CHCl_3$ and with the extinction maxima as excitation wavelength.

Initial calculations of the QY compared to Ph in R^2 showed that substitution with an electron-withdrawing group reduces the QY in all combinations, whereas substitution with an electron-donating group results in either the same or lower QY in most cases (**figure 5**). In contrast, the introduction of a methyl in the *ortho* position of the Ph led to a consistent increase in QY. A further observation was that electron-poor substituents in R^1 always had a higher QY than electron-rich ones, and here it was also evident that the *ortho* position of R^1 should not be substituted. In particular, *N*-heteroaromatics showed a strong influence on the QY. It was therefore assumed that a sterically demanding electron-donating moiety in R^2 and an electron-poor *para* substituted residue in R^1 is the most influential combination. In a broader study with 2-pyrimidinyl in R^1, simple sterically large groups such as 9--anthryl and 1-naphthyl showed only a minor influence on the QY, while moieties that were additionally more electron-donating led to a strong increase in QY. In particular, PhO and carbazole-9-yl showed very high liquid phase QY of 85% and 81%. This is a significantly higher QY than for imidazo[1,5-*a*]pyridines[68,69], more than twice as high for some comparable systems, and imidazo[1,5-*a*]quinolines investigated previously also exhibited a QY only up to 39%.[26,41,43] However, further investigations with PhO in R^2 showed that combinations with electron-deficient aromatics in R^1 did not exceed a QY of 54% and even the introduction of more nitrogen into the aromatic ring in the case of 2-*s*-triazine did not achieve any further increase. The only exception is again the nitro substituent, which is known to quench emissions from 450-630 nm.[70]

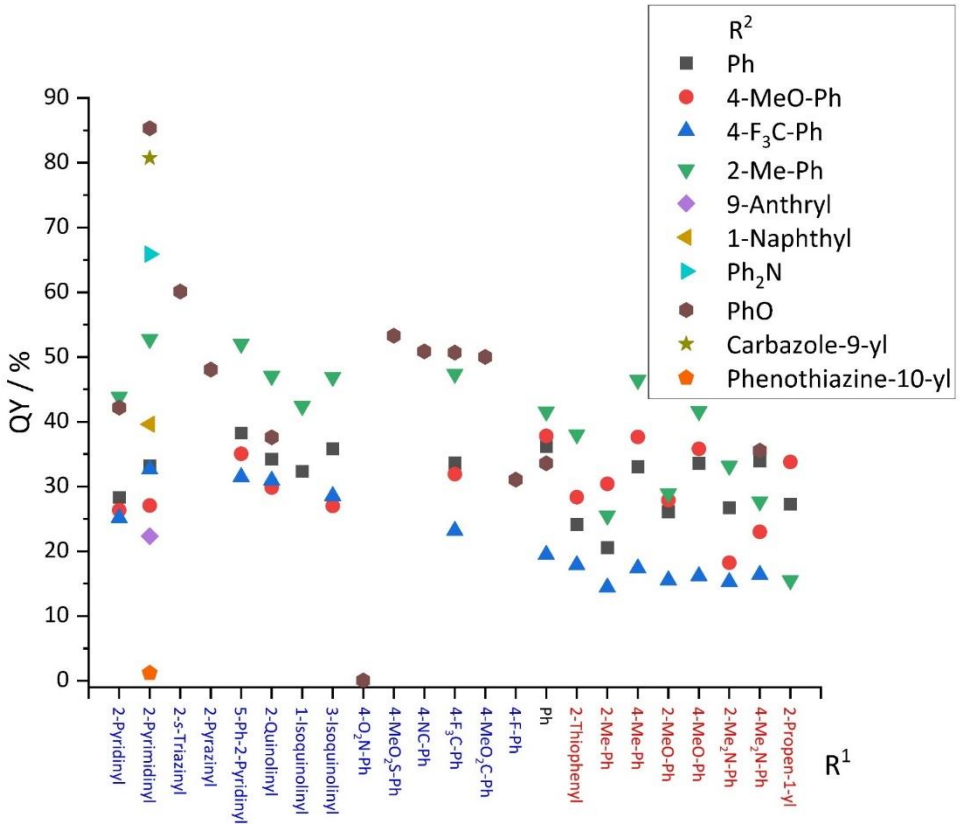

Figure 5. Calculated QY for all measured systems in proportion to quinine sulfate.

A further investigation of the PhO system by CV showed that no combination with electron-deficient substituents or Ph in R^1 showed a reduction. Only 4-Me_2N-Ph showed a reduction, which could explain why it is the only electron-rich substituent that leads to high QYs. Non-reversible oxidation is a property for the imidazo[1,5-*a*]quinolines that has already been observed by us.[26] However, it is very interesting that in this system it seems to be dependent on the substituents. While IPs typically show reversible reduction for both electron-poor and rich substituents.[41,69] HOMO and LUMO energies were also calculated from the measured CV data (**figure 6**). The calculations were conducted according to the literature, with ferrocene as standard.[71] It was observed that HOMO and LUMO did not differ greatly for the individual systems and in all cases was approximately -5 eV for the HOMO and -2.5 eV for the LUMO. This also results in a constant band gap of about 3 eV, which is typical for blue emitters. Standard DFT calculations also showed no strong deviation for the measured HOMO energies.[72] The constantly increased LUMO energies can be attributed to the calculation method applied.[73] As already mentioned in the emission section, the HOMO/LUMO energies could be dependent on the longest linear segment in the molecule. [65–67] Since this segment is not directly substituted, the orbital energies are not directly affected.

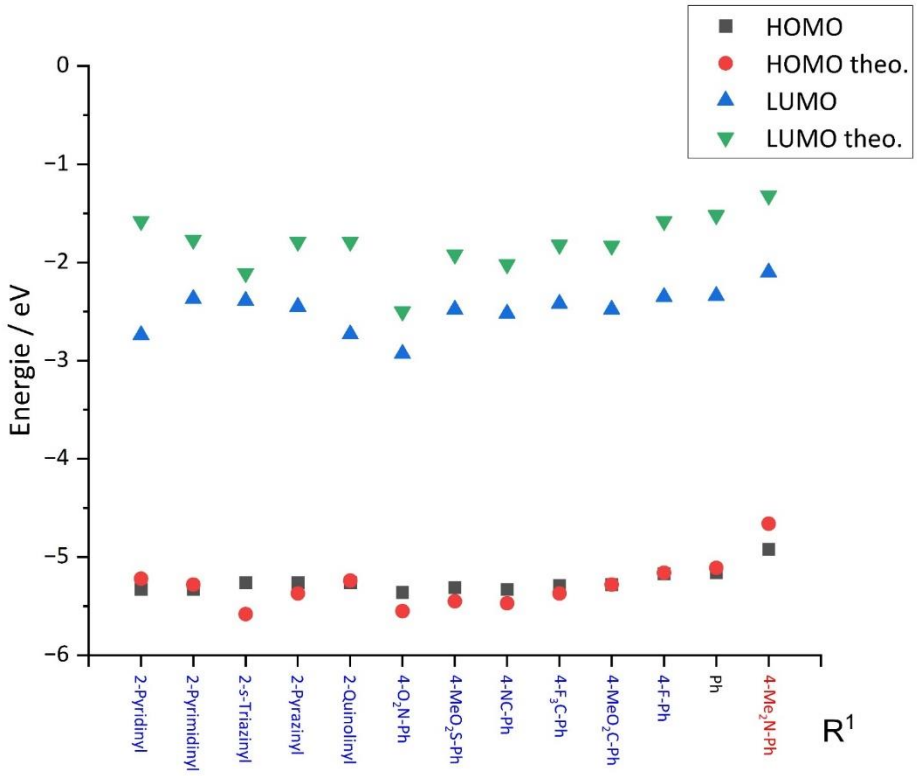

Figure 6. Calculated HOMO/LUMO energies for the PhO system in proportion to ferrocene from the measured CV data and from a DFT approach.

Due to the complexity of measuring QY in solid phase (QY (s)), only four compounds were measured as they already showed sufficient emission in the crystalline state under a UV lamp. The investigation was carried out on the basis of literature specifications, with magnesium oxide as reference material.[74] The first observation is that both extinction and emission maxima shift bathochromically by about 50 nm, with the pattern of the spectrum being similar to that in solution. However, the QY (s) decreased considerably, so that the combination of PhO and 2-*s*-triazinyl and 4-MeO_2S-Ph could not exceed a QY (s) of 15%. This reduction in QY (s) was even greater for the combination of PhO and 2-pyrimidinyl, which decreased from 85% in solution to only 21% in solid state. Surprisingly, the combination of Ph_2N and 2-pyrimidinyl only showed a halving from 66% to 32%. A possible explanation for this can be identified in the spectra, since the combination of Ph_2N and 2-pyrimidinyl is the only one that has only a small overlap of extinction and emission (**figure 7**). The other systems potentially lose far more QY (s) through re-absorption of emitted photons. In solution, the *Stoke* shift for each of the measured compounds was large enough to prevent this. Nevertheless, a QY (s) of 31% is higher than that of many imidazo[1,5-*a*]pyridines based materials[75] and comparable with more established emitter materials.[76] This could form a foundation for the future integration of imidazo[1,5-*a*]quinolines as emitter materials in OLEDs.

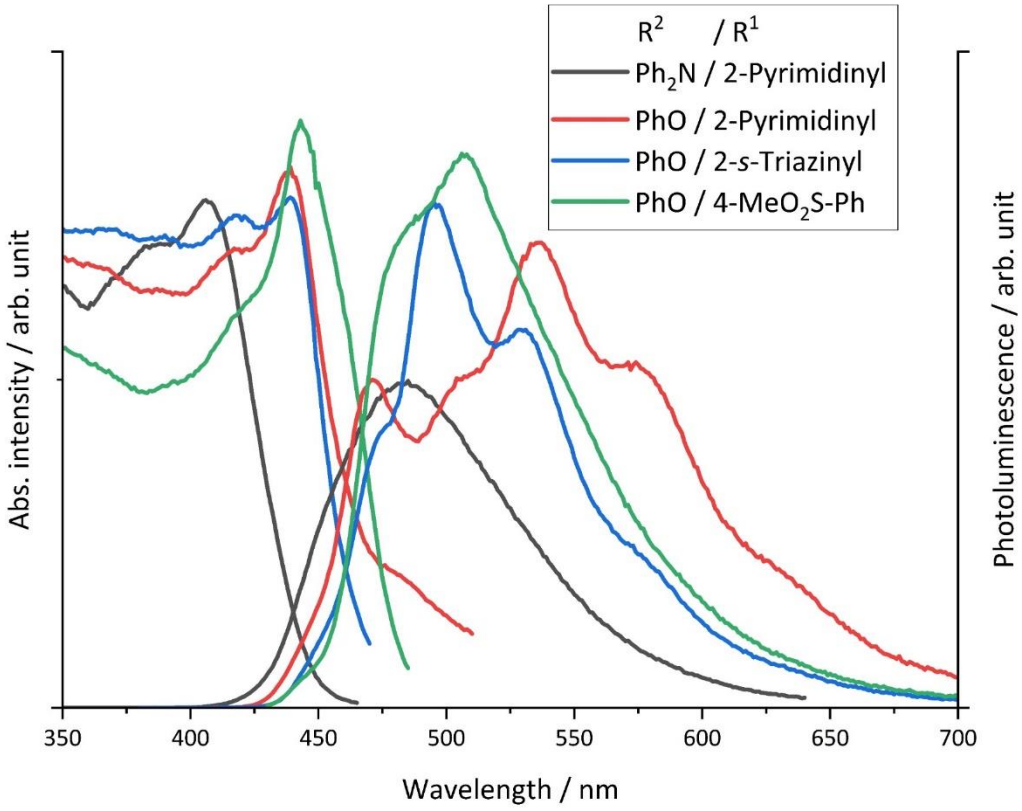

Figure 7. Measured extinction spectra (left) and emission spectra (right) for the selected systems.

3. Tuberculosis

Among the communicable infectious diseases that affect the human, Tuberculosis (TB) has a special place. Even with global efforts and modern medicine, it remained one of the world's deadliest diseases of the past two decades.[77] New infections reached 10.6 million and deaths with TB infection were reported at 1.3 million in 2023 worldwide, according to the World Health Organization (WHO).[78] The main pathogen of TB is *Mycobacterium tuberculosis* (*Mtb*) and although it is mainly pulmonary, it can cause diseases throughout the body. In addition, TB as a disease must be considered on a spectrum from asymptomatic infection to life-threatening disease.[79] This spectrum consists of four stages between which the infection can shift, depending on the host immunity and comorbidities (**figure 8**).[80] When exposed to *Mtb*, the pathogen can either be completely neutralized by the immune system or the bacterium reaches a quiescent or latent state. In this latent TB infection (LTBI) state, the patient is completely asymptomatic and non-infectious, because bacterial growth is completely suppressed by persistent immune response. Just 5% to 15% of those LTBI develop an active TB disease within a few months or years.[81] This active TB disease can be either symptomatic or asymptomatic, in which case it is classified as subclinical. Symptoms may include, among others fever, fatigue, loss of appetite, weight loss, persistent cough and, if the infection reaches a large extent pulmonary necrosis, haemoptysis and cavitary lesions.[82]

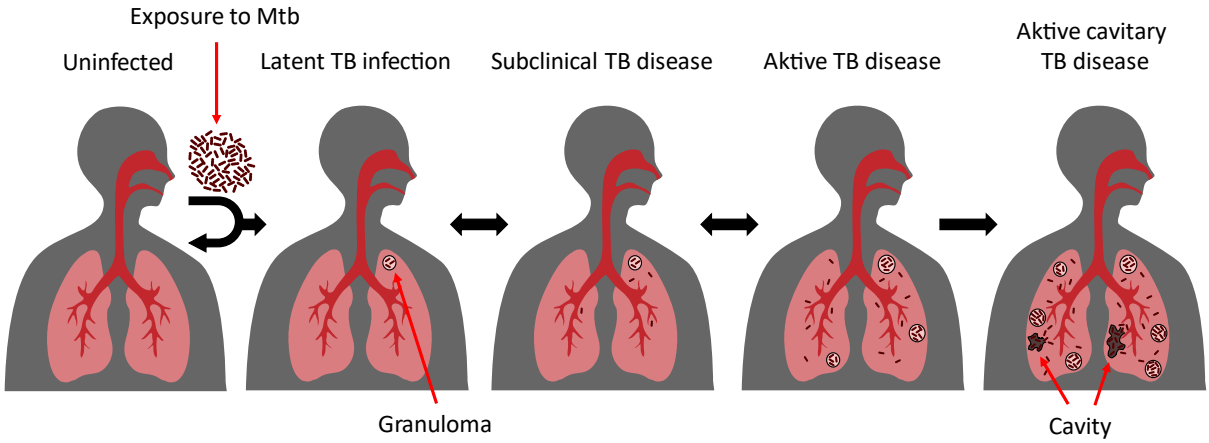

Figure 8. Spectrum of TB from infection to outbreak of the fully active disease.

The prescribed treatment for active TB disease involves the administration of a combination of isoniazid, rifampicin, pyrazinamide and ethambutol over several months.[83] This therapy is complicated by the emergence of rifampicin-resistant TB (RR-TB), multidrug-resistant TB (MDR-TB) and even extensively drug-resistant TB (XDR-TB). In these cases, even second-line antibiotics such as aminoglycosides and fluoroquinolones can often only achieve limited treatment success.[78] The WHO reports that 3.6% of new TB cases and 20.2% of previously treated cases are estimated to have MDR-

TB and it has been a growing concern for a long time.[84] Contributions to the battle against TB are therefore of great importance. As a large number of new molecules were synthesized, it was also sensible to test their biological properties. This led to the discovery of activity against *Mtb* and further characterization of this class of molecules through extended investigations.[55] These results will be the subject of the following sections, starting with our synthetic approach.

3.1 Biological properties of imidazo[1,5-*a*]quinolines

Antibacterial properties of imidazo[1,5-*a*]quinolines were not described in the literature for any system. Consequently, we were surprised that they showed good activity against *Mtb* in a small screening. As already described in the introduction the class of imidazoquinolines shows antibacterial properties, but only one case of antimycobacterial activity of an imidazo[4,5-*c*]quinoline is known.[85] This discovery was therefore not only unexpected, but also improbable.

In an initial study, the Minimum inhibitory concentration (MIC) was determined on a selection of four microbial indicator strains and cytotoxicity was evaluated using an epithelia cell line from human lung carcinoma (Calu-3) applying procedures described in the literature.[55,86] The selected strains were *Escherichia coli* (*Ec*) ATCC35218, *Staphylococcus aureus* (*Sa*) ATCC33592, *Septoria tritici* (*Str*) MUCL45408 and *Mycobacterium tuberculosis* (*Mtb*) H37Ra. For the activity, a strong dependence on a nitrogen in *ortho* position in R^1 and the size of this moiety can be observed (**table 1**). While pyridine **11** shows only a low activity, this can be increased by introducing more nitrogen atoms in *ortho* position (**13** and **16**), but an increase to a quinoline **12** or extension with Ph **14** leads to a reduction. Whereby an isoquinoline **15** in R^1 and 1-napthyl **20** in R^2 also exhibited a strong increase in activity, which indicates a required specific orientation of the moiety in R^1 and R^2. The activity could also be increased by chelation with Zn^{2+}, Fe^{3+} and Cu^{2+} for all ligands, so that **C5** and **C3** even displayed minor activity against *Sa* and *Str*. These MICs of 1 - 2 µM are comparable with those of the reference drugs used (MIC of gentamicin = 4 µM and rifampicin = 0.07 µM) and other drugs known from the literature (MIC of isoniazid = 0.3 - 1.4 µM, levofloxacin = 0.8 - 1.4 µM, amikacin = 0.4 - 1.7 µM, bendaquiline = 0.03 - 1 µM, ethambutol = 0.3 - 3 µM or ethionamide = 10 µM).[87] However, some of these compounds also exhibit cytotoxicity and are therefore of no interest for further consideration.

In a second study, inhibition against the virulent wild-type *Mtb* ATCC 35801 was observed at 20 µM and if the value was above 80%, the inhibitory concentration ($IC_{50/90}$) was also determined. The inhibition step was skipped for some complexes. The cytotoxicity was also re-evaluated with a human liver cancer cell line HepG2. Of the most promising non-toxic compounds **15**, **C1**, **C2** and **C7**, only **C1** and **C7** were able to transfer their activity against *Mtb* H37Ra to the wild-type. Compound **15** was no longer active against the wild-type and **C2** did not show inhibition. While the low cytotoxicity was maintained for all four compounds. The influence of Zn^{2+}, Cu^{2+} and others like $V^{4+/5+}$ or Co^{2+} on anti-

mycobacterial activity is known from literature for many complexes.[88] Nevertheless, it is unexpected that chelation with Zn^{2+} would demonstrate such a strong influence on activity, even compared to the wild-type.

Table 1. Minimum inhibitory concentration (MIC) and inhibition percentage and inhibitory concentration ($IC_{50/90}$) against wild-type *Mtb* ATCC 35801 of investigated imidazo[1,5-*a*]quinolines. Epithelia cell line from lung carcinoma (Calu-3), "-" indicates no effect at 100 µM and "+" toxic effects at 100 µM. Further cytotoxicity investigation on human liver cancer cell line HepG2. All MICs and ICs values are in µM.

Nr.	R^2 / R^1	MIC in µM				Calu-3	*Mtb* ATCC 35801			HepG2
		Ec	*Sa*	*Str*	*Mtb*		Inhibition at 20 µM	IC_{50}	IC_{90}	IC_{50}
9	Ph / 2-Thiophenyl	>196	>196	>196	>196	-	17%	n.d.	n.d.	n.d.
10	Ph / Ph	>200	>200	>200	>200	-	2%	n.d.	n.d.	n.d.
11	Ph / 2-Pyridinyl	>199	>199	>199	25	+	21%	n.d.	n.d.	n.d.
12	Ph / 2-Quinolinyl	>172	>172	>172	86-43	-	1%	n.d.	n.d.	n.d.
13	Ph / 2-Pyrimidinyl	>148	>148	>148	1	+	65%	n.d.	n.d.	n.d.
14	Ph / 2-(5-Ph-Pyridinyl)	>136	>136	>136	34	-	8%	n.d.	n.d.	n.d.
15	Ph / 2-Isoquinolinyl	>144	>144	>144	1-0.5	-	82%	86.5	132.2	>100
16	Ph / 2-Me_2N-Ph	>127	>127	>127	2	+	-8%	n.d.	n.d.	n.d.
17	Ph / MeO-Ph	>183	>183	>183	46	-	15%	n.d.	n.d.	n.d.
18	2-Pyridinyl / 2-Pyridinyl	>198	>198	>198	12-6	-	41%	n.d.	n.d.	n.d.
19	2-Pyridinyl / Ph	>199	>199	>199	50-25	+	40%	n.d.	n.d.	n.d.
20	1-Naphthyl / 2-Pyridinyl	>172	>172	>172	5-1	+	83%	12.7	26.8	28.2
21	NPh_2 / 2-Pyridinyl	>155	>155	>155	>155	-	2%	n.d.	n.d.	n.d.
Nr.	**Complex formula**									
C1	[$ZnCl_2$**11**]	>140	>140	>140	2	-	90%	6	7.7	>100
C2	[$FeCl_2$(**11**)$_2$]$FeCl_4$	>132	>132	>132	2	-	26%	n.d.	n.d.	n.d.
C3	[$Cu(OAc)_2$**11**]	>127	>127	16-8	2	+	n.d.	9.7	14.4	4.5
C4	[$ZnCl_2$**20**]	>126	31.5	63	2-1	+	n.d.	7.4	9.6	17.8
C5	[$ZnCl_2$**13**]	>140	17 - 9	17	2-1	+	n.d.	3.6	7.2	>100
C6	[$ZnCl_2$**14**]	>120	>120	>120	8	-	n.d.	44.7	80.0	>100
C7	[$ZnCl_2$**15**]	>126	>126	>126	2-1	-	n.d.	9.1	17.7	83.3
C8	[$ZnCl_2$**21**]	>117	>117	>117	>117	-	n.d.	98.5	>100	>100

4. Summary and Perspective

The main focus of this work was to investigate the photoluminescent and biological properties of imidazo[1,5-*a*]quinolines. Previous photophysical measurements have shown that imidazo[1,5-*a*]quinolines exhibit strong blue emission and have acceptable QY, paired with exceptional oxidative stability. These properties characterize these materials particularly in relation to visual applications and it has been demonstrated that imidazo[1,5-*a*]quinolines are suitable as emitter materials in OLEDs. In the course of this, a dependence of the QY and the substitution pattern on the imidazole ring was

observed. Particularly noteworthy is a strong increase in QY upon substitution with 2-*N*-heteroaromatics. Strong deviations in QY depending on the selected combination of substituents could not be converted into an exact pattern. Nevertheless, the significance of the substitution pattern was clearly recognizable and became the central topic of this work. A secondary subject was the expansion of the understanding of the less researched biological characteristics of imidazo[1,5-*a*]quinolines.

In order to investigate the dependence of the photoluminescent properties on the substitution pattern on the imidazole ring, a versatile synthesis was required. Our developed synthesis provides access to a wide variety of substituent combinations in a high efficiency. Starting with quinoline *N*-oxide, the 2-methylamine was obtained in excellent yields in two steps (compare **scheme 7** and chapter 4.1). From this starting material, the first substituent was introduced as an acid chloride in an *Einhorn* acylation. After a *Vilsmeier*-type ring closure, the imidazole ring could be selectively brominated in high yield. This bromide was used as a coupling partner in a *Negishi* coupling to produce a wide range of products in very good yields. In addition, a selective and high-yield substitution with *s*-triazine was achieved (compare **scheme 8** and chapter 4.3). To explore the effects of substitution patterns, various combinations of electron-rich and electron-poor moieties, both individually and in conjunction with each other, were synthesized.

It could be proven that the basic properties of the investigated IQs are only slightly dependent on the substitution pattern at the imidazole ring. While the extinction maximum of these compounds still shows a fairly wide range between about 350 - 400 nm, they only emit in a narrow range of 440 - 480 nm (**figure 3** and **4**). In a CV measurement it could also be shown that the HOMO for all measured compounds is around -5.5 eV and the LUMO is -2.5 eV (**figure 6**). This relative independence from the substitution pattern may be related to the fact that the quinoline ring is the structural element of the imidazo[1,5-*a*]quinolines that determines these properties. Since only the imidazole ring is substituted, these properties are not directly affected. However, a strong dependence of the QY on the chosen combination of substituents was observed (**figure 5**). In particular, the combination of an electron-donating residue in position 1 of the imidazole ring and an electron-withdrawing 2-*N*-heteroaromatic in position 3 showed a strong increase in the QY. The substitution of a phenyl ether as electron donor and 2-pyrimidinyl as electron acceptor could increase the QY up to 86%. This represents a more than twofold increase of the QY compared to previous compounds. Further investigation of the behavior of these compounds in the solid phase showed that the extinction and emission maxima shift bathochromically by approximately 50 nm (compare **figure 7** and chapter 4.3). In addition, the QY (s) dropped sharply, although an appropriate value of 31% was still reached.

During the evaluation of the biological activity against selected strains of different pathogens, a strong impact against *Mtb* was observed. Especially, chelating compounds showed good MICs of 1 - 2 µM.

Subsequent investigation of Zn^{2+}, Fe^{3+} and Cu^{2+} complexes with these ligands showed that the activity can be conferred not only against the non-virulent variant but also against the infectious wild-type. Structurally, a combination of a sterically demanding substituent in position 1 and a 2-pyridinyl moiety in position 3 showed the highest activity. Which could be further increased by incorporation into a zinc complex, while retaining no toxicity in human lung and liver cancer lines. These properties could make imidazo[1,5-*a*]quinolines a potential target for further drug development against *Mtb*.

In summary, we have developed a versatile and productive synthetic route through which we were able to identify a favorable substitution pattern on the imidazole ring to optimize the photoluminescent properties of imidazo[1,5-*a*]quinolines. In addition, the transition from photoluminescence in solution and in the solid state could be investigated and demonstrated in more detail. This would pave the way for possible integration as emitter materials in an OLED. Additionally, our research provides important foundational insights into the biological properties of imidazo[1,5-*a*]quinolines, particularly in relation to the activity against *Mtb*.

5. References

1 G. Domagk, *Dtsch. med. Wochenschr.*, 1935, **61**, 250–253.

2 a) X.-Y. Sun, R. Wu, X. Wen, L. Guo, C.-P. Zhou, J. Li, Z.-S. Quan and J. Bao, *Eur. J. Med. Chem.*, 2013, **60**, 451–455; b) M. Fujita, H. Egawa, M. Kataoka, T. Miyamoto, J. Nakano and J. Matsumoto, *Chem. Pharm. Bull.*, 1995, **43**, 2123–2132;

3 R. Kayarmar, G. K. Nagaraja, M. Bhat, P. Naik, K. P. Rajesh, S. Shetty and T. Arulmoli, *Med. Chem. Res.*, 2014, **23**, 2964–2975.

4 a) J. D. Seixas, S. A. Luengo-Arratta, R. Diaz, M. Saldivia, D. I. Rojas-Barros, P. Manzano, S. Gonzalez, M. Berlanga, T. K. Smith, M. Navarro and M. P. Pollastri, *J. Med. Chem.*, 2014, **57**, 4834–4848; b) A. K. Pandey, R. Sharma, A. Singh, S. Shukla, K. Srivastava, S. K. Puri, B. Kumar and P. M. S. Chauhan, *RSC Adv.*, 2014, **4**, 26757–26770;

5 a) Z. Zhu, B. Lippa and L. B. Townsend, *J. Org. Chem.*, 1999, **64**, 4159–4168; b) A. Carta, I. Briguglio, S. Piras, P. Corona, G. Boatto, M. Nieddu, P. Giunchedi, M. E. Marongiu, G. Giliberti, F. Iuliano, S. Blois, C. Ibba, B. Busonera and P. La Colla, *Bioorg. Med. Chem.*, 2011, **19**, 7070–7084;

6 a) M. Hranjec, M. Kralj, I. Piantanida, M. Sedić, L. Suman, K. Pavelić and G. Karminski-Zamola, *J. Med. Chem.*, 2007, **50**, 5696–5711; b) N. Perin, L. Uzelac, I. Piantanida, G. Karminski-Zamola, M. Kralj and M. Hranjec, *Bioorg. Med. Chem.*, 2011, **19**, 6329–6339;

7 M. W. Moon, J. K. Morris, R. F. Heier, C. G. Chidester, W. E. Hoffmann, M. F. Piercey, J. S. Althaus, P. F. von Voigtlander, D. L. Evans and L. M. Figur, *J. Med. Chem.*, 1992, **35**, 1076–1092.

8 a) H. N. Nagesh, A. Suresh, M. N. Reddy, N. Suresh, J. Subbalakshmi and K. V. G. Chandra Sekhar, *RSC Adv.*, 2016, **6**, 15884–15894; b) J. Sun, Z. Liu, Y. Wang, S. Xiao, M. Pei, X. Zhao and G. Zhang, *RSC Adv.*, 2015, **5**, 100873–100878;

9 H. v. Bidder and H. Rupe, *Helv. Chim. Acta*, 1939, **22**, 1268–1278.

10 Q. Cai, Z. Li, J. Wei, L. Fu, C. Ha, D. Pei and K. Ding, *Org. Lett.*, 2010, **12**, 1500–1503.

11 J.-R. Huang, Q.-R. Zhang, C.-H. Qu, X.-H. Sun, L. Dong and Y.-C. Chen, *Org. Lett.*, 2013, **15**, 1878–1881.

12 A. Cappelli, M. Anzini, F. Castriconi, G. Grisci, M. Paolino, C. Braile, S. Valenti, G. Giuliani, S. Vomero, A. Di Capua, L. Betti, G. Giannaccini, A. Lucacchini, C. Ghelardini, L. Di Cesare Mannelli, M. Frosini, L. Ricci, G. Giorgi, M. P. Mascia and G. Biggio, *J. Med. Chem.*, 2016, **59**, 3353–3372.

13 a) K. Sasaki, A. Tsurumori and T. Hirota, *J. Chem. Soc., Perkin Trans. 1*, 1998, 3851–3856; b) Y. Yan, Y. Zhang, Z. Zha and Z. Wang, *Org. Lett.*, 2013, **15**, 2274–2277;

14 Q. Wang, S. Zhang, F. Guo, B. Zhang, P. Hu and Z. Wang, *J. Org. Chem.*, 2012, **77**, 11161–11166.

15 K. C. Langry, *Org. Prep. Proced. Int.*, 1994, **26**, 429–438.

16 G. Pelletier and A. B. Charette, *Org. Lett.*, 2013, **15**, 2290–2293.

17 Z. Li, S.-S. Wu, Z.-G. Luo, W.-K. Liu, C.-T. Feng and S.-T. Ma, *J. Org. Chem.*, 2016, **81**, 4386–4392.

18 Z. Tan, H. Zhao, C. Zhou, H. Jiang and M. Zhang, *J. Org. Chem.*, 2016, **81**, 9939–9946.

19 M. Li, Y. Xie, Y. Ye, Y. Zou, H. Jiang and W. Zeng, *Org. Lett.*, 2014, **16**, 6232–6235.

20 H. Wang, W. Xu, Z. Wang, L. Yu and K. Xu, *J. Org. Chem.*, 2015, **80**, 2431–2435.

21 H. Wang, W. Xu, L. Xin, W. Liu, Z. Wang and K. Xu, *J. Org. Chem.*, 2016, **81**, 3681–3687.

22 A. Cappelli, G. Giuliani, M. Anzini, D. Riitano, G. Giorgi and S. Vomero, *Bioorg. Med. Chem.*, 2008, **16**, 6850–6859.

23 R. Lyapchev, P. Petrov, M. Dangalov and N. G. Vassilev, *J. Organomet. Chem.*, 2017, **851**, 194–209.

24 H. Yasuda, R. Nakano, S. Ito and K. Nozaki, *J. Am. Chem. Soc.*, 2018, **140**, 1876–1883.

25 a) R. Nakano and K. Nozaki, *J. Am. Chem. Soc.*, 2015, **137**, 10934–10937; b) S. Akita, R. Nakano, S. Ito and K. Nozaki, *Organometallics*, 2018, **37**, 2286–2296; c) W. Tao, R. Nakano, S. Ito and K. Nozaki, *Angew. Chem., Int. Ed.*, 2016, **55**, 2835–2839;

26 G. Albrecht, J. M. Herr, M. Steinbach, H. Yanagi, R. Göttlich and D. Schlettwein, *Dyes Pigments*, 2018, **158**, 334–341.

27 C. W. Tang and S. A. VanSlyke, *Appl. Phys. Lett.*, 1987, **51**, 913–915.
28 Precedence Research, *OLED Market Size Expected to Reach USD 344.58 Billion by 2034,* available at: https://finance.yahoo.com/news/oled-market-size-expected-reach-150000573.html?guccounter=1, accessed 17 October 2024.
29 J. N. Bardsley, *IEEE J. Select. Topics Quantum Electron.*, 2004, **10**, 3–9.
30 C. R. Ronda, *Luminescence. From Theory to Applications*, Wiley-VCH, Weinheim, 2007.
31 a) J. A. Howell and L. G. Hargis, *Anal. Chem.*, 1986, **58**, 108–124; b) N. S. Lewis, *Acc. Chem. Res.*, 1990, **23**, 176–183;
32 a) C. Adachi and A. S. D. Sandanayaka, *CCS Chem.*, 2020, **2**, 1203–1216; b) M. Reddy and K. S. Bejoymohandas, *Journal of Photochemistry and Photobiology C: Photochemistry Reviews*, 2016, **29**, 29–47;
33 N. J. Turro, *Modern Molecular Photochemistry*, University Science Books, Mill Valley, California, 1991.
34 M. A. Baldo, D. F. O'Brien, M. E. Thompson and S. R. Forrest, *Phys. Rev. B*, 1999, **60**, 14422–14428.
35 D. Di, Le Yang, J. M. Richter, L. Meraldi, R. M. Altamimi, A. Y. Alyamani, D. Credgington, K. P. Musselman, J. L. MacManus-Driscoll and R. H. Friend, *Adv. Mater.*, 2017, **29**, 1605987.
36 a) B.-Y. Lin, C. J. Easley, C.-H. Chen, P.-C. Tseng, M.-Z. Lee, P.-H. Sher, J.-K. Wang, T.-L. Chiu, C.-F. Lin, C. J. Bardeen and J.-H. Lee, *ACS Appl. Mater. Interfaces*, 2017, **9**, 10963–10970; b) N. T. Tierce, C.-H. Chen, T.-L. Chiu, C.-F. Lin, C. J. Bardeen and J.-H. Lee, *Phys. Chem. Chem. Phys.*, 2018, **20**, 27449–27455;
37 a) R. J. Holmes, S. R. Forrest, Y.-J. Tung, R. C. Kwong, J. J. Brown, S. Garon and M. E. Thompson, *Appl. Phys. Lett.*, 2003, **82**, 2422–2424; b) M. A. Baldo, S. Lamansky, P. E. Burrows, M. E. Thompson and S. R. Forrest, *Appl. Phys. Lett.*, 1999, **75**, 4–6;
38 a) X. Cai and S.-J. Su, *Adv. Funct. Mater.*, 2018, **28**, 1802558; b) I. Hladka, D. Volyniuk, O. Bezvikonnyi, V. Kinzhybalo, T. J. Bednarchuk, Y. Danyliv, R. Lytvyn, A. Lazauskas and J. V. Grazulevicius, *J. Mater. Chem. C*, 2018, **6**, 13179–13189; c) T. Matulaitis, P. Imbrasas, N. A. Kukhta, P. Baronas, T. Bučiūnas, D. Banevičius, K. Kazlauskas, J. V. Gražulevičius and S. Juršėnas, *J. Phys. Chem. C*, 2017, **121**, 23618–23625;
39 a) C. Adachi, M. A. Baldo, S. R. Forrest, S. Lamansky, M. E. Thompson and R. C. Kwong, *Appl. Phys. Lett.*, 2001, **78**, 1622–1624; b) R. Braveenth, H. Lee, S. Kim, K. Raagulan, S. Kim, J. H. Kwon and K. Y. Chai, *J. Mater. Chem. C*, 2019, **7**, 7672–7680; c) Y.-C. Cheng, X.-C. Fan, F. Huang, X. Xiong, J. Yu, K. Wang, C.-S. Lee and X.-H. Zhang, *Angew. Chem., Int. Ed.*, 2022, **61**, e202212575; d) C.-L. Ho, H. Li and W.-Y. Wong, *J. Organomet. Chem.*, 2014, **751**, 261–285; e) H. Nakanotani, T. Higuchi, T. Furukawa, K. Masui, K. Morimoto, M. Numata, H. Tanaka, Y. Sagara, T. Yasuda and C. Adachi, *Nat. Commun.*, 2014, **5**, 1–7; f) X. Yang, G. Zhou and W.-Y. Wong, *Chem. Soc. Rev.*, 2015, **44**, 8484–8575; g) Y. Zhang, Y. Wang, J. Song, J. Qu, B. Li, W. Zhu and W.-Y. Wong, *Adv. Opt. Mater.*, 2018, **6**, 1800466;
40 a) J. Lee, C. Jeong, T. Batagoda, C. Coburn, M. E. Thompson and S. R. Forrest, *Nat. Commun.*, 2017, **8**, 1–9; b) N. C. Giebink, B. W. D'Andrade, M. S. Weaver, P. B. Mackenzie, J. J. Brown, M. E. Thompson and S. R. Forrest, *J. Appl. Phys.*, 2008, **103**, 44509;
41 G. Albrecht, C. Rössiger, J. M. Herr, H. Locke, H. Yanagi, R. Göttlich and D. Schlettwein, *Phys. Status Solidi B*, 2020, **257**, 1900677.
42 G. Albrecht, C. Geis, J. M. Herr, J. Ruhl, R. Göttlich and D. Schlettwein, *Org. Electron.*, 2019, **65**, 321–326.
43 J. M. Herr, C. Rössiger, H. Locke, M. Wilhelm, J. Becker, W. Heimbrodt, D. Schlettwein and R. Göttlich, *Dyes Pigments*, 2020, **180**, 108512.
44 N. Kulhanek, N. Martin and R. Göttlich, *Eur. J. Org. Chem.*, 2024, **27**, e202301007.

45 N. Kulhanek, K. V. Borysova, M. Kirchner, K. Müller-Buschbaum and R. Göttlich, *Eur. J. Org. Chem.*, 2024, e202400783.
46 a) P. Qian, Z. Yan, Z. Zhou, K. Hu, J. Wang, Z. Li, Z. Zha and Z. Wang, *Org. Lett.*, 2018, **20**, 6359–6363; b) P. Qian, Z. Zhou, K. Hu, J. Wang, Z. Li, Z. Zha and Z. Wang, *Org. Lett.*, 2019, **21**, 6403–6407; c) H. Liu, X. Wang and C. Ma, *Synthesis*, 2018, **50**, 2761–2767; d) Z. Yan, C. Wan, Y. Yang, Z. Zha and Z. Wang, *RSC Adv.*, 2018, **8**, 23058–23065; e) M. Sandeep, P. Swati Dushyant, B. Sravani and K. Rajender Reddy, *Eur. J. Org. Chem.*, 2018, **2018**, 3036–3047;
47 D. Sustac Roman, V. Poiret, G. Pelletier and A. B. Charette, *Eur. J. Org. Chem.*, 2015, **2015**, 67–71.
48 a) W. K. Fife, *J. Org. Chem.*, 1983, **48**, 1375–1377; b) W. K. Fife and B. D. Boyer, *Heterocycles*, 1984, **22**, 1121–1124; c) T. Sakamoto, S. Kaneda, S. Nishimura and H. Yamanaka, *Chem. Pharm. Bull.*, 1985, **33**, 565–571; d) H. Vorbrüggen and K. Krolikiewicz, *Synthesis*, 1983, **1983**, 316–319;
49 M. Henze, *Ber. dtsch. Chem. Ges. A/B*, 1936, **69**, 1566–1568.
50 a) R. O. Hutchins and M. G. K. Hutchins, in *The Chemistry of triple-bonded functional groups*. *Part 1*, ed. S. Patai and Z. Rappoport, Wiley, Chichester West Sussex, New York, 1983, 571–601; b) Y. Kikugawa, M. Kuramoto, I. Saito and S. Yamada, *Chem. Pharm. Bull.*, 1973, **21**, 1927–1937;
51 a) A. M. Maj, I. Suisse, C. Hardouin and F. Agbossou-Niedercorn, *Tetrahedron*, 2013, **69**, 9322–9328; b) J. R. Quinn and S. C. Zimmerman, *J. Org. Chem.*, 2005, **70**, 7459–7467;
52 A. Einhorn, F. Hollandt and M. von Alfred Einhorn, *Justus Liebigs Ann. Chem.*, 1898, **301**, 95–115.
53 a) A. Vilsmeier and A. Haack, *Ber. dtsch. Chem. Ges. A/B*, 1927, **60**, 119–122; b) M. Alcarazo, S. J. Roseblade, A. R. Cowley, R. Fernández, J. M. Brown and J. M. Lassaletta, *J. Am. Chem. Soc.*, 2005, **127**, 3290–3291;
54 F. Shibahara, E. Yamaguchi, A. Kitagawa, A. Imai and T. Murai, *Tetrahedron*, 2009, **65**, 5062–5073.
55 M. Marner, N. Kulhanek, J. Eichberg, K. Hardes, M. D. Molin, J. Rybniker, M. Kirchner, T. F. Schäberle and R. Göttlich, *RSC Med. Chem.*, 2024, **15**, 1746–1750.
56 M. Hapke, L. Brandt and A. Lützen, *Chem. Soc. Rev.*, 2008, **37**, 2782–2797.
57 a) L.-C. Campeau and K. Fagnou, *Chem. Soc. Rev.*, 2007, **36**, 1058–1068; b) E. Tyrrell and P. Brookes, *Synthesis*, 2003, **2003**, 469–483; c) X. A. F. Cook, A. de Gombert, J. McKnight, L. R. E. Pantaine and M. C. Willis, *Angew. Chem., Int. Ed.*, 2021, **60**, 11068–11091;
58 G. R. Newkome, A. K. Patri, E. Holder and U. S. Schubert, *Eur. J. Org. Chem.*, 2004, **2004**, 235–254.
59 W. F. Bailey and J. J. Patricia, *J. Organomet. Chem.*, 1988, **352**, 1–46.
60 R. P. Sonawane, V. Sikervar and S. Sasmal, in *Comprehensive Heterocyclic Chemistry IV*, Elsevier, Amsterdam, 2022, 181–283.
61 W. M. Boesveld, P. B. Hitchcock and M. F. Lappert, *J. Chem. Soc., Perkin Trans. 1*, 2001, 1103–1108.
62 W. M. Boesveld and M. F. Lappert, *Chem. Commun.*, 1997, 2091–2092.
63 A. Kreutzberger, *Angew. Chem., Int. Ed.*, 1967, **6**, 940.
64 a) A. M. Brouwer, *Pure Appl. Chem.*, 2011, **83**, 2213–2228; b) D. F. Eaton, *Pure Appl. Chem.*, 1988, **60**, 1107–1114;
65 E. Mayo Yanes, S. Chakraborty and R. Gershoni-Poranne, *Sci. Data*, 2024, **11**, 97.
66 S. Chakraborty, E. Mayo Yanes and R. Gershoni-Poranne, *Beilstein J. Org. Chem.*, 2024, **20**, 1817–1830.
67 A. Wahab, L. Pfuderer, E. Paenurk and R. Gershoni-Poranne, *J. Chem. Inf. Model.*, 2022, **62**, 3704–3713.
68 a) E. Yamaguchi, F. Shibahara and T. Murai, *J. Org. Chem.*, 2011, **76**, 6146–6158; b) G. Volpi, B. Lace, C. Garino, E. Priola, E. Artuso, P. Cerreia Vioglio, C. Barolo, A. Fin, A. Genre and C. Prandi, *Dyes Pigments*, 2018, **157**, 298–304; c) G. Volpi, S. Galliano, R. Buscaino, G. Viscardi and C. Barolo, *J. Lumin.*, 2022, **242**, 118529;
69 G. Volpi, C. Garino, E. Fresta, E. Casamassa, M. Giordano, C. Barolo and G. Viscardi, *Dyes Pigments*, 2021, **192**, 109455.

70 C.-X. Zhao, T. Liu, M. Xu, H. Lin and C.-J. Zhang, *Chin. Chem. Lett.*, 2021, **32**, 1925–1928.
71 a) J. C. Costa, R. J. Taveira, C. F. Lima, A. Mendes and L. M. Santos, *Opt. Mater.*, 2016, **58**, 51–60; b) B. D'Andrade, S. Datta, S. Forrest, P. Djurovich, E. Polikarpov and M. Thompson, *Org. Electron.*, 2005, **6**, 11–20;
72 a) A. D. Becke, *J. Chem. Phys.*, 1993, **98**, 5648–5652; b) A. D. Becke and E. R. Johnson, *J. Chem. Phys.*, 2005, **123**, 154101; c) S. Grimme, J. Antony, S. Ehrlich and H. Krieg, *J. Chem. Phys.*, 2010, **132**, 154104; d) E. R. Johnson and A. D. Becke, *J. Chem. Phys.*, 2006, **124**, 174104; e) C. Lee, W. Yang and R. G. Parr, *Phys. Rev. B*, 1988, **37**, 785–789; f) A. Schäfer, C. Huber and R. Ahlrichs, *J. Chem. Phys.*, 1994, **100**, 5829–5835; g) P. J. Stephens, F. J. Devlin, C. F. Chabalowski and M. J. Frisch, *J. Phys. Chem.*, 1994, **98**, 11623–11627;
73 A. J. Garza and G. E. Scuseria, *J. Phys. Chem. Lett.*, 2016, **7**, 4165–4170.
74 a) A. E. Sedykh, M. Becker, M. T. Seuffert, D. Heuler, M. Maxeiner, D. G. Kurth, C. E. Housecroft, E. C. Constable and K. Müller-Buschbaum, *Chem. Photo. Chem.*, 2023, **7**, e202200244; b) M. S. Wrighton, D. S. Ginley and D. L. Morse, *J. Phys. Chem.*, 1974, **78**, 2229–2233;
75 a) L. Valla, D. Pitrat, J.-C. Mulatier, T. Le Bahers, E. Jeanneau, L. M. A. Ali, C. Nguyen, M. Gary-Bobo, C. Andraud and Y. Bretonnière, *J. Org. Chem.*, 2024, **89**, 8407–8419; b) G. Colombo, A. Cinco, G. A. Ardizzoia and S. Brenna, *Colorants*, 2023, **2**, 179–193; c) G. Colombo, G. Attilio Ardizzoia and S. Brenna, *Inorganica Chim. Acta*, 2022, **535**, 120849;
76 a) X. Yang, G. Mu, K. Weng and X. Tang, *Photonics*, 2024, **11**, 864; b) D. R. Lee, M. Kim, S. K. Jeon, S.-H. Hwang, C. W. Lee and J. Y. Lee, *Adv. Mater.*, 2015, **27**, 5861–5867; c) J.-H. Lee, C.-H. Chen, P.-H. Lee, H.-Y. Lin, M. Leung, T.-L. Chiu and C.-F. Lin, *J. Mater. Chem. C*, 2019, **7**, 5874–5888; d) H. Uoyama, K. Goushi, K. Shizu, H. Nomura and C. Adachi, *Nature*, 2012, **492**, 234–238; e) Q. Zhang, B. Li, S. Huang, H. Nomura, H. Tanaka and C. Adachi, *Nature Photon*, 2014, **8**, 326–332;
77 a) I. Barberis, N. L. Bragazzi, L. Galluzzo and M. Martini, *J. Prev. Med. Hyg.*, 2017, **58**, E9-E12; b) T. M. Daniel, J. H. Bates and K. A. Downes, in *Tuberculosis*. *Pathogenesis, protection, and control*, ed. B. R. Bloom, ASM Press, Washington, D.C, 1994, 13–24; c) T. Paulson, *Nat.*, 2013, **502**, S2-3;
78 World Health Organization, *Global Tuberculosis Report 2023*, WHO, Geneva, 2023.
79 a) H. Esmail, C. E. Barry, D. B. Young and R. J. Wilkinson, *Phil. Trans. R. Soc. B*, 2014, **369**, 20130437; b) C. E. Barry, H. I. Boshoff, V. Dartois, T. Dick, S. Ehrt, J. Flynn, D. Schnappinger, R. J. Wilkinson and D. Young, *Nat. Rev. Microbiol.*, 2009, **7**, 845–855;
80 M. Pai, M. A. Behr, D. Dowdy, K. Dheda, M. Divangahi, C. C. Boehme, A. Ginsberg, S. Swaminathan, M. Spigelman, H. Getahun, D. Menzies and M. Raviglione, *Nat. Rev. Dis. Primers*, 2016, **2**, 16076.
81 E. Vynnycky and P. E. Fine, *Epidemiol. Infect.*, 1997, **119**, 183–201.
82 V. A. Dartois and E. J. Rubin, *Nat. Rev. Microbiol.*, 2022, **20**, 685–701.
83 a) National Health Service (NHS), *Clinical Commissioning Policy Statement: Treatment for defined patients with MDR-TB and XDR-TB including bedaquiline and delamanid*, England, 2019; b) Centers for Disease Control and Prevention (CDC), *Treatment for TB Disease*, USA, 2023;
84 World Health Organization, *Antimicrobial resistance: global report on surveillance*, WHO, Geneva, 2014.
85 G. G. Ladani and M. P. Patel, *Heterocycl. Lett.*, 2016, **6**, 459–469.
86 a) I. D. M. Kresna, Z. G. Wuisan, J.-M. Pohl, U. Mettal, V. L. Otoya, M. Gand, M. Marner, L. L. Otoya, N. Böhringer, A. Vilcinskas and T. F. Schäberle, *J. Nat. Prod.*, 2022, **85**, 888–898; b) M. Marner, M. A. Patras, M. Kurz, F. Zubeil, F. Förster, S. Schuler, A. Bauer, P. Hammann, A. Vilcinskas, T. F. Schäberle and J. Glaeser, *J. Nat. Prod.*, 2020, **83**, 2607–2617;
87 a) M. T. Heinrichs, R. J. May, F. Heider, T. Reimers, S. K. B Sy, C. A. Peloquin and H. Derendorf, *Int. J. Mycobacteriol.*, 2018, **7**, 156–161; b) K. Kaniga, D. M. Cirillo, S. Hoffner, N. A. Ismail, D. Kaur, N. Lounis, B. Metchock, G. E. Pfyffer and A. Venter, *J. Clin. Microbiol.*, 2016, **54**, 2956–2962; c) T. Schön, J. Werngren, D. Machado, E. Borroni, M. Wijkander, G. Lina, J. Mouton, E. Matuschek, G.

Kahlmeter, C. Giske, M. Santin, D. M. Cirillo, M. Viveiros and E. Cambau, *Clin. Microbiol. Infect.*, 2020, **26**, 1488–1492; d) N. J. E. Waller, C.-Y. Cheung, G. M. Cook and M. B. McNeil, *Nat. Commun.*, 2023, **14**, 1517;

88 a) I. Correia, P. Adão, S. Roy, M. Wahba, C. Matos, M. R. Maurya, F. Marques, F. R. Pavan, C. Q. F. Leite, F. Avecilla and J. Costa Pessoa, *J. Inorg. Biochem.*, 2014, **141**, 83–93; b) M. C. Mandewale, B. Thorat, D. Shelke and R. Yamgar, *Bioinorg. Chem. Appl.*, 2015, **2015**, 153015; c) M. N. Matada and K. Jathi, *J. Coord. Chem.*, 2019, **72**, 1994–2014; d) P. P. Netalkar, S. P. Netalkar, S. Budagumpi and V. K. Revankar, *Eur. J. Med. Chem.*, 2014, **79**, 47–56; e) D. A. Paixão, I. M. Marzano, E. H. L. Jaimes, M. Pivatto, D. L. Campos, F. R. Pavan, V. M. Deflon, P. I. S. Da Maia, A. M. Da Costa Ferreira, I. A. Uehara, M. J. B. Silva, F. V. Botelho, E. C. Pereira-Maia, S. Guilardi and W. Guerra, *J. Inorg. Biochem.*, 2017, **172**, 138–146; f) J.-H. Pan, Y. Chen, Y.-H. Huang, Y.-W. Tao, J. Wang, Y. Li, Y. Peng, T. Dong, X.-M. Lai and Y.-C. Lin, *Arch Pharm. Res.*, 2011, **34**, 1177–1181; g) R. Pati, R. Sahu, J. Panda and A. Sonawane, *Sci. Rep.*, 2016, **6**, 24184, https://www.nature.com/articles/srep24184; h) C. B. Scarim, R. Lira de Farias, A. Vieira de Godoy Netto, C. M. Chin, J. Leandro Dos Santos and F. R. Pavan, *Eur. J. Med. Chem.*, 2021, **214**, 113166;

6. Publications

6.1 Highly Versatile Preparation of Imidazo[1,5-*a*]quinolines and Characterization of Their Photoluminescent Properties

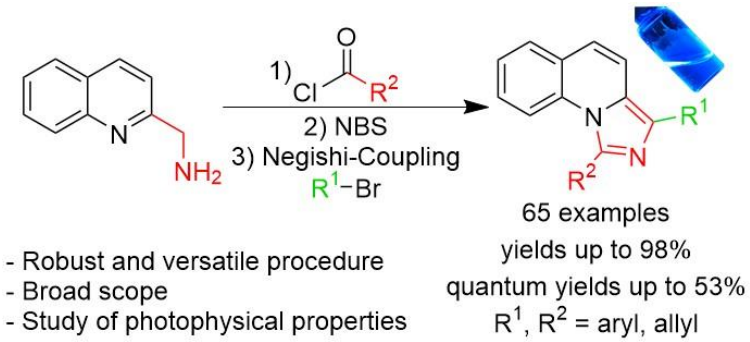

In this work we show a robust and versatile procedure for the synthesis of substituted imidazo[1,5-*a*]quinolines and examine the influence of this substituents on the photophysical properties of this system.

Reference

N. Kulhanek, N. Martin and R. Göttlich, *Eur. J. Org. Chem.*, 2024, **27**, e202301007. (DOI: 10.1002/ejoc.202301007)

Check for updates

EurJOC
European Journal of Organic Chemistry

Research Article
doi.org/10.1002/ejoc.202301007

Chemistry Europe
European Chemical Societies Publishing

www.eurjoc.org

Highly Versatile Preparation of Imidazo[1,5-a]quinolines and Characterization of Their Photoluminescent Properties

Niclas Kulhanek,[a] Niklas Martin,[a] and Richard Göttlich*[a]

In this work, we describe a simple and robust synthetic approach for the formation of 1,3-substituted imidazo[1,5-*a*]quinolines. This was achieved by developing a mild and selective bromination with N-bromosuccinimide (NBS) in 3-position of the imidazole ring. This was followed by a Negishi coupling, which we performed with various coupling partners, resulting in a wide range of different combinations, usually unattainable by other approaches and similar coupling reactions. Fluorescence measurements identified beneficial substitution patterns for the future use of imidazo[1,5-*a*]quinolines in optical applications, such as organic light-emitting diodes (OLEDs).

Introduction

Since their introduction in 1987 by Tang and VanSlyke, organic light-emitting diodes (OLEDs) have become a fundamental part of the modern lighting industry.[1] To this day, there have been several OLED generations produced utilizing different strategies to improve the internal quantum efficiency (IQE).[2] Regardless of the generation, blue OLED emitter materials are particularly challenging, due to a band gap of around 3 eV and long exciton lifetime (μs), which are higher than for green or red OLED emitter materials. The interaction of excitons and polarons creates hot exciton states that can lead to decomposition of the material. This means that the lifetime of blue emitters is more limited, which makes materials with blue emission and high stability very important.[3]

Imidazo[1,5-*a*]*N*-heteroaromatic ring systems are a common structural motif in pharmacologically and biologically active agents.[4] This important class also includes imidazo[1,5-*a*]pyridines and imidazo[1,5-*a*]quinolines, which are of particular interest because these compounds possess interesting photophysical properties. The simple and small imidazo[1,5-*a*]pyridines show blue emission with good quantum yields (QYs) in combination with a large Stokes shift, qualifying them as emitter materials for OLED application.[5] They can also be used as ligands with various central atoms, without losing their characteristic photoluminescent properties.[6] Weber *et al.* successfully implemented an imidazo[1,5-*a*]pyridine complex into an optical device.[7]

While the synthesis of imidazo[1,5-*a*]pyridines and recently imidazo[5,1-*a*]isoquinolines were the main topic of many studies, imidazo[1,5-*a*]quinolines have been examined less.[8,9] Classically, approaches to the preparation of imidazo[1,5-*a*]quinolines involve ring closure of a carbonyl species. This could be achieved *via* a Vilsmeier-type reaction starting from an amide, but in the modern variant by Pelletier *et al.*, the cyclization can occur under milder conditions (Scheme 1a).[10,11] Wang and Xu *et al.* prepared imidazo[1,5-*a*]quinolines using a copper-catalyzed decarboxylative cyclization of ketones or aldehydes with primary amines and amino acids (Scheme 1b).[12] Wu *et al.* formed the carbonyl species *in situ*, using a copper-promoted oxidative amination (Scheme 1c).[13]

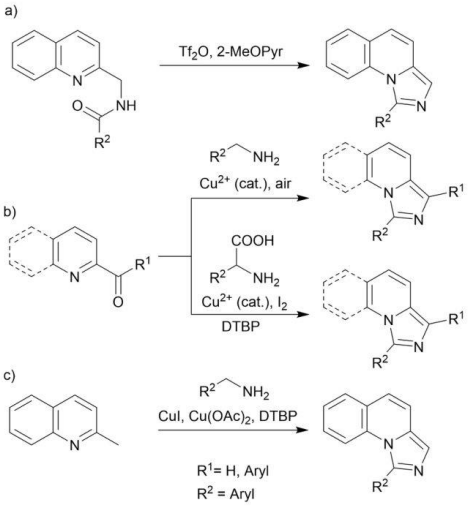

Scheme 1. Known strategies for direct formation of imidazo[1,5-*a*]quinolines using various carbonyl compounds. Di-*t*-butyl peroxide (DTBP).

[a] *N. Kulhanek, N. Martin, Prof. Dr. R. Göttlich*
Institute of Organic Chemistry
Justus-Liebig-University
Heinrich-Buff-Ring 17
35392 Giessen, Germany
E-mail: Richard.Goettlich@org.chemie.uni-giessen.de

Supporting information for this article is available on the WWW under https://doi.org/10.1002/ejoc.202301007

In our group we have already characterized some imidazo[1,5-*a*]quinoline derivatives and they possessed similar photophysical characteristics as imidazo[1,5-*a*]pyridines, but with higher QY and better stability.[14] We observed that the QY of imidazo[1,5-*a*]quinolines was dependent on the residues R^1 and R^2 (Figure 1), but we were not able to identify a clear trend.[15] In addition, we were able to successfully construct an OLED with **PCIC** as the dopant, in order to show that these compounds could be used as blue light-emitting materials (Figure 1).[16] Since imidazo[1,5-*a*]quinolines are suitable as blue OLED emitters, and showed interesting properties in complexes, we wanted to investigate this system further.

The focus of this study is to examine the effects of R^1 and R^2 residues on the emission, especially the impact of electron-rich, electron-poor, and sterically demanding residues in these positions. Thus, the goal is to develop a synthesis that allows the simple preparation of imidazo[1,5-*a*]quinolines with different residues R^1 and R^2.

Results and Discussion

Synthesis of the imidazo[1,5-a]quinolines

To achieve maximum flexibility we decided to close the imidazole ring with a suitable amide of R^2 and introduce R^1 separately, using a cross-coupling reaction (Scheme 2).

To obtain the required amine **3**, we reduced quinolin-2-carbonitrile **2**, which was excessed from quinoline *N*-oxide **1**, with conditions described in literature.[17]

We utilized an Einhorn acylation with an excess of triethylamine (TEA) to introduce R^2, using a variety of acid chlorides to form the amides **4**. To study the effect of R^2, the chosen residues used were a basic system with phenyl **4a**, an electron-rich aromatic group **4b**, an electron-poor aromatic group **4c** and a sterically demanding group **4d**. Purification of these compounds proved to be difficult. Therefore, we used the crude amides **4**. For the ring closure, we chose the Pelletier approach because it proved to be particularly reliable.[11] Following the procedure, we obtained the desired imidazo[1,5-*a*]quinolines **5** in excellent yields (Scheme 3). Initially we wanted to perform a halogenation with bromine in the 3-position of the imidazole ring system as reported by Shibahara *et al.*[18] However, this approach led to undesired side products, so we performed the bromination at −20 °C with NBS. This granted us the bromide **6** in excellent yields for all compounds (Scheme 3). It must be noted that such bromides can also be accessed directly, as shown by Sandeep and Tan *et al.*[19] These procedures were not used because they lacked the scalability needed for our project.

2-Boronic acids of *N*-heteroaromatics are known to be unstable and the boronic acid of **6** could not be isolated, making a Suzuki coupling not possible.[20] Therefore, we chose a Negishi coupling as our final reaction. Synthesis with **6** as the metallo-organic component resulted in better yields. Thus, in all experiments, bromide **6** was lithiated at −78 °C and transmetalated using an excess of $ZnCl_2$ in THF. We screened for a suitable Pd catalyst (Table 1). Pd(II) catalysts (entry 1–5) showed similar activity to Pd(0) (entry 6–10). However, the yields with Pd(II) did not improve with the addition of ligands, while the Pd(0) complexes led to higher yields in combination with an electron-rich and sterically demanding ligand. The best reactivity in this cross-coupling reaction was obtained with 3 mol% $[Pd_2(dba)_3]\cdot CHCl_3$ and 6 mol% $P(t\text{-}Bu)_3$ (entry 10). Therefore, the conditions of entry 10 were adapted for all of the following experiments.

It should be noted that we applied two different workups in the following procedures. The presence of $ZnCl_2$ during the coupling reaction led to the formation of Zn complexes for all chelating compounds **7**–**10a**–**f**, which could be simply filtered off then treated with conc. NH_3 solution to isolate the products directly. The other compounds **g**–**p** were purified by liquid column chromatography.

We started with the coupling of **6a** and the electron-poor substrates and obtained them in very good yields (Table 2). The only exception is **7e**, which was formed in only 13% yield, a sterically demanding substrates can be problematic for the Negishi reaction.[21] This trend continued with the *ortho*-substituted aryl bromides. Thus, **7j** and **7n** were formed in lower yields than their *para*-substituted equivalents. Surpris-

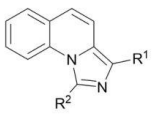

PCIC, R^2 = 2-Pyridyl, R^1 = 2-Quinolyl

Figure 1. General structure and example for imidazo[1,5-*a*]quinoline from our group.

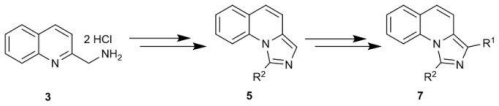

Scheme 2. General approach to the synthesis.

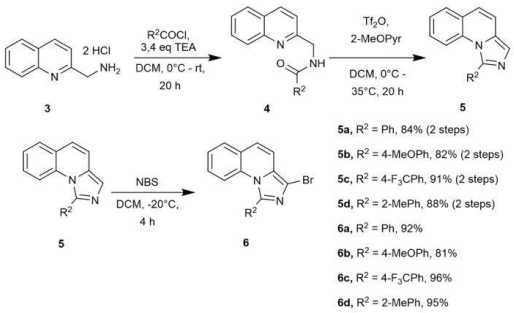

Scheme 3. Introduction of the first selectable residue R^2 using an Einhorn acylation. The crude amides **4** were then cyclized using triflic anhydride (Tf_2O) and 2-MeO-pyridine. After bromination with NBS the first coupling component was obtained.

Table 1. Screening results for the desired Negishi coupling.

6a **7a**

Entry	Cat.	Ligand	Yield/%
1[a]	$Pd(OAc)_2$	PPh_3	69
2[a]	$Pd(OAc)_2$	$P(t\text{-}Bu)_3$	71
3[b]	$[PdCl_2COD]$	–	66
4[b]	$[PdCl_2(MeCN)_2]$	–	61
5[b]	$[PdCl_2(PPh_3)_2]$	–	61
6[b]	$[Pd(PCy_3)_2]$	–	50
7[b]	$[Pd(PPh_3)_4]$	–	69
8[c]	$[Pd_2(dba)_3]\cdot CHCl_3$	PPh_3	72
9[c]	$[Pd_2(dba)_3]\cdot CHCl_3$	dppf	77
10[c]	$[Pd_2(dba)_3]\cdot CHCl_3$	$P(t\text{-}Bu)_3$	83

Reaction conditions: [a] 6 mol% cat., 12 mol% ligand. [b] 6 mol% cat. [c] 3 mol% cat., 6 mol% ligand.

Table 2. Isolated products for the couplings with **6a**, using the conditions of entry 10[c] (Table 1).

Nr.	R^2	R^1	Yield/%
7a	Ph	2-Pyridinyl	73
7b	Ph	2-Pyrimidinyl	60
7c	Ph	2-(5-Ph-Pyridinyl)	70
7d	Ph	2-Quinolinyl	79
7e	Ph	1-Isoquinolinyl	13
7f	Ph	3-Isoquinolinyl	79
7g	Ph	2-Thiophenyl	58
7h	Ph	4-F3 C-Ph	77
7i	Ph	Ph	84
7j	Ph	2-Me-Ph	52
7k	Ph	4-Me-Ph	78
7l	Ph	2-MeO-Ph	84
7m	Ph	4-MeO-Ph	61
7n	Ph	2-Me_2N-Ph	40
7o	Ph	4-Me_2N-Ph	68
7p	Ph	Allyl	47

ingly **7l** opposes this trend. It could be possible that the methoxy group stabilizes the intermediate by coordination to the Pd. This chelation would be stronger for a dimethylamine group which could inhibit the reductive elimination and hinder the coupling reaction, resulting in lower yield for **7n**. The coupling with allylic bromide was also successful, but the obtained mixture contained a large amount of various undefined side products. Purification was therefore challenging and only 47% of **7p** could be isolated.

The general trends observed for the phenyl system **7** largely followed the other coupling systems (Table 3). The 1-isoquinoline substrate could only be isolated in two cases and in low yields. The sterically demanding products **7–10j** and **7–10n** were formed in lower yields, and **7–10l** in higher yield than their equivalents. The allylic product was not formed for **9p** and the other products **7p**, **8p** and **10p** were isolated in lower yields. Surprisingly, the products **10a–f** were isolated in lower yields. The Zn complexes for these systems are presumably more soluble in THF and could not be isolated by filtration in the same amount as the other products.

Photophysical measurements

Optical measurements were conducted using a 0.1 mM chloroform solution at room temperature. A 0.1 mM solution of quinine sulfate in 0.5 M H_2SO_4 was used as the reference.[22] The fluorescence QY was calculated as described in the literature.[23] All measurements were performed under non-inert conditions. The extinction and emission spectra of all measured compounds are provided in the supporting information.

The measurements showed that no strong deviation of the extinction in the individual systems occurred. No major shift in the extinction maxima was observed, staying in a range of 350–390 nm (Table 4). In addition, the molar extinction coefficient log ε varied at approximately 4 $L\cdot mol^{-1}\cdot cm^{-1}$ (Table 5) and matches the findings of Volpi *et al.* with a similar system.[9]

Table 3. Isolated products in % for all performed coupling reactions using the conditions of entry 10[c] (Table 1).

	R^1	R^2			
		Ph **7**	4-MeO-Ph **8**	4-F_3C-Ph **9**	2-Me-Ph **10**
a	2-Pyridinyl	73	76	61	52
b	2-Pyrimidinyl	60	73	65	25
c	2-(5-Ph-Pyridinyl)	70	89	88	45
d	2-Quinolinyl	79	91	76	46
e	1-Isoquinolinyl	13	–	–	17
f	3-Isoquinolinyl	79	95	75	12
g	2-Thiophenyl	58	88	98	61
h	4-F_3C-Ph	77	51	53	96
i	Ph	84	95	68	84
j	2-Me-Ph	52	52	27	44
k	4-Me-Ph	78	69	49	56
l	2-MeO-Ph	84	97	77	77
m	4-MeO-Ph	61	75	71	66
n	2-Me_2N-Ph	40	25	62	67
o	4-Me_2N-Ph	68	84	76	74
p	Allyl	47	35	–	48

Research Article
doi.org/10.1002/ejoc.202301007

Table 4. Measured extinction maxima in nm for all isolated products. Every measurement was performed using a 1 μM solution of the compound in chloroform at 25 °C in air.

	R^1	R^2			
		Ph **7**	4-MeO-Ph **8**	4-F_3C-Ph **9**	2-Me-Ph **10**
a	2-Pyridinyl	373	374	360	373
b	2-Pyrimidinyl	369	369	364	369
c	2-(5-Ph-Pyridinyl)	383	385	368	383
d	2-Quinolinyl	390	392	386	389
e	1-Isoquinolinyl	380	–	–	377
f	3-Isoquinolinyl	367	368	365	368
g	2-Thiophenyl	375	374	368	375
h	4-F_3C-Ph	359	361	354	363
i	Ph	361	362	359	360
j	2-Me-Ph	355	354	350	352
k	4-Me-Ph	364	364	362	364
l	2-MeO-Ph	355	355	356	359
m	4-MeO-Ph	364	368	365	366
n	2-Me_2N-Ph	360	339	357	362
o	4-Me_2N-Ph	377	377	378	381
p	Allyl	349	348	–	344

Table 5. Calculated molar extinction coefficient log ε in $L \cdot mol^{-1} \cdot cm^{-1}$ for all isolated products in 1 μM solution with 1 cm cuvette length.

	R^1	R^2			
		Ph **7**	4-MeO-Ph **8**	4-F_3C-Ph **9**	2-Me-Ph **10**
a	2-Pyridinyl	4.20	4.11	4.26	4.26
b	2-Pyrimidinyl	4.27	4.20	4.32	4.41
c	2-(5-Ph-Pyridinyl)	4.18	4.23	4.41	4.38
d	2-Quinolinyl	4.34	4.11	4.34	4.40
e	1-Isoquinolinyl	4.08	–	–	4.23
f	3-Isoquinolinyl	4.15	4.36	4.36	4.41
g	2-Thiophenyl	4.04	4.08	3.90	4.18
h	4-F_3C-Ph	4.15	4.08	4.20	4.26
i	Ph	4.08	4.04	4.08	4.08
j	2-Me-Ph	4.08	4.04	4.04	4.04
k	4-Me-Ph	4.00	4.04	4.04	4.04
l	2-MeO-Ph	4.04	4.08	4.08	4.15
m	4-MeO-Ph	3.95	4.08	4.08	4.15
n	2-Me_2N-Ph	3.95	3.78	3.95	4.04
o	4-Me_2N-Ph	4.00	4.11	4.11	4.15
p	Allyl	3.85	3.95	–	3.95

The measured emission data for the base system **7** showed minor red shifts for **7e**, **7g** and **7o** compared to **7i** (Table 6, Figure 2). Lower emission wavelengths were observed for **7b** and **7p**. Electron-rich and -poor systems in position R^1 seem to have only small effects on the emission wavelength. Therefore,

Table 6. Measured emission maxima for the base system **7**. Every measurement was performed using a 1 μM solution of the compound in chloroform at 25 °C in air. The extinction maxima of the specific compound was chosen as the excitation wavelength.

Nr.	R^2	R^1	Emission/nm	QY / %
7a	Ph	2-Pyridinyl	455	28.35
7b	Ph	2-Pyrimidinyl	447	33.23
7c	Ph	2-(5-Ph-Pyridinyl)	462	38.27
7d	Ph	2-Quinolinyl	463	34.24
7e	Ph	1-Isoquinolinyl	475	32.35
7f	Ph	3-Isoquinolinyl	462	35.83
7g	Ph	2-Thiophenyl	483	24.16
7h	Ph	4-F3 C-Ph	460	33.64
7i	Ph	Ph	464	36.16
7j	Ph	2-Me-Ph	462	20.58
7k	Ph	4-Me-Ph	465	33.07
7l	Ph	2-MeO-Ph	452	26.10
7m	Ph	4-MeO-Ph	467	33.58
7n	Ph	2-Me_2N-Ph	456	26.73
7o	Ph	4-Me_2N-Ph	475	33.94
7p	Ph	Allyl	430	27.31

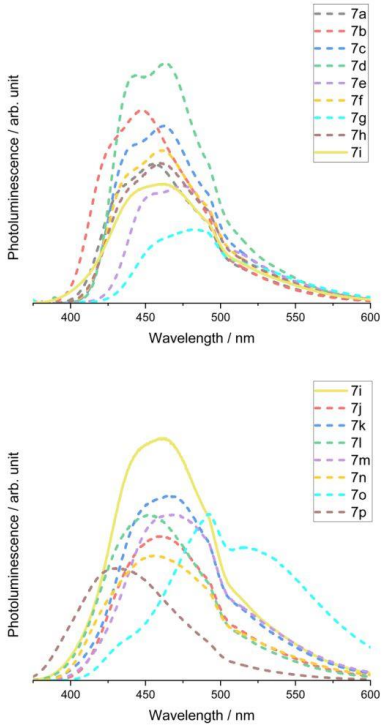

Figure 2. Photoluminescence spectra as 0.1 mM chloroform solution of electron-poor (top) and electron-rich substituted (bottom) base system **7**.

all of **7** displayed a strong blue emission around 450 nm. The QY of **7** was negatively affected by more sterically demanding substituents R^1. Compared to **7i** and their *para*-substituted equivalents, the *ortho*-substituted systems **7j**, **7l** and **7n** showed much lower QYs (Table 6). *N*-heteroaromatic substituents showed higher QYs, which could be increased by extension of their π-system (compare **7a** to **7c**) or introduction of more nitrogen centers (compare **7a** to **7b**). This presumably countered the negative steric effect of the R^1-substituent in **7d**, **7e** and **7f**. Thiophen **7g** and the non-conjugated allyl in **7p** decreased the QY significantly.

Table 7. Measured emission maxima in nm for all isolated products. Every measurement was performed using a 1 μM solution of the compound in chloroform at 25 °C in air. The extinction maxima of the specific compound was chosen as the excitation wavelength.

	R^1	R^2			
		Ph **7**	4-MeO-Ph **8**	4-F_3C-Ph **9**	2-Me-Ph **10**
a	2-Pyridinyl	455	462	457	441
b	2-Pyrimidinyl	447	458	445	428
c	2-(5-Ph-Pyridinyl)	462	468	461	449
d	2-Quinolinyl	463	456	461	452
e	1-Isoquinolinyl	475	–	–	466
f	3-Isoquinolinyl	462	464	463	448
g	2-Thiophenyl	483	477	485	473
h	4-F_3C-Ph	460	470	460	448
i	Ph	464	459	465	456
j	2-Me-Ph	462	453	459	454
k	4-Me-Ph	465	464	470	460
l	2-MeO-Ph	452	457	458	451
m	4-MeO-Ph	467	467	479	466
n	2-Me_2N-Ph	456	459	486	470
o	4-Me_2N-Ph	475	493	493	482
p	Allyl	430	437	–	442

Table 8. Calculated QYs in % for all measured systems.

	R^1	R^2			
		Ph **7**	4-MeO-Ph **8**	4-F_3C-Ph **9**	2-Me-Ph **10**
a	2-Pyridinyl	28.35	26.36	25.14	43.83
b	2-Pyrimidinyl	33.23	27.06	32.64	52.76
c	2-(5-Ph-Pyridinyl)	38.27	35.05	31.48	52.04
d	2-Quinolinyl	34.24	29.85	30.94	47.06
e	1-Isoquinolinyl	32.35	–	–	42.43
f	3-Isoquinolinyl	35.83	27.00	28.55	46.91
g	2-Thiophenyl	24.16	28.36	17.88	38.05
h	4-F_3C-Ph	33.64	31.92	23.19	47.41
i	Ph	36.16	37.82	19.47	41.58
j	2-Me-Ph	20.58	30.43	14.43	25.50
k	4-Me-Ph	33.07	37.67	17.38	46.43
l	2-MeO-Ph	26.10	27.89	15.54	28.89
m	4-MeO-Ph	33.58	35.83	16.19	41.63
n	2-Me_2N-Ph	26.73	18.25	15.27	33.17
o	4-Me_2N-Ph	33.94	23.02	16.40	27.69
p	Allyl	27.31	33.79	–	15.51

The trends of the base system **7** persisted for **8**–**10** (Table 7) and no radical changes of the spectra (Figure 2) could be observed. Comparing **7**–**9**, the measured emission wavelengths were similar. Only **10** showed slightly lower emission wavelengths. The R^2 substituent seems to have only a limited effect on the emission. In general, it is notable that the imidazo[1,5-*a*]quinolines maintained their blue luminescence. We expected a wide range of emission colors, as observed for the imidazo[1,5-*a*]pyridines measured by Shibahara *et al.*[18]

The trends for substitution in R^1 observed for the base system **7** were also observed for the other compounds (Table 8). The more electron-rich system **8** showed a slight reduction in QY for all substitutions. While the electron-poor system **9** also reduced the QY slightly for all electron-poor residues **9a**–**h**, it showed a significant decrease for the more electron-rich residues **9i**–**o**. The introduction of a sterically demanding group R^2 for system **10** led to a strong increase in QY, especially in combination with electron-poor residues **10a**–**h**. The nitrogen-rich pyrimidyl **10b** and the substituted pyridyl **10c** showed a very high QY of around 52%. **10o** underwent slow decomposition in solution. In addition, we obtained a much lower QY for this compound. Substitution with an electron-poor or -rich aromatic group in R^2 led to no significant impact. But the introduction of a sterically demanding group showed an impact on the photoluminescent properties. The combination with *N*-heteroaromatics or electron-poor substituents in R^1 increased the QY even further (Figure 3). *N*-heteroaromatic compounds have already shown this effect earlier.[14] We suspect that the planar orientation of all the π-systems leads to more orbital overlap and therefore better QYs. The substitution of a phenyl at R^1 for pyridinyl or pyrimidyl removes hydrogen in the *ortho* positions and could create more overlap with the aromatic core.

Conclusions

We were successful in designing an easy and reliable synthesis to obtain large numbers of imidazo[1,5-*a*]quinoline derivatives.

Figure 3. Demonstration of QY increase of compounds as 0.02 M DCM solution (left to right: **9j**, **7j**, **8d**, **7i**, **7c**, **10h**, **10b**).

The developed Negishi coupling conditions are widely applicable for various coupling partners. Optical measurements have identified that a combination of a sterically demanding group in R^2 and an electron-withdrawing group in R^1 is beneficial for the emission; especially electron-poor *N*-heteroaromatics improved the QY significantly, with **10b** showing a QY of 53% in solution. Electron-rich residues as R^1 lowered the emission, apart from dimethylamine-substituted residues. In addition, we showed that *ortho*-substituted residues as R^1 reduce the QY considerably.

Experimental Section

All solvents were purified by distillation prior to use. Anhydrous solvents were used from ACROS Organics™ as AcroSeal™ bottles. Commercially available chemicals were used as obtained from the supplier, unless otherwise stated. Syntheses prepared under anhydrous conditions were generally performed using standard Schlenk technique in nitrogen atmosphere. For purification by column chromatography, silica gel 60 (Merck) was used. ^{1}H and ^{13}C NMR spectra were recorded on the Bruker Avance II 400, the Bruker Avance III 400 and the Bruker Avance II 200 "Microbay" spectrometers in deuterated solvents. ^{1}H and ^{13}C chemical shifts were determined by reference to the residual solvent signals. High-resolution ESI mass spectra were recorded in methanol with an ESImicroTOF spectrometer from Bruker Daltonics in positive ion mode, unless otherwise stated. As a power supply, the Sky Toppower PS1110 was used. UV-Vis extinction was measured with an Analytik Jena Specord 200 Plus spectrometer and fluorescence emission data were obtained from a Jasco Germany FP 8300 spectrometer. Melting points were determined with a Gallenkamp Melting Point Apparatus.

General procedure for imidazole ring closure adapted from Pelletier et al.[11]

60 mL of dry DCM was added to 2-(aminomethyl)quinoline dihydrochloride **3** (1 eq) under N_2 atmosphere. The suspension was cooled to 0 °C and dry TEA (3.4 eq) was added. The yellow solution was kept at 0 °C for 30 min. Acid chloride R^2COCl (1.1 eq) was added, and the solution was stirred for 20 h at room temperature. Finally, 60 mL sat. Na_2CO_3 solution was added, and the aqueous phase was extracted twice with 60 mL DCM. The combined organic phases were dried over Na_2SO_4, filtered, and the solvent removed *in vacuo*. The crude quinoline amide **4** (1 eq) was placed in 60 mL of dry DCM under N_2 atmosphere and cooled to 0 °C. The solution was first treated with 2-methoxypyridine (1.1 eq), followed by slow addition of Tf_2O (1.2 eq). The reaction solution was stirred at 35 °C for 20 h. Then, 20 mL sat. Na_2CO_3 solution was added slowly, and the aqueous phase was extracted twice with 60 mL DCM. The combined organic phases were dried over Na_2SO_4, filtered and the solvent removed *in vacuo*. Purification was carried out by silica chromatography.

General procedure for bromination

The imidazo[1,5-*a*]quinoline **5** was placed in 60 mL dry DCM under N_2 atmosphere and cooled to −20 °C. 1.1 eq NBS was slowly added to the solution. The reaction solution was stirred at −20 °C for 4 h. Then, 20 ml sat. $Na_2S_2O_3$ solution was added and the aqueous phase extracted twice with 40 mL DCM. The combined organic phases were dried over Na_2SO_4, filtered, and the solvent removed *in vacuo*. Purification was carried out by silica chromatography.

General procedure methods for the Negishi coupling

0.400 g (1 eq) 3-bromoimidazo[1,5-*a*]quinoline **6** was dissolved in 10 mL dry THF under N_2 atmosphere and cooled to −78 °C. 1.2 eq of *n*-BuLi (1.6 M) were slowly added dropwise and the solution was kept at −78 °C for 30 min. 2.5 eq $ZnCl_2$ in dry THF (1 M) were added at −78 °C and then stirred at room temperature for 1 h. 3 mol% of $[Pd_2(dba)_3]\cdot CHCl_3$, 6 mol% of $P(t\text{-}Bu)_3$ and 2 eq of the chosen coupling bromide were added and the reaction solution was stirred at 70 °C for 20 h. Depending on the compound, two different methods for workup were applied.

Method A for **7**–**10a**–**f**:

The precipitate was filtered off and washed first with THF, then with H_2O and again with THF. The solid was treated with 15 mL conc. $NH_{3(aq)}$ solution and the aqueous phase was extracted three times with 20 mL DCM. The pure product was obtained after concentration *in vacuo* of the combined organic phases.

Method B for **7**–**10g**–**p**:

15 mL conc. $NH_{3(aq)}$ solution was added and the aqueous phase was extracted three times with 20 mL DCM. The combined organic phases were concentrated *in vacuo* and the impure product was purified by silica chromatography.

Supporting Information

Experimental procedures, optical values and spectra for all measured compounds and analytical data of all compounds are provided in the online Supporting Information. Additional references cited within the Supporting Information (Ref. [24]).

Acknowledgements

Open Access funding enabled and organized by Projekt DEAL.

Conflict of Interests

The authors declare no conflict of interest.

Data Availability Statement

The data that support the findings of this study are available in the supplementary material of this article.

Keywords: emitter material · imidazo[1,5-*a*]quinolines · Negishi coupling · nitrogen heterocycles · photoluminescence

[1] C. W. Tang, S. A. VanSlyke, *Appl. Phys. Lett.* **1987**, *51*, 913–915.
[2] a) C. Adachi, M. A. Baldo, S. R. Forrest, S. Lamansky, M. E. Thompson, R. C. Kwong, *Appl. Phys. Lett.* **2001**, *78*, 1622–1624; b) C.-L. Ho, H. Li, W.-Y. Wong, *J. Organomet. Chem.* **2014**, *751*, 261–285; c) H. Nakanotani, T. Higuchi, T. Furukawa, K. Masui, K. Morimoto, M. Numata, H. Tanaka, Y. Sagara, T. Yasuda, C. Adachi, *Nat. Commun.* **2014**, *5*, 4016.
[3] N. C. Giebink, B. W. D'Andrade, M. S. Weaver, P. B. Mackenzie, J. J. Brown, M. E. Thompson, S. R. Forrest, *J. Appl. Phys.* **2008**, *103*, 44509.

[4] a) M. S. Malamas, Y. Ni, J. Erdei, H. Stange, R. Schindler, H.-J. Lankau, C. Grunwald, K. Y. Fan, K. Parris, B. Langen, U. Egerland, T. Hage, K. L. Marquis, S. Grauer, J. Brennan, R. Navarra, R. Graf, B. L. Harrison, A. Robichaud, T. Kronbach, M. N. Pangalos, N. Hoefgen, N. J. Brandon, *J. Med. Chem.* **2011**, *54*, 7621–7638; b) A. Kamal, G. Ramakrishna, P. Raju, A. V. S. Rao, A. Viswanath, V. L. Nayak, S. Ramakrishna, *Eur. J. Med. Chem.* **2011**, *46*, 2427–2435; c) D. Kim, L. Wang, J. J. Hale, C. L. Lynch, R. J. Budhu, M. Maccoss, S. G. Mills, L. Malkowitz, S. L. Gould, J. A. DeMartino, M. S. Springer, D. Hazuda, M. Miller, J. Kessler, R. C. Hrin, G. Carver, A. Carella, K. Henry, J. Lineberger, W. A. Schleif, E. A. Emini, *Bioorg. Med. Chem. Lett.* **2005**, *15*, 2129–2134.

[5] a) F. Shibahara, R. Sugiura, E. Yamaguchi, A. Kitagawa, T. Murai, *J. Org. Chem.* **2009**, *74*, 3566–3568; b) G. Volpi, G. Magnano, I. Benesperi, D. Saccone, E. Priola, V. Gianotti, M. Milanesio, E. Conterosito, C. Barolo, G. Viscardi, *Dyes Pigm.* **2017**, *137*, 152–164; c) E. Yamaguchi, F. Shibahara, T. Murai, *J. Org. Chem.* **2011**, *76*, 6146–6158; d) G. Volpi, B. Lace, C. Garino, E. Priola, E. Artuso, P. Cerreia Vioglio, C. Barolo, A. Fin, A. Genre, C. Prandi, *Dyes Pigm.* **2018**, *157*, 298–304.

[6] a) F. Yagishita, T. Kinouchi, K. Hoshi, Y. Tezuka, Y. Jibu, T. Karatsu, N. Uemura, Y. Yoshida, T. Mino, M. Sakamoto, Y. Kawamura, *Tetrahedron* **2018**, *74*, 3728–3733; b) G. A. Ardizzoia, G. Colombo, B. Therrien, S. Brenna, *Ber. Dtsch. Chem. Ges. A* **2019**, *2019*, 1825–1831; c) S. Durini, G. A. Ardizzoia, B. Therrien, S. Brenna, *New J. Chem.* **2017**, *41*, 3006–3014; d) C. Garino, T. Ruiu, L. Salassa, A. Albertino, G. Volpi, C. Nervi, R. Gobetto, K. I. Hardcastle, *Ber. Dtsch. Chem. Ges. A* **2008**, *2008*, 3587–3591; e) L. Salassa, C. Garino, A. Albertino, G. Volpi, C. Nervi, R. Gobetto, K. I. Hardcastle, *Organometallics* **2008**, *27*, 1427–1435.

[7] M. D. Weber, C. Garino, G. Volpi, E. Casamassa, M. Milanesio, C. Barolo, R. D. Costa, *Dalton Trans.* **2016**, *45*, 8984–8993.

[8] a) J. Wang, L. Dyers, R. Mason, P. Amoyaw, X. R. Bu, *J. Org. Chem.* **2005**, *70*, 2353–2356; b) M. Li, Y. Xie, Y. Ye, Y. Zou, H. Jiang, W. Zeng, *Org. Lett.* **2014**, *16*, 6232–6235; c) Z. Hu, J. Hou, J. Liu, W. Yu, J. Chang, *Org. Biomol. Chem.* **2018**, *16*, 5653–5660; d) S. Chandrasekar, S. Sangeetha, G. Sekar, *ChemistrySelect* **2019**, *4*, 5651–5655; e) A. Joshi, D. C. Mohan, S. Adimurthy, *J. Org. Chem.* **2016**, *81*, 9461–9469.

[9] M. Giordano, G. Volpi, C. Garino, F. Cardano, C. Barolo, G. Viscardi, A. Fin, *Dyes Pigm.* **2023**, *218*, 111482.

[10] J. D. Bower, G. R. Ramage, *J. Chem. Soc.* **1955**, 2834.

[11] G. Pelletier, A. B. Charette, *Org. Lett.* **2013**, *15*, 2290–2293.

[12] a) H. Wang, W. Xu, L. Xin, W. Liu, Z. Wang, K. Xu, *J. Org. Chem.* **2016**, *81*, 3681–3687; b) H. Wang, W. Xu, Z. Wang, L. Yu, K. Xu, *J. Org. Chem.* **2015**, *80*, 2431–2435.

[13] Z. Li, S.-S. Wu, Z.-G. Luo, W.-K. Liu, C.-T. Feng, S.-T. Ma, *J. Org. Chem.* **2016**, *81*, 4386–4392.

[14] G. Albrecht, C. Rössiger, J. M. Herr, H. Locke, H. Yanagi, R. Göttlich, D. Schlettwein, *Phys. Status Solidi B* **2020**, *257*, 1900677.

[15] J. M. Herr, C. Rössiger, H. Locke, M. Wilhelm, J. Becker, W. Heimbrodt, D. Schlettwein, R. Göttlich, *Dyes Pigm.* **2020**, *180*, 108512.

[16] G. Albrecht, C. Geis, J. M. Herr, J. Ruhl, R. Göttlich, D. Schlettwein, *Org. Electron.* **2019**, *65*, 321–326.

[17] a) M. Henze, *Ber. Dtsch. Chem. Ges. A* **1936**, *69*, 1566–1568; b) K. C. Langry, *Org. Prep. Proced. Int.* **1994**, *26*, 429–438.

[18] F. Shibahara, E. Yamaguchi, A. Kitagawa, A. Imai, T. Murai, *Tetrahedron* **2009**, *65*, 5062–5073.

[19] a) M. Sandeep, P. Swati Dushyant, B. Sravani, K. Rajender Reddy, *Eur. J. Org. Chem.* **2018**, *2018*, 3036–3047; b) Z. Tan, H. Zhao, C. Zhou, H. Jiang, M. Zhang, *J. Org. Chem.* **2016**, *81*, 9939–9946.

[20] a) E. Tyrrell, P. Brookes, *Synthesis* **2003**, *2003*, 469–483; b) M. Hapke, L. Brandt, A. Lützen, *Chem. Soc. Rev.* **2008**, *37*, 2782–2797; c) L.-C. Campeau, K. Fagnou, *Chem. Soc. Rev.* **2007**, *36*, 1058–1068.

[21] J. E. Milne, S. L. Buchwald, *J. Am. Chem. Soc.* **2004**, *126*, 13028–13032.

[22] D. F. Eaton, *Pure Appl. Chem.* **1988**, *60*, 1107–1114.

[23] A. M. Brouwer, *Pure Appl. Chem.* **2011**, *83*, 2213–2228.

[24] a) J. R. Quinn, S. C. Zimmerman, *J. Org. Chem.* **2005**, *70*, 7459–7467; b) P. Qian, Z. Yan, Z. Zhou, K. Hu, J. Wang, Z. Li, Z. Zha, Z. Wang, *Org. Lett.* **2018**, *20*, 6359–6363.

Manuscript received: October 2, 2023
Revised manuscript received: November 21, 2023
Accepted manuscript online: November 22, 2023
Version of record online: December 19, 2023

6.2 Design, synthesis and antimycobacterial activity of Imidazo[1,5-*a*]quinolines and their Zinc-complexes

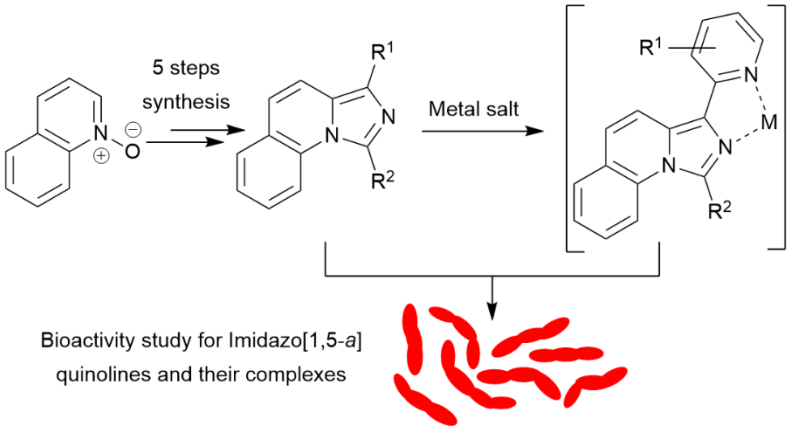

In this study, we report the novel bioactivity of imidazo[1,5-*a*]quinolines and their complexes against *Mycobacterium tuberculosis Mtb*.

Reference

M. Marner, N. Kulhanek, J. Eichberg, K. Hardes, M. D. Molin, J. Rybniker, M. Kirchner, T. F. Schäberle and R. Göttlich, *RSC Med. Chem*., 2024, **15**, 1746–1750. (DOI: 10.1039/D4MD00086B)

Michael Marner and Niclas Kulhanek contributed equally to this work.

RSC Medicinal Chemistry

ROYAL SOCIETY OF CHEMISTRY

RESEARCH ARTICLE

View Article Online
View Journal | View Issue

Cite this: *RSC Med. Chem.*, 2024, **15**, 1746

Design, synthesis and antimycobacterial activity of imidazo[1,5-*a*]quinolines and their zinc-complexes†

Michael Marner, ‡[a] Niclas Kulhanek,‡[b] Johanna Eichberg,[ah] Kornelia Hardes,[ah] Michael Dal Molin,[ef] Jan Rybniker,[efg] Michael Kirchner,[b] Till F. Schäberle [acd] and Richard Göttlich *[b]

Received 2nd February 2024,
Accepted 10th March 2024

DOI: 10.1039/d4md00086b

rsc.li/medchem

Tuberculosis has remained one of the world's deadliest infectious diseases. The complexity and numerous adverse effects of current treatment options as well as the emergence of multi-drug resistant *M. tuberculosis* (Mtb) demand research and innovation efforts to yield new anti-mycobacterial agents. In this study, we synthesized a series of imidazo[1,5-*a*]quinolines, including 4 new analogs, and evaluated their activity against Mtb. Inspired by previous studies, we also designed 8 compounds featuring a coordinated metal ion, determined their absolute configuration by single-crystal X-ray diffraction and included them in the bioactivity study. Remarkably, the metal complexation of **5c** with either Zn^{2+} or Fe^{2+} increased the Mtb inhibitory activity of the compound 12.5-fold and reduced its cytotoxicity. Ultimately, out of the 21 analyzed imidazo[1,5-*a*]quinoline analogs, two zinc complexes (**C1** and **C7**) showed the strongest, specific activity against Mtb H37Rv *in vitro* (IC_{90} = 7.7 and 17.7 μM).

Introduction

Tuberculosis (TB) is a communicable infectious disease caused by *Mycobacterium tuberculosis* (Mtb). Despite global efforts, TB remains one of the world's deadliest killers of the past two decades.[1–3] In 2023, the World Health Organization (WHO) reported 10.6 million new cases and 1.3 million deaths caused by TB.[4] In addition, the COVID-19 pandemic is considered to have erased the progress made in the years up to 2019.[5,6] The net reduction of the TB incidence from 2015 to 2022 was only 8.7%, missing the important key milestone of the WHO *End TB Strategy* by far (50% reduction until 2025).

Recommended treatment regimens for drug-sensitive Mtb are long and complex (high doses of 4 antibiotics over 4 to 6 months or longer).[7,8] Non-compliance, *e.g.* misused or mismanaged antibiotic therapy, facilitates the emergence and spread of rifampicin-resistant TB, multidrug-resistant TB and even extensively drug-resistant TB (RR-TB/MDR-TB/XDR-TB). In 2021, the number of MDR-TB cases increased to 450 000. Chemotherapy against MDR-TB and XDR-TB is even

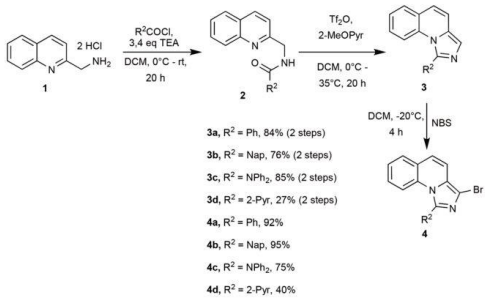

Scheme 1 General synthesis route and isolated yields.

[a] *Fraunhofer-Institute for Molecular Biology and Applied Ecology (IME) Branch Bioresources, Ohlebergsweg 12, 35392 Giessen, Germany*
[b] *Institute of Organic Chemistry, Justus-Liebig-University, Heinrich-Buff-Ring 17, Giessen 35392, Germany*
[c] *Institute for Insect Biotechnology, Justus-Liebig-University Giessen, Ohlebergsweg 12, 35392, Giessen, Germany*
[d] *German Center for Infection Research (DZIF), Partner Site Giessen-Marburg-Langen, Ohlebergsweg 12, 35392 Giessen, Germany*
[e] *Department I of Internal Medicine, University of Cologne, 50937 Cologne, Germany*
[f] *Center for Molecular Medicine Cologne (CMMC), University of Cologne, 50931 Cologne, Germany*
[g] *German Center for Infection Research (DZIF), Partner Site Bonn-Cologne, Cologne, Germany*
[h] *BMBF Junior Research Group in Infection Research "ASCRIBE", Branch for Bioresources of the Fraunhofer Institute for Molecular Biology and Applied Ecology IME, Ohlebergsweg 12, 35392 Giessen, Germany*

† Electronic supplementary information (ESI) available: General procedures, material and methods. CCDC 2284388, 2284389 and 2284387. For ESI and crystallographic data in CIF or other electronic format see DOI: **https://doi.org/10.1039/d4md00086b**

‡ The authors contributed equally.

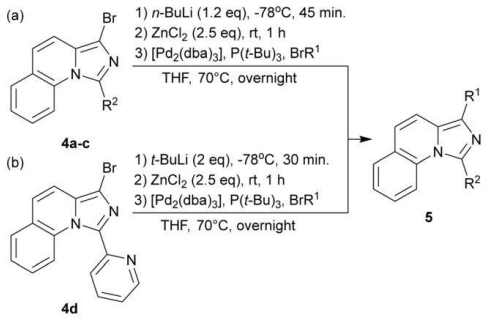

Scheme 2 Employed coupling strategies for the final products.

Table 1 Yields for Negishi coupling

Number	R^2	R^1	Isolated product/%
5a[a]	Ph	2-Thiophenyl	58
5b[a]	Ph	Ph	84
5c[a]	Ph	2-Pyridinyl	73
5d[a]	Ph	2-Quinolinyl	79
5e[b]	Ph	2-Pyrimidinyl	60
5f[b]	Ph	2-(5-Ph-Pyridinyl)	70
5g[b]	Ph	3-Isoquinolinyl	79
5h[a]	Ph	2-Me_2N-Ph	40
5i[a]	Ph	2-MeO-Ph	84
6a[c]	2-Pyridyl	2-Pyridinyl	26
6b[c]	2-Pyridyl	Ph	39
7a[a]	Nap	2-Pyridinyl	68
8a[a]	NPh_2	2-Pyridinyl	66

Reaction conditions: [a] Conditions shown in Scheme 2a. [b] conditions shown in Scheme 2a, products were isolated as hydrochloride salts. [c] conditions shown in Scheme 2b.

more complicated, and the clinical outcome is generally poor.[5] Therefore, continuous research and innovation towards new and improved TB active agents is of great importance. A promising approach to improve the potency of anti-mycobacterial agents is their combination with further antimicrobial molecules.

Transition metals, such as zinc (Zn^{2+}), are involved in many physiological processes and are appreciated for their pharmaceutical potential. As part of the innate immune response towards pathogens, macrophages can deploy phagosomal zinc intoxication defence mechanisms.[9] Antibacterial,[10–12] antifungal[13] and antiparasitic[14,15] features of metal-drug complexes have been observed in many studies.

Sonawane *et al.* demonstrated that the activity of rifampicin could be increased by complexing it with Zn^{2+} and encapsulating it into transferrin-conjugated silver quantum dots.[16] In addition, other metal complexes with Cu^{2+} and $V^{5+/4+}$ showed good anti-mycobacterial activity, highlighting the potential use of complexes in TB treatment.[17,18]

In this early discovery study, we set out to design, synthesize and evaluate the *in vitro* activity of imidazo[1,5-*a*] quinolines. Compounds featuring this core motif have already been reported to exhibit diverse biological activities.[19–21] However, these scaffolds were never evaluated for their potency towards Mtb. Hence, in the first step, we expanded a set of literature-known imidazo[1,5-*a*]quinolines (**5a–i**)[22] with four new structures (**6a**, **6b**, **7a**, and **8a**) by diversifying substitutions at R^1 and R^2. The substitution of the imidazole ring was selected based on its synthetic feasibility and reaction yield. Next, we prepared metal complexes of the most intriguing compounds and evaluated their antimycobacterial activity.

Results and discussion

Synthesis and crystal structures

We employed our versatile synthetic route reported in an earlier publication (Scheme 1).[22] Here, we introduced R^2 over an Einhorn acylation and established the imidazo ring system by nucleophilic substitution. **3a–d** was then selectively brominated with *N*-bromosuccinimide at −20 °C.

Table 2 General procedure of the complexation reaction and molecular formula of synthesised complexes with yields

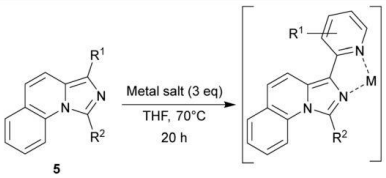

Number	Ligand	Metal salt	Molecular formular	Isolated product/%
C1	**5c**	$ZnCl_2$	[$ZnCl_2$**5c**]	95
C2	**5c**	$FeCl_3$	[$FeCl_2$(**5c**)$_2$]$FeCl_4$	97
C3	**5c**	$Cu(OAc)_2$	[$Cu(OAc)_2$**5c**]	98
C4	**7a**	$ZnCl_2$	[$ZnCl_2$**7a**]	44
C5	**5e**	$ZnCl_2$	[$ZnCl_2$**5e**]	40
C6	**5f**	$ZnCl_2$	[$ZnCl_2$**5f**]	64
C7	**5g**	$ZnCl_2$	[$ZnCl_2$**5g**]	74
C8	**8a**	$ZnCl_2$	[$ZnCl_2$**8a**]	64

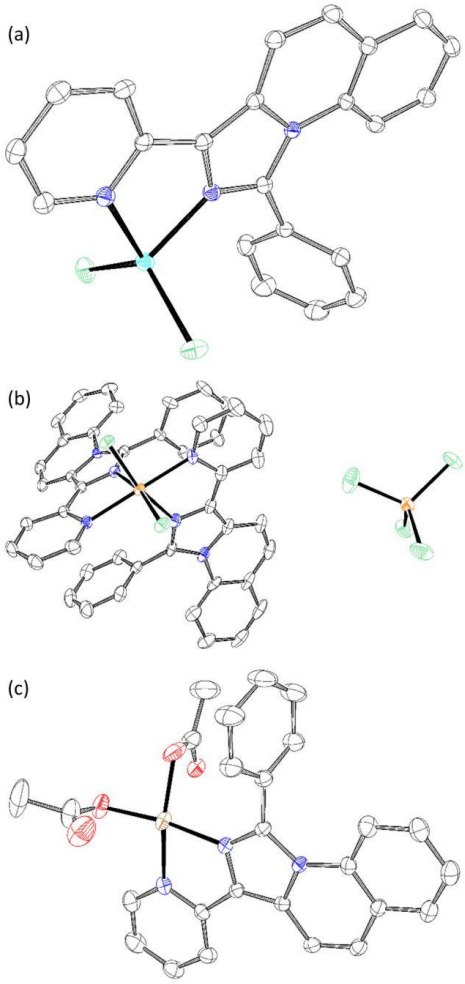

Scheme 3 Crystal structures for (a) **C1**, (b) **C2**, and (c) **C3**. Analysed by XRD measurements, solved with ShelXL and visualized with ORTEP-3. Hydrogen atoms are hidden for better visibility (white = carbon, blue = nitrogen, red = oxygen, green = chlorine, cyan = zinc, orange = iron and brown = copper).

Bromides (**4a–c**) were transmetalated with *n*-BuLi and $ZnCl_2$ by Negishi coupling (Scheme 2a). The excess of $ZnCl_2$ in the solution led to the formation of bidentate Zn complexes. The transmetalation with *n*-BuLi resulted in the alkylation of the nitrogen within the pyridine moity of **4d**, forming *n*-butylbromide. We eliminated the presence of halogenoalkanes in the solution using 2 eq. of *t*-BuLi (Scheme 2b).

The majority of products were isolated in good yields of 58–84%. **6a–b** and **5h** were isolated in lower yields even with the improved reaction conditions. We observed a high percentage of **3d** – an effect that we could not prevent even by longer reaction time or elevated temperature. The ligand character of **3** might have inhibited the activity of the Pd-catalyst. Similarly, the +M-substituent in the R^1 position of **5h** might have resulted in a deactivating chelating effect. **5e–5g** was converted into their hydrochloride salts to improve their solubility in water (Table 1).

Chelation was performed with the listed ligands (Table 2) in THF. Besides Zn, compound **5c** was also combined with $FeCl_3$ and $Cu(OAc)_2$. The structures of **C1** (Scheme 3a), **C2** (Scheme 3b) and **C3** (Scheme 3c) were analysed by XRD from single crystals. The M^{2+}-central atoms showed square planar orientation. **C2** formed an octahedral complex by the displacement of chloride, resulting in a charged complex and, thus, good solvability in water. However, the solubility of the complexes also influenced the isolation yield. The most soluble complexes (**C4–8**) were retrieved in poor yields

Table 3 Minimum inhibitory concentration (MIC) of investigated imidazo[1,5-*a*]quinolines. Ec: *Escherichia coli* ATCC35218, Sa: *Staphylococcus aureus* ATCC33592; Str: *Septoria tritici* MUCL45408, Mtb: *Mycobacterium tuberculosis* H37Ra; MICs given in μM. Calu-3: epithelia cell line from lung carcinoma, "—" indicates no effect at 100μM and "+" toxic effects at 100 μM

Number	Ec	Sa	Str	Mtb	Calu-3
5a	>196	>196	>196	>196	—
5b	>200	>200	>200	>200	—
5c	>199	>199	>199	25	+
5d	>172	>172	>172	86–43	—
5e	>148	>148	>148	1	+
5f	>136	>136	>136	34	—
5g	>144	>144	>144	1–0.5	—
5h	>127	>127	>127	2	+
5i	>183	>183	>183	46	—
6a	>198	>198	>198	12–6	—
6b	>199	>199	>199	50–25	+
7a	>172	>172	>172	5–1	+
8a	>155	>155	>155	>155	—
C1	>140	>140	>140	2	—
C2	>132	>132	>132	2	—
C3	>127	>127	16–8	2	+
C4	> 126	31.5	63	2–1	+
C5	>140	17–9	17	2–1	+
C6	>120	>120	>120	8	—
C7	>126	126	126	2–1	—
C8	>117	>117	>117	>117	—

Table 4 $IC_{50/90}$ values of prioritized compounds against BSL-3 *M. tuberculosis* ATCC 35801. Prioritization was based on primary antimicrobial screening results. Values are given in μM

	Mtb ATCC 35801			HepG2
Number	Inhibition at 20 μM	IC_{50}	IC_{90}	IC_{50}
5g	82%	86.5	136.2	>100
C1	90%	6	7.7	>100
C2	26%	n.d.	n.d.	n.d.
C7	n.d.	9.1	17.7	83.3

after the washing step. The data evaluation is provided in the supplementary information.

Antimycobacterial activity

The antimicrobial effect of the 21 synthesized compounds was initially accessed against a panel of 4 microbial indicator strains (*Escherichia coli* ATCC35218, *Staphylococcus aureus* ATCC33592, *Septoria tritici* MUCL45408 and *Mycobacterium tuberculosis* H37Ra). Cytotoxicity was investigated using an epithelia cell line from human lung carcinoma (Calu-3). The results are summarized in Tables 3 and S1.†

From the investigated compounds, 13 showed no cytotoxicity at a high dose of 100 μM. Simultaneously, 4 (**5g**, **C1**, **C2**, **C7**) of the non-toxic compounds exhibited an intriguing MIC of ≤2 μM against our surrogate Mtb strain H37Ra. These values are in range or only slightly higher than MICs of the reference drugs used in this study (MIC of gentamicin against H37Ra = 4 μM and MIC of rifampicin 0.07 μM; see Table S1 in ESI†) and literature reported values against various Mtb strains (*e.g.* isoniazid = 0.3–1.4 μM; levofloxacin = 0.8–1.4 μM, amikacin = 0.4–1.7 μM, bendaquiline = 0.03–1 μM, ethambutol = 0.3–3 μM or ethionamide = 10 μM).[23–26]

Interestingly, the low antimycobacterial activity of **5c** against H37Ra (25 μM) could be potentiated by a factor of 12.5 by complexation with either Zn^{2+} (**C1**), $Fe3^{+}$ (**C2**) or $Cu2^{+}$ (**C3**). Although the copper-acetate complex maintained the initially observed cytotoxic properties of **5c**, we observed no toxicity of the Zn^{2+} and Fe^{3+} complexes towards the Calu-3 lung carcinoma cell line at 100 μM.

The inhibitory effects of **5g**, **C1**, **C2**, and **C7** were specifically observed against Mtb, while the other test strains were not affected. These 4 compounds were then screened in a second-tier assay against wild-type *Mycobacterium tuberculosis* strain ATCC 35801. After activity confirmation at a high dose of 20 μM, the MIC values were determined. Cytotoxicity was also revaluated in the human liver cancer cell line HepG2 (Table 4, Fig. S1–S6†).

Although the promising activity of **C1** against H37Ra could be transferred to the wild-type strain ATCC 35801 ($IC_{50/90}$ = 6/7.7 μM), **C2** showed no growth inhibitory effects against this strain. Similarly, the initially promising growth inhibitory activity of **5g** against the Mtb surrogate (1 μM) could not be transferred to the virulent Mtb strain ($IC_{50/90}$ = 86.5/132.2 μM), but the potency was strongly increased ($IC_{50/90}$ = 9.14/17.72 μM) upon Zn^{2+} complexation (**C7**). The other designed imidazo[1,5-*a*]quinoline-Zn^{2+} complexes were either cytotoxic (**C4**–**C5**) or inactive (**C6**, **C8**).

Conclusions

In summary, we synthesized a series of 21 imidazo[1,5-*a*] quinolines and screened them against the surrogate strain *M. tuberculosis* HR37a, as well as against *Escherichia coli, Staphylococcus aureus,* the fungal plant pathogen *Septoria tritici* and lung carcinoma cell line Calu-3. Inspired by previous reports, we also decided to include metal-chelated variants in the compound series. To the best of our knowledge, the present study is the first to describe the antimycobacterial effects of imidazo[1,5-*a*]quinolines. Interestingly, the initially moderate antimycobacterial activity of **5c** against H37Ra (25 μM) could be potentiated by a factor of 12.5 by complexation with either Zn^{2+} or Fe^{2+}, while the cytotoxic effect was reduced (>100 μM).

Besides compounds **C1** and **C2**, two additional compounds (**5g** and **C7**) exhibited specific HR37a activity (<2 μM) and were therefore followed up in a second-tier assay against BSL-3 *Mycobacterium tuberculosis* ATCC 35801. Ultimately, we identified two zinc complexes **C1** and **C7**, with intriguing anti-tuberculosis activity and low cytotoxicity. Although these compounds surfaced from a relatively small derivative library, their *in vitro* potency was comparable to that of developed Mtb drugs. However, the major challenge regarding TB is the treatment of multi-drug resistant forms of the disease for which currently available drugs are not effective.[27] Hence, it would be of interest to profile our candidates against RR-TB, MDR-TB and XDR-TB strains. Additional work investigating the mode of action, frequency of resistance, cross resistance, collateral susceptibility effects as well as ADME Tox properties of target compounds is crucial to evaluate their clinical potential.

Author contributions

M. Marner performed the biological studies and prepared the draft. N. Kulhanek performed the synthesis and analytics and prepared the draft. N. Kulhanek and M. Marner contributed equally to this publication. Johanna Eichberg performed cytotoxicity analysis and Michael Dal Molin conducted BSL-3 work. M. Kirchner analysed and solved the XRD data.

Conflicts of interest

There are no conflicts to declare.

Acknowledgements

The authors would like to thank K. S. Bommersheim for her technical support during the MIC determinations. The work in the Schäberle lab was supported by the State Ministry of Higher Education, Research and Arts of the state Hessen through the LOEWE program for the Center for Insect Biotechnology and Bioresources and by the German Center for Infection Research. The work in the Junior Research Group in Infection Research "ASCRIBE" of K. Hardes was supported by the Federal Ministry of Education and Research (BMBF).

References

1 T. M. Daniel, J. H. Bates and K. A. Downes, in *Tuberculosis*, ed. B. R. Bloom, ASM Press, Washington, D. C, 1994, pp. 13–24.

2 I. Barberis, N. L. Bragazzi, L. Galluzzo and M. Martini, *J. Prev. Med. Hyg.*, 2017, **58**, E9–E12.
3 T. Paulson, *Nature*, 2013, **502**, S2–S3.
4 World Health Organization, *Global Tuberculosis Report 2023*, WHO, Geneva, 2023, **https://www.who.int/teams/global-tuberculosis-programme/tb-reports/global-tuberculosis-report-2023**, (accessed 19 February 2024).
5 World Health Organization, *Global Tuberculosis Report 2022*, WHO, Geneva, 2022, **https://www.who.int/teams/global-tuberculosis-programme/tb-reports/global-tuberculosis-report-2022**, (accessed 9 October 2023).
6 C. F. McQuaid, A. Vassall, T. Cohen, K. Fiekert and R. G. White, *Int. J. Tuberc. Lung. Dis.*, 2021, **25**, 436–446.
7 Centers for Disease Control and Prevention (CDC), *Treatment for TB Disease*, USA, 2023, **https://www.cdc.gov/tb/topic/treatment/tbdisease.htm**, (accessed 9 October 2023).
8 National Health Service (NHS), *Clinical Commissioning Policy Statement: Treatment for defined patients with MDR-TB and XDR-TB including bedaquiline and delamanid*, England, 2019, **https://www.england.nhs.uk/commissioning/wp-content/uploads/sites/12/2019/07/clinical-commissioning-policy-statement-treatment-for-defined-patients-with-mdr-tb-and-xdr-updated-dec-20.pdf**, (accessed 9 October 2023).
9 C. J. Stocks, J. B. von Pein, J. E. B. Curson, J. Rae, M.-D. Phan, D. Foo, N. J. Bokil, T. Kambe, K. M. Peters, R. G. Parton, M. A. Schembri, R. Kapetanovic and M. J. Sweet, *J. Leukocyte Biol.*, 2021, **109**, 287–297.
10 S. Hayet, M. Ghrayeb, D. N. Azulay, Z. Shpilt, E. Y. Tshuva and L. Chai, *RSC Med. Chem.*, 2023, **14**, 983–991.
11 T. Damena, D. Zeleke, T. Desalegn, T. B. Demissie and R. Eswaramoorthy, *ACS Omega*, 2022, **7**, 4389–4404.
12 B. Duffy, C. Schwietert, A. France, N. Mann, K. Culbertson, B. Harmon and J. P. McCue, *Biol. Trace Elem. Res.*, 1998, **64**, 197–213.
13 Z. H. Chohan, H. Pervez, A. Rauf, K. M. Khan and C. T. Supuran, *J. Enzyme Inhib. Med. Chem.*, 2004, **19**, 417–423.
14 J. A. de Azevedo-França, R. Granado, S. T. de Macedo Silva, G. D. Santos-Silva, S. Scapin, L. P. Borba-Santos, S. Rozental, W. de Souza, É. S. Martins-Duarte, E. Barrias, J. C. F. Rodrigues and M. Navarro, *Antimicrob. Agents Chemother.*, 2020, **64**(5), DOI: **10.1128/aac.01980-19**.
15 T. J. Hubin, P. N.-A. Amoyaw, K. D. Roewe, N. C. Simpson, R. D. Maples, T. N. Carder Freeman, A. N. Cain, J. G. Le, S. J. Archibald, S. I. Khan, B. L. Tekwani and M. O. F. Khan, *Bioorg. Med. Chem.*, 2014, **22**, 3239–3244.
16 R. Pati, R. Sahu, J. Panda and A. Sonawane, *Sci. Rep.*, 2016, **6**, 24184.
17 D. A. Paixão, I. M. Marzano, E. H. L. Jaimes, M. Pivatto, D. L. Campos, F. R. Pavan, V. M. Deflon, P. I. S. Da Maia, A. M. Da Costa Ferreira, I. A. Uehara, M. J. B. Silva, F. V. Botelho, E. C. Pereira-Maia, S. Guilardi and W. Guerra, *J. Inorg. Biochem.*, 2017, **172**, 138–146.
18 I. Correia, P. Adão, S. Roy, M. Wahba, C. Matos, M. R. Maurya, F. Marques, F. R. Pavan, C. Q. F. Leite, F. Avecilla and J. Costa Pessoa, *J. Inorg. Biochem.*, 2014, **141**, 83–93.
19 A. Cappelli, M. Anzini, F. Castriconi, G. Grisci, M. Paolino, C. Braile, S. Valenti, G. Giuliani, S. Vomero, A. Di Capua, L. Betti, G. Giannaccini, A. Lucacchini, C. Ghelardini, L. Di Cesare Mannelli, M. Frosini, L. Ricci, G. Giorgi, M. P. Mascia and G. Biggio, *J. Med. Chem.*, 2016, **59**, 3353–3372.
20 D. C. Mungra, M. P. Patel and R. G. Patel, *Med. Chem. Res.*, 2011, **20**, 782–789.
21 V. Srinivasulu, M. Khanfar, H. A. Omar, R. ElAwady, S. M. Sieburth, A. Sebastian, D. M. Zaher, F. Al-Marzooq, F. Hersi and T. H. Al-Tel, *J. Org. Chem.*, 2019, **84**, 14476–14486.
22 N. Kulhanek, N. Martin and R. Göttlich, *Eur. J. Org. Chem.*, 2024, **27**(1), DOI: **10.1002/ejoc.202301007**.
23 K. Kaniga, D. M. Cirillo, S. Hoffner, N. A. Ismail, D. Kaur, N. Lounis, B. Metchock, G. E. Pfyffer and A. Venter, *J. Clin. Microbiol.*, 2016, **54**, 2956–2962.
24 M. T. Heinrichs, R. J. May, F. Heider, T. Reimers, S. K. B. Sy, C. A. Peloquin and H. Derendorf, *Int. J. Mycobact.*, 2018, **7**, 156–161.
25 N. J. E. Waller, C.-Y. Cheung, G. M. Cook and M. B. McNeil, *Nat. Commun.*, 2023, **14**, 1517.
26 T. Schön, J. Werngren, D. Machado, E. Borroni, M. Wijkander, G. Lina, J. Mouton, E. Matuschek, G. Kahlmeter, C. Giske, M. Santin, D. M. Cirillo, M. Viveiros and E. Cambau, *Clin. Microbiol. Infect.*, 2020, **26**, 1488–1492.
27 I. Barilar, T. Fernando, C. Utpatel, C. Abujate, C. M. Madeira, B. José, C. Mutaquiha, K. Kranzer, T. Niemann, N. Ismael, L. de Araujo, T. Wirth, S. Niemann and S. Viegas, *Lancet Infect. Dis.*, 2024, **24**, 297–307.

6.3 Characterization and Optimization of the Photoluminescent Properties of Imidazo[1,5-*a*]quinolines

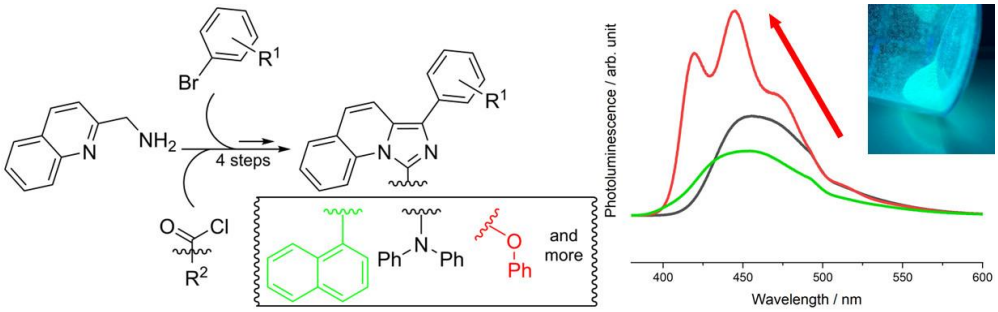

In this work, we have investigated the relationship between imidazole ring substitution in the R^2-position and the blue photoluminescent properties of imidazo[1,5-*a*]quinolines in more detail. For this purpose, a four-step synthesis was implemented and findings from previous work were extended upon. This allowed us to identify an advantageous substitution pattern to optimize the quantum yield in solution and in solid phase.

Reference

N. Kulhanek, K. V. Borysova, M. Kirchner, K. Müller-Buschbaum and R. Göttlich, *Eur. J. Org. Chem*., 2024, e202400783. (DOI: 10.1002/ejoc.202400783)

Check for updates

EurJOC
European Journal of Organic Chemistry

Research Article
doi.org/10.1002/ejoc.202400783

Chemistry Europe
European Chemical Societies Publishing

www.eurjoc.org

Characterization and Optimization of the Photoluminescent Properties of Imidazo[1,5-*a*]quinolines

Niclas Kulhanek,[a] Kateryna V. Borysova,[b] Michael Kirchner,[a] Klaus Müller-Buschbaum,[b] and Richard Göttlich*[a]

In our previous work we could show, that Imidazo[1,5-*a*]quinolines are compounds with interesting optical properties. In this work, we optimized the photoluminescent properties of imidazo[1,5-*a*]quinolines by following outlined trends in our previous work. By introducing electron-rich and electron-poor residual groups on the imidazole ring, the quantum yield (QY) could be significantly increased. This indicated a clear advantageous substitution pattern for this system. In addition, cyclic voltammetric and UV/vis measurements in solid state lay the foundation for applications, such as organic light-emitting diodes (OLEDs).

Introduction

Modern display and lighting technology are increasingly dominated by OLEDs. Since their introduction by Tang and VanSlyke, they were developed and improved greatly in terms of efficiency.[1] Different strategies have been pursued to increase the internal quantum efficiency (IQE), resulting in a large number of green and red emitter materials with good IQEs and stability.[2] The development of molecules with blue emission was particularly challenging. Most of these blue emitter materials have a short lifetime and lower efficiency, as the required band gap of approximately 3 eV leads to long exciton lifetimes (μs). The resulting hot exciton states can decompose the emitter material and thus shorten the lifetime of the entire OLED.[3] Therefore, the development of new organic molecules with blue emission and high stability is an important contribution to an illuminated future.[4]

Blue emission combined with stability is therefore rare in organic molecules.[5] Imidazo[1,5-*a*]*N*-heteroaromatic ring systems are a structural motif frequently incorporated in pharmacologically and biologically active agents and are also found in natural products.[6] Imidazo[1,5-*a*]pyridines in particular have proven to be materials for various applications, such as in nonlinear optics (NLO), confocal microscopy or fluorescence sensing.[7,8] In addition, these simple molecules have uncommon photophysical properties. Some imidazo[1,5-*a*]pyridines have a strong blue emission with a good quantum yield (QY) and a large Stokes shift.[8–11] Especially as ligands, they have already been incorporated into many complexes and successfully implemented into an optical device by Weber *et al.*[12] A less studied but promising subclass are the imidazo[1,5-*a*]quinolines, which possess similar photophysical properties and will be the focus of this work (Scheme 1).

In our group, we have already investigated some imidazo[1,5-*a*]quinolines and found that this class not only showed a strong blue emission with better QY, but was also more stable than imidazo[1,5-*a*]pyridines (Scheme 1).[13] Imidazo[1,5-*a*]quinolines proved to have high stability under physical vapor deposition conditions and the increase in melting point temperature simplifies their implementation as emitter materials in this process. We were able to successfully integrate one of these molecules into an OLED and consequently investigated the influence of various residual groups on the QY.[14] In a large-scale screening, we could identify a preferred substitution pattern.[15] On the one hand, combinations of aromatic electron-rich residues in R^2-position and electron-poor residues in R^1-position lead to increased QY. Particularly advantageous in the R^1-position proved to be *N*-heteroaromatic substituents, i.e. 2-pyrimidinyl in this position lead to a very high QY. On the other hand, a slight steric influence of groups in R^2-position on the QY could be observed. In this work, we will continue these studies towards steric influences on the QY by introduction of sterically demanding electron-rich residues in R^2 and conduct further measurements

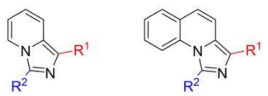

imidazo[1,5-*a*]pyridines imidazo[1,5-*a*]quinolines

Scheme 1. General structures for imidazo[1,5-*a*]pyridines and imidazo[1,5-*a*]quinolines.

[a] *N. Kulhanek, M. Kirchner, R. Göttlich*
Institute of Organic Chemistry, Justus-Liebig-University, Heinrich-Buff-Ring 17, 35392 Giessen, Germany
E-mail: Richard.Goettlich@org.chemie.uni-giessen.de

[b] *K. V. Borysova, K. Müller-Buschbaum*
Institute of Inorganic Chemistry, Justus-Liebig-University, Heinrich-Buff-Ring 17, 35392 Giessen, Germany

Supporting information for this article is available on the WWW under https://doi.org/10.1002/ejoc.202400783

to characterize this class of molecules and improve their optical properties.

Results and Discussion

Synthesis of the imidazo[1,5-*a*]quinolines

On the basis of the highlighted trends, we applied a synthetic route that we already presented in an earlier publication (Scheme 2).[15] In this route we started from 2-aminomethylquinolin dihydrochloride 1, which is available *via* a two steps synthesis known from literature.[16] Compound 1 was reacted with acid chloride R^2COCl and the resulting amides 2 were cyclized with Tf_2O.[17] To study steric effects, sterically large and electron-rich aromatic systems were chosen as R^2. While the cyclization with 9-anthryl and OPh could be performed well, the amides of 9H-carbazole-9-yl and 10H-phenothiazine-10-yl were prone to decomposition which lead to a lower yield of cyclized products 3c and 3 d. The subsequent bromination with NBS could be achieved in excellent yields with all systems.

The obtained bromides **4** were coupled with 2-bromopyrimidine *via* Negishi coupling (Scheme 3 route 1) and since OPh proved to be a particularly good substituent in the subsequent measurements, **4b** was combined with a large number of electron-poor aromatic compounds. The introduction of a 2-*s*-triazinyl residue *via* this coupling route is impractical, as the corresponding halides are commercially not available. Therefore, *s*-triazine was reacted directly with the lithiated bromide **4b** and the resulting dihydro-*s*-triazine was aromatized with DDQ to form the product **6c** (Scheme 3 route 2).[18]

The Negishi coupling lead in most cases to very good yields of the desired products (Scheme 4), only sterically very demanding substrates lead to reduced yields. Thus, sterically demanding residues in position R^2 obstruct the coupling for **7-10b**. To enlarge the scope, bromides from one of our earlier works were included.[19] The newly developed substitution with *s*-triazine was also achieved with very good yields.

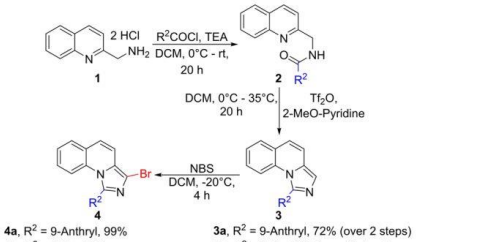

4a, R^2 = 9-Anthryl, 99% **3a**, R^2 = 9-Anthryl, 72% (over 2 steps)
4b, R^2 = OPh, 89% **3b**, R^2 = OPh, 72% (over 2 steps)
4c, R^2 = 9H-Carbazole-9-yl, 83% **3c**, R^2 = 9H-Carbazole-9-yl, 32% (over 2 steps)
4d, R^2 = 10H-Phenothiazine-10-yl, 89% **3d**, R^2 = 10H-Phenothiazine-10-yl, 20% (over 2 steps)

Scheme 2. General synthetic route for the cyclisation and bromination of the new imidazo[1,5-a]quinolines.

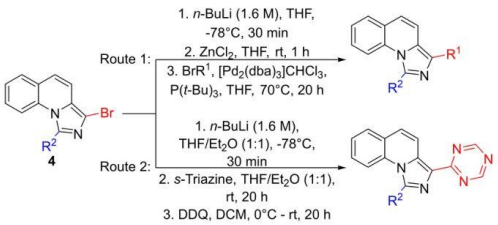

Scheme 3. Subsequent reaction of the bromides 4 in a Negishi coupling *via* route 1 and a substitution with *s*-triazine *via* route 2.

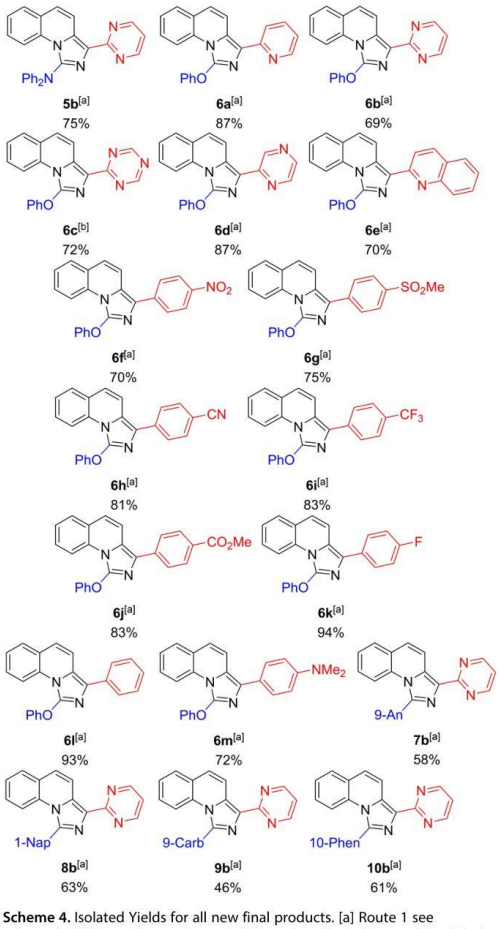

Scheme 4. Isolated Yields for all new final products. [a] Route 1 see scheme 1, [b] Route 2 see scheme 1. (9-An = 9-Anthryl, 1-Nap = 1-Naphthyl, 9-Carb = 9H-Carbazole-9-yl, 10-Phen = 10H-Phenothiazine-10-yl).

Research Article
doi.org/10.1002/ejoc.202400783

Photophysical Measurements in Liquid Phase

Optical measurements were conducted using a 0.1 μM chloroform solution at room temperature. A 0.1 μM solution of quinine sulfate in 0.5 M H_2SO_4 was used as the reference.[20] The fluorescence QY was calculated as described in the literature.[21] All measurements were performed under air. The extinction and emission spectra as well as molar extinction coefficients log ε of all measured compounds are provided in the supporting information.

The measurements of the extinction with different residues in R^2-position showed that all compounds had a maximum around 369 nm (Scheme 5). This observation could also be validated for the emission, as almost all systems displayed a blue emission at about 450 nm (Figure 1 top). The only compound that differed greatly was **7b**, which had a slight cyan coloration. Larger differences could be observed in the QY. The increase of the residue in R^2 from the base system **11b** to **8b** and **9b** first displayed an increase from 33% to 40% when naphthyl was introduced. However, this was almost halved to only 22% by the enlargement of the R^2-position to 9-anthryl in **7b**. The strongest increase was observed when an oxygen- or nitrogen-center was introduced as a link between the residue and the imidazole ring. Here, **5b** displayed a QY of 66% and **6b** with 85% a significantly higher QY than our best compound so far, **14b**. Direct linkage of the phenyl residues in **5b** to carbazole in **9b** yielded an increase of the QY to 81%, while bridging with sulfur in **10b** almost completely canceled the emission. From these data, it is evident that a purely sterically demanding residue in the R^2-position is disadvantageous, as none of the new compounds with solely large R^2 residues showed a significantly better QY than **14b**. This changes when a heteroatom is used as a linker, resulting in significantly different QY.

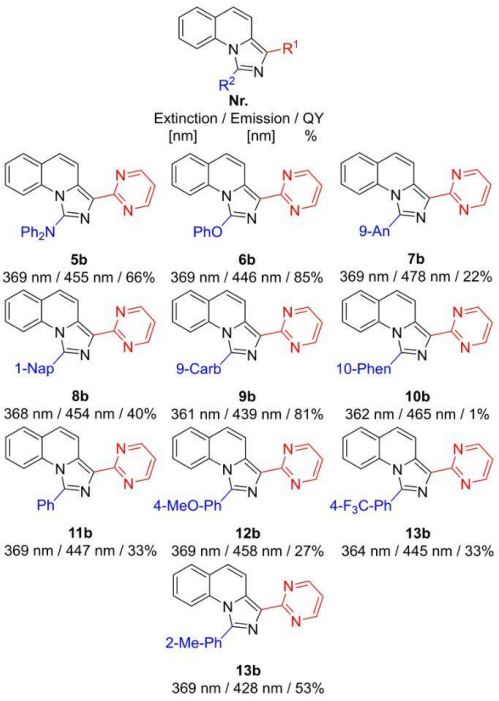

Scheme 5. Extinction, Emission maximas and calculated QYs for different rests in R^2-position and 2-pyrimidinyl in R^1-positions. Measured at 25 °C, under air, 0.1 μM solution in $CHCl_3$ and with the extinction maxima as excitation wavelength. (9-An = 9-Anthryl, 1-Nap = 1-Naphthyl, 9-Carb = 9H-Carbazole-9-yl, 10-Phen = 10H-Phenothiazine-10-yl)

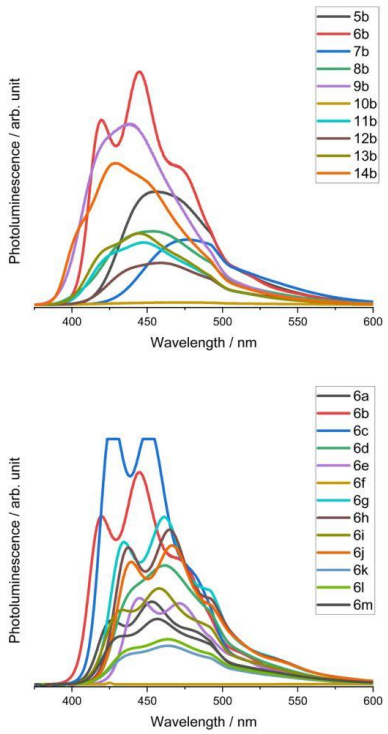

Figure 1. F-Spectra for different rests in R^2-position and 2-pyrimidinyl in R^1-position (top) and different rests in R^1-position and OPh in R^2-position (bottom). Measured at 25 °C, under air, 0.1 μM solution in $CHCl_3$ and with the extinction maxima as excitation wavelength.

Since the OPh residue proved to be the best group in R^2-position, an attempt was made to identify other suitable electron-poor residues in the R^1-position. The extinction varied greatly with the different residual groups (Scheme 6). The strongly electron-withdrawing nitro group in particular resulted in a strong bathochromic shift. In contrast, the emission of the other studied compounds remained largely at a value of approximately 460 nm (Figure 1 top). Likewise, the nitro group led to a significant deviation in the emission wavelength. By

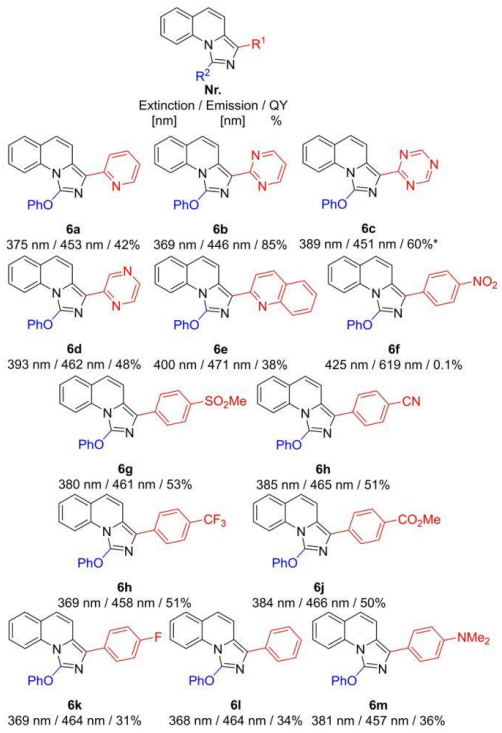

Scheme 6. Extinction, Emission maximas and calculated QYs for different rests in R^1-position and OPh in R^2-positions. Measured at 25 °C, under air, 0.1 μM solution in $CHCl_3$ and with the extinction maxima as excitation wavelength. * Emission could not be fully measured. QY calculated with the incomplete measured Emission.

substitution of the carbon in 2-position of the phenyl ring with more nitrogen, the QY could be greatly increased compared to **6l** from 34% to **6a** with 42%, up to **6b** with 85%. The influence of the substitution pattern of the residues was demonstrated by the introduction of 2-pyrazinyl **6d** for which we observed a decreased QY of 48% compared to **6b**. Enlargement of the *N*-heteroaromatic system size also resulted in a decrease in QY, as can be observed for **6e**. Showing that a sterically small substituent is also advantageous in R^1-position. Surprisingly, the QY with a *s*-triazinyl residue could not be increased any further. Although **6c** had such a strong emission that it could not be fully measured, it also had a higher molar extinction coefficient (Figure 1 bottom). It can also be observed that all phenoxy based systems **6** have a characteristic second weak emission maximum before the main maximum. As the *para*-substitution proved to be the most effective for phenyl, only these were synthesized.[15] The substitution with dimethylamine **6m** and fluorine **6k** in *para*-position did not show any significant change. Dimethylamine had proven to be the only exception for + M substituents in our previous work.[15] This substitution of compounds **6m** and **6k** did only result in minor changes of the QY compared to **6l**. By increasing the electron-withdrawing effect to a methyl ester **6j**, the QY could be improved to 50%. However, it could not be increased above this value by further increasing the electron withdrawing effect of the substituent in *para*-position to trifluoromethyl **6i**, nitrile **6h** and methylsulfonyl **6g**. Substitution with a nitro group completely extinguished the emission. This quenching effect of photo emissions between 450–630 nm is well known from literature.[22]

Increasing the electron deficiency through *para*-substitution alone proved to be insufficient. The strongest improvement was observed with the substitution of the carbon in 2-position of the phenyl ring with more nitrogen, with the 2-pyrimidinyl residue being the best substituent in the R^1-position. It is possible that this results in a less hindered rotation of the substituent in the R^1-position leading to a better interaction between the residue in R^1-position and the imidazole ring core.

In general, it is surprising that the imidazo[1,5-*a*]quinolines retained their blue emission in almost all cases, while imidazo[1,5-*a*]pyridines showed a wide variety of emission wavelengths due to substitutions with a wide variety of functional groups.[11] Comparable imidazo[1,5-*a*]pyridines systems achieved QYs between 7–50% and emission between 430–480 nm.[10,13,23] Similar properties were observed forimidazo[5,1-*a*]isoquinolines, which also show an emission range of 430–450 nm and 5–48% QY.[24] While the emission range and pattern are the same compared to imidazo[5,1-*a*]isoquinolines and imidazo[1,5-*a*]pyridines, we were able to significantly increase the QY to over 80% with the substitution with 2-pyrimidinyl and other *N*-heterocycles.

Photophysical Measurements in Solid Phase

For comparison, absolute QYs (s) were determined in the solid state under air at 25 °C by measuring each sample as well as a reference material several times (4 times sample/3 times reference) with subsequent calculation of QY value (an average value) and standard deviation that represents the measurement error. Magnesium oxide was utilized as a reference material.

Due to the preparative complexity, only molecules that already exhibited sufficient emission and QY in solution were measured. For this reason, **5b**, **6a**, **6b**, **6c**, **6g** and **9b** were selected. Unexpectedly, despite showing strong emission in solution, **6a** and **9b** did not possess a sufficiently high emission in their solid state for the measurements and were excluded. The UV/vis and F maxima shifted approximately 50 nm towards the red spectrum for the measured systems (Scheme 7). Noteworthy here is **6b**, as a very strong shift in extinction and emission was observed (Figure 2). Compound **6b** also lost over 60% of its QY (s) compared to the liquid phase, while **5b** only displayed a reduction of 30%. Molecules **6c** and **6g** could not exceed 15% QY (s). The comparatively weak emission of **6c** was particularly surprising, as it emitted exceptionally strongly in solution. It can be concluded that 2-pyrimidinyl is a very good substituent for the R^1-position even in the solid phase. However,

Research Article
doi.org/10.1002/ejoc.202400783

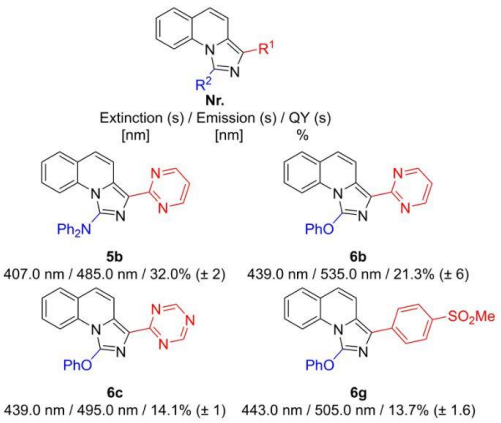

Scheme 7. Extinction, Emission maximas and calculated QYs (s) in solid state for the measured systems. Measured under air and 25 °C (5b, λ_{ex} = 330 nm; 6b, λ_{ex} = 360 nm; 6c, λ_{ex} = 360 nm; 6 g, λ_{ex} = 415 nm).

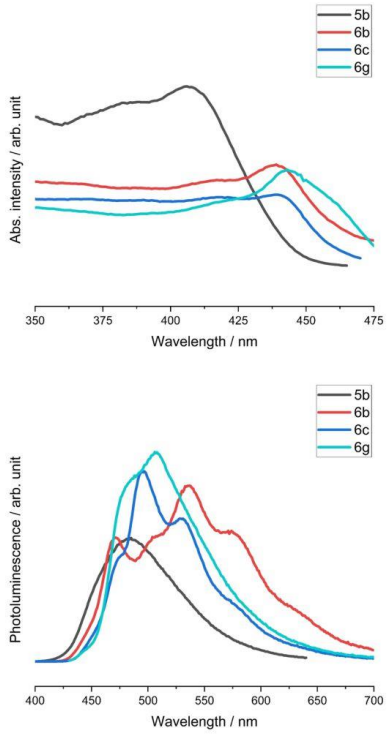

Figure 2. UV/vis (top) and F-Spectra (bottom) in solid state for the measured systems at 25 °C and under air (black **5 b**, λ_{ex} = 330 nm; red **6 b**, λ_{ex} = 360 nm; blue **6 c**, λ_{ex} = 360 nm; cyan **6 g**, λ_{ex} = 415 nm).

the QY (s) loss in **5 b** was mitigated to a greater extent than in **6 b**.

Cyclic Voltammetric Measurements and DFT-Calculations

Cyclic voltammetry (CV) measurements were performed with a glassy carbon electrode as working electrode, a platinum/titanium electrode as counter electrode and an Ag/AgCl reference electrode. The HOMO energy was estimated by using this literature procedure with ferrocene as standard[25] and the LUMO energy was calculated from the HOMO energy and the bandgap (BG) energy, which was obtained by a linear fit of the extinction edge and conversion of the intersection wavelength into an energy value.[26] The 5 mM sample solution was dissolved in a 0.1 M tetrabutylammonium tetrafluoroborate DMF-solution, measured at 25 °C, under inert atmosphere.

All density functional theory computations were carried out using the Orca 5.0.3 program package. For structural optimizations and the acquisition of HOMO and LUMO energies, the B3LYP hybrid functional[27] with the Karlsruhe basis set def2-TZVP[28] was deployed. The D3 scheme[29] with Becke-Johnson dampening[30] was used to account for dispersion interactions.

The 2-pyrimidinyl substituted systems displayed all very similar results in the CV measurements. A reversible oxidation could be shown for all substances without a reduction being measured (Figure 3 top). Only **5 b** showed two oxidation maxima, but again without reduction. With OPh in R^2-position, two oxidation maxima were measured with **6 f**, **6 i**, **6 k** and **6 l** whereas the other systems showed only one oxidation maximum (Figure 3 bottom). An exception is **6 m**, which not only displayed two oxidation maxima, but also two reduction maxima. This could explain the unique properties of **6 m**, as it is the only electron-rich substituent that has high QYs.

Non-reversible oxidation distinguishes the imidazo[1,5-*a*]quinolines from the imidazo[1,5-*a*]pyridines, which typically show reversibility of oxidation. Moreover, the potential of the imidazo[1,5-*a*]quinolines at around 1.3 V is considerably higher than that of the imidazo[1,5-*a*]pyridines at approximately 0.4 V.[10,13]

Energy levels for HOMO is consistent at below −5 eV, with 2-pyrimidinyl substituted system tending more towards < −5.5 eV (Table 1). Very large systems **7 b** and **10 b** and heteroatom-linked systems **5 b** and **6 b** show slightly higher HOMO energies. This trend can also be observed for LUMO Energies. While most systems are around −2.5 eV, the systems mentioned above show slightly higher energies. The HOMO and LUMO energies are similar to those of the imidazo[1,5-*a*]pyridines.[10,13] This results in a consistent BG of 3 eV for 2-pyrimidinyl substituted systems, with the remaining systems having a BG below 3 eV.

The DFT calculations showed very good agreement with HOMO energies, while LUMO energies deviated strongly (Table 2). This discrepancy in the use of this approach is well known in the literature.[31] However, it can be observed that these deviations are constant at around + 0.6 eV. This excess also resulted to higher values for BG energies, which remained

Research Article
doi.org/10.1002/ejoc.202400783

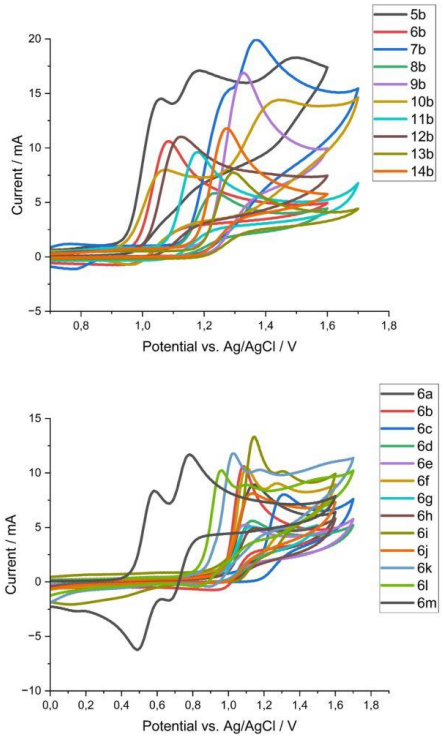

Figure 3. CV-Spectra for different rests in R^2-position with 2-pyrimidinyl in R^1-position (top) and for different rests in R^1-position with OPh in R^2-position (bottom). Measured at 25 °C, under inert atmosphere, 5 mM sample-solution dissolved in a 0.1 M tetrabutylammonium tetrafluoroborate DMF-solution, at a scan rate of 200 mVs^{-1}.

constant at around 3.5 eV for all systems. An exception to this was **6f**, which also had a small BG in the CV measurement.

Conclusions

We were successful in expending on the trends we observed for the 1,3-substitution of imidazo[1,5-a]quinolines. By introduction of sterically large heteroatom-linked residues in the R^2-position and combination with *N*-heteroaromatics in the R^1-position. In particular, the use of diphenylamine or phenyl ether in conjunction with 2-pyrimidinyl increased the QY to over 80% in solution. The best system in solution was **6b** with 86% QY. While in the solid phase **5b** with 32% displayed the highest QY (s) compared to the other systems. By CV measurements it could also be determined that all systems possess a BG of about 3 eV, with HOMO and LUMO energies varying only slightly between different substitutions. In summary we were able to develop and prepare new imidazo[1,5-a]quinolines that show a high fluorescence quantum yield in solution as well as in the solid state. Further experiments towards applying these new emitter molecules for OLED applications are currently performed in our group.

Experimental Section

All solvents were purified by distillation prior to use. Anhydrous solvents were used from ACROS Organics™ as AcroSeal™ bottles. Commercially available chemicals were used as obtained from the supplier, unless otherwise stated. Syntheses prepared under anhydrous conditions were generally performed using standard Schlenk technique in nitrogen atmosphere. For purification by column chromatography, silica gel 60 (Merck) was used. ^1H and ^{13}C NMR spectra were recorded on the Bruker Avance II 400, the Bruker Avance III 400 and the Bruker Avance II 200 "Microbay" spectrometers in deuterated solvents. ^1H and ^{13}C chemical shifts were determined by reference to the residual solvent signals. High-resolution ESI mass spectra were recorded in methanol with an ESImicroTOF spectrometer from Bruker Daltonics in positive ion mode, unless otherwise stated. As a power supply, the Sky Toppower PS1110 was used. Melting points were determined with a Gallenkamp Melting Point Apparatus. The CHN elemental analysis was performed using the CHN-Analysator: Thermo Flash EA-1112 Series. UV-vis extinction in solution was measured with an Analytik Jena Specord 200 Plus spectrometer and fluorescence emission data were obtained from a Jasco Germany FP 8300 spectrometer. Cyclic voltammetry measurements were performed with a glassy carbon electrode as working electrode, a platinum/titanium electrode as counter electrode and an Ag/AgCl reference electrode. Ferrocene was used as standard and the electrochemical data were recorded with an e-corder 410 eDAQ (eDAQ, Colorado Springs, US) and the program eChem. Solid-state photoluminescence properties were studied on Horiba Jobin Yvon Fluorolog 3 equipped with 450 W xenon lamp as a light source, double-grated monochromators (emission and excitation) and photomultiplier tube R928P (Horiba). FluorEssence software by Horiba was used to carry out the measurements. Quantum yield (QY (s)) for solid samples was measured using previously mentioned Horiba Jobin Yvon Fluorolog 3 combined with a Quanta-Phi integrating sphere F-3029 (by Horiba). Magnesium oxide was utilized as a reference material.

General procedure for imidazole ring closure adapted from Pelletier *et al.*[17]:

60 mL of dry DCM was added to 2-(aminomethyl)quinoline dihydrochloride 1 (1 eq) under N_2 atmosphere. The suspension was cooled to 0 °C and dry TEA (3.4 eq) was added. The yellow solution was kept at 0 °C for 30 min. Acid chloride R^2COCl (1.1 eq) was added, and the solution was stirred for 20 h at room temperature. Finally, 60 mL sat. Na_2CO_3 solution was added, and the aqueous phase was extracted twice with 60 mL DCM. The combined organic phases were dried over Na_2SO_4, filtered, and the solvent removed *in vacuo*. The crude quinoline amide 2 (1 eq) was placed in 60 mL of dry DCM under N_2 atmosphere and cooled to 0 °C. The solution was first treated with 2-methoxypyridine (1.1 eq), followed by slow addition of Tf_2O (1.2 eq). The reaction solution was stirred at 35 °C for 20 h. Then, 20 mL sat. Na_2CO_3 solution was added slowly, and the aqueous phase was extracted twice with 60 mL DCM. The combined organic phases were dried over Na_2SO_4, filtered and the solvent removed *in vacuo*. Purification was carried out by silica chromatography.

General procedure for bromination:

The imidazo[1,5-*a*]quinoline 3 was placed in 60 mL dry DCM under N_2 atmosphere and cooled to −20 °C. 1.1 eq NBS was slowly added

Research Article
doi.org/10.1002/ejoc.202400783

Table 1. CV–Data for different rest at R^2 and R^1-position. Measured at 25 °C, under inert atmosphere, 5 mM sample-solution dissolved in a 0.1 M tetrabutylammonium tetrafluoroborate DMF-solution.

Nr.	R^2	R^1	HOMO/eV	LUMO/eV	BG/eV
5b	NPh_2	2-Pyrimidinyl	−5.27	−2.30	2.97
6b	OPh	2-Pyrimidinyl	−5.33	−2.37	2.97
7b	9-Anthryl	2-Pyrimidinyl	−5.26	−2.20	3.06
8b	1-Naphthyl	2-Pyrimidinyl	−5.56	−2.51	3.06
9b	9H-Carbazole-9-yl	2-Pyrimidinyl	−5.59	−2.47	3.12
10b	10H-Phenothiazine-10-yl	2-Pyrimidinyl	−5.26	−2.23	3.03
11b	Ph	2-Pyrimidinyl	−5.56	−2.53	3.03
12b	4-MeO-Ph	2-Pyrimidinyl	−5.45	−2.49	2.97
13b	4-F_3C-Ph	2-Pyrimidinyl	−5.64	−2.60	3.03
14b	2-Me-Ph	2-Pyrimidinyl	−5.59	−2.52	3.07
6a	OPh	2-Pyridinyl	−5.33	−2.74	2.59
6c	OPh	2-*s*-Triazinyl	−5.26	−2.39	2.87
6d	OPh	2-Pyrazinyl	−5.26	−2.45	2.81
6e	OPh	2-Quinolinyl	−5.26	−2.73	2.53
6f	OPh	4-O_2N-Ph	−5.36	−2.93	2.43
6g	OPh	4-MeO_2S-Ph	−5.31	−2.48	2.83
6h	OPh	4-NC-Ph	−5.33	−2.52	2.81
6i	OPh	4-F_3C-Ph	−5.29	−2.42	2.87
6j	OPh	4-MeO_2C-Ph	−5.28	−2.48	2.81
6k	OPh	4-F-Ph	−5.17	−2.35	2.82
6l	OPh	Ph	−5.16	−2.34	2.83
6m	OPh	4-Me_2N-Ph	−4.92	−2.10	2.81

Table 2. DFT-Calculation results for HOMO/LUMO of the specific molecules.

Nr.	R^2	R^1	theo. HOMO/eV	theo. LUMO/eV	theo. BG/eV
5b	NPh_2	2-Pyrimidinyl	−5.21	−1.74	3.47
6b	OPh	2-Pyrimidinyl	−5.28	−1.77	3.51
7b	9-Anthryl	2-Pyrimidinyl	−5.41	−2.04	3.37
8b	1-Naphthyl	2-Pyrimidinyl	−5.41	−1.73	3.68
9b	9H-Carbazole-9-yl	2-Pyrimidinyl	−5.64	−1.85	3.79
10b	10H-Phenothiazine-10-yl	2-Pyrimidinyl	−5.31	−1.80	3.51
11b	Ph	2-Pyrimidinyl	−5.39	−1.77	3.62
12b	4-MeO-Ph	2-Pyrimidinyl	−5.25	-1.70	3.55
13b	4-F_3C-Ph	2-Pyrimidinyl	−5.61	−1.97	3.64
14b	2-Me-Ph	2-Pyrimidinyl	−5.43	−1.72	3.71
6a	OPh	2-Pyridinyl	−5.22	−1.58	3.64
6c	OPh	2-*s*-Triazinyl	−5.58	−2,11	3,47
6d	OPh	2-Pyrazinyl	−5.37	−1.79	3.58
6e	OPh	2-Quinolinyl	−5.24	−1.79	3.45
6f	OPh	4-O_2N-Ph	−5.55	−2.50	3.05
6g	OPh	4-MeO_2S-Ph	−5.45	−1.92	3.53
6h	OPh	4-NC-Ph	−5.47	−2.02	3.45
6i	OPh	4-F_3C-Ph	−5.37	−1.82	3.55
6j	OPh	4-MeO_2C-Ph	−5.28	−1.83	3.45
6k	OPh	4-F-Ph	−5.16	−1.58	3.58
6l	OPh	Ph	−5.11	−1.52	3.59
6m	OPh	4-Me_2N-Ph	−4.66	−1.32	3.34

to the solution. The reaction solution was stirred at −20 °C for 4 h. Then, 20 ml sat. $Na_2S_2O_3$ solution was added and the aqueous phase extracted twice with 40 mL DCM. The combined organic phases were dried over Na_2SO_4, filtered, and the solvent removed *in vacuo*. Purification was carried out by silica chromatography.

General procedure for the Negishi coupling (Route 1):

0.400 g (1 eq) 3-bromoimidazo[1,5-*a*]quinoline 4 was dissolved in 10 mL dry THF under N_2 atmosphere and cooled to −78 °C. 1.2 eq of *n*-BuLi (1.6 M) were slowly added dropwise and the solution was kept at −78 °C for 30 min. 2.5 eq $ZnCl_2$ in dry THF (1 M) were added at −78 °C and then stirred at room temperature for 1 h. 3 mol% of $[Pd_2(dba)_3]{\cdot}CHCl_3$, 6 mol% of P(*t*-Bu)$_3$ and 2 eq of the chosen coupling bromide were added and the reaction solution was stirred at 70 °C for 20 h. 15 mL conc. $NH_{3(aq)}$ solution was added and the aqueous phase was extracted three times with 20 mL DCM. The combined organic phases were concentrated *in vacuo* and the impure product was purified by silica chromatography.

Procedure for *s*-Triazin formation (Route 2):

0.400 g (1 eq, 1.18 mmol) 3-bromo-1-(phenylether)imidazo[1,5-*a*]quinoline 4b was dissolved in 10 mL dry THF/Et_2O (1 : 1) under N_2 atmosphere and cooled to −78 °C. 0.81 mL (1.1 eq, 1.3 mmol) of *n*-BuLi (1.6 M) were slowly added dropwise and the solution was kept at −78 °C for 30 min. 0.124 g (1.3 eq, 1.53 mmol) of *s*-Triazine was added and the solution was warmed up to room temperature. A yellow participate formed slowly and the solution was stirred at room temperature overnight. 0.05 ml of dest. water was added and the solution stirred for 30 min. Then 20 mL of dest. water and 20 DCM were added and the organic phase separated. The water phase was extracted twice with 20 mL DCM. The combined organic phases were concentrated *in vacuo* and the crude product was dissolved in 20 of dry DCM under N_2 atmosphere and cooled to 0 °C. To this cooled solution 0.321 g (1.2 eq, 1.42 mmol) of DDQ was added and stirred at room temperature overnight. 20 mL dest. water was added and the organic phase was separated. The water phase was extracted twice with 20 mL DCM and the combined organic phases were concentrated *in vacuo*. The crude mixture was purified by silica chromatography (1 : 1 ethyl acetate:*n*-hexane). The product was obtained as a yellow solid (0.287 g, 0.85 mmol, 72% over 2 steps). 1H NMR (400 MHz, $CDCl_3$): δ = 8.94 (s, 2H), 8.62 (d, J = 9.06 Hz, 1H), 8.41 (d, J = 9.58 Hz, 1H), 7.59 (dd, J = 7.83, 1.62 Hz, 1H), 7.45 (ddd, J = 8.69, 7.24, 1.60 Hz, 1H), 7.34 (td, J = 7.55, 1.12 Hz, 1H), 7.31–7.20 (m, 5H), 7.11–7.05 (m, 1H) ppm; 13 C NMR (101 MHz, $CDCl_3$): δ = 167.9, 165.8, 154.4, 147.8, 132.5, 131.8, 130.2, 129.5, 128.6, 126.7, 126.3, 125.4, 125.3, 122.7, 119.2, 118.7, 117.7 ppm; HRMS(ESI): m/z calculated for $C_{20}H_{13}N_5O$ $\{M+Na^+\}$: 362.1012. Found: 362.1014. Elemental Analysis theo.: N = 20.64, C = 70.79, H = 3.86; found: N = 20.61, C = 70.53, H = 3.84.

Supporting Information Summary

Additional references cited within the Supporting Information.[32] Experimental procedures, physical values and spectra for all measured compounds and analytical data of all compounds are provided in the online Supporting Information.

Acknowledgements

Open Access funding enabled and organized by Projekt DEAL.

Conflict of Interests

The authors declare no conflict of interest.

Data Availability Statement

The data that support the findings of this study are available in the supplementary material of this article.

Keywords: Imidazo[1,5-*a*]quinolines · Photoluminescence · Emitter material · Blue luminescence · Nitrogen heterocycles

[1] a) C. W. Tang, S. A. VanSlyke, *Appl. Phys. Lett.* **1987**, *51*, 913–915; b) G. Hong, X. Gan, C. Leonhardt, Z. Zhang, J. Seibert, J. M. Busch, S. Bräse, *Adv. Mater.* **2021**, *33*, e2005630.
[2] a) C. Adachi, M. A. Baldo, S. R. Forrest, S. Lamansky, M. E. Thompson, R. C. Kwong, *Appl. Phys. Lett.* **2001**, *78*, 1622–1624; b) C.-L. Ho, H. Li, W.-Y. Wong, *J. Organomet. Chem.* **2014**, *751*, 261–285; c) H. Nakanotani, T. Higuchi, T. Furukawa, K. Masui, K. Morimoto, M. Numata, H. Tanaka, Y. Sagara, T. Yasuda, C. Adachi, *Nat. Commun.* **2014**, *5*, 4016.
[3] N. C. Giebink, B. W. D'Andrade, M. S. Weaver, P. B. Mackenzie, J. J. Brown, M. E. Thompson, S. R. Forrest, *J. Appl. Phys.* **2008**, *103*, 44509.
[4] a) Y. Im, S. Y. Byun, J. H. Kim, D. R. Lee, C. S. Oh, K. S. Yook, J. Y. Lee, *Adv. Funct. Mater.* **2017**, *27*, 1603007; b) W.-C. Chen, C.-S. Lee, Q.-X. Tong, *J. Mater. Chem. C* **2015**, *3*, 10957–10963.
[5] Z. Xu, J. Gu, X. Qiao, A. Qin, B. Z. Tang, D. Ma, *ACS Photonics* **2019**, *6*, 767–778.
[6] a) R. G. S. Berlinck, R. Britton, E. Piers, L. Lim, M. Roberge, R. Da Moreira Rocha, R. J. Andersen, *J. Org. Chem.* **1998**, *63*, 9850–9856; b) M. S. Malamas, Y. Ni, J. Erdei, H. Stange, R. Schindler, H.-J. Lankau, C. Grunwald, K. Y. Fan, K. Parris, B. Langen, U. Egerland, T. Hage, K. L. Marquis, S. Grauer, J. Brennan, R. Navarra, R. Graf, B. L. Harrison, A. Robichaud, T. Kronbach, M. N. Pangalos, N. Hoefgen, N. J. Brandon, *J. Med. Chem.* **2011**, *54*, 7621–7638; c) A. Kamal, G. Ramakrishna, P. Raju, A. V. S. Rao, A. Viswanath, V. L. Nayak, S. Ramakrishna, *Eur. J. Med. Chem.* **2011**, *46*, 2427–2435; d) D. Kim, L. Wang, J. J. Hale, C. L. Lynch, R. J. Budhu, M. Maccoss, S. G. Mills, L. Malkowitz, S. L. Gould, J. A. DeMartino, M. S. Springer, D. Hazuda, M. Miller, J. Kessler, R. C. Hrin, G. Carver, A. Carella, K. Henry, J. Lineberger, W. A. Schleif, E. A. Emini, *Bioorg. Med. Chem. Lett.* **2005**, *15*, 2129–2134; e) F. Peytam, Z. Emamgholipour, A. Mousavi, M. Moradi, R. Foroumadi, L. Firoozpour, F. Divsalar, M. Safavi, A. Foroumadi, *Bioorg. Chem.* **2023**, *140*, 106831; f) G. Volpi, E. Laurenti, R. Rabezzana, *Molecules* **2024**, *29*, 2668; g) P. A. Chaudhran, A. Sharma, *Crit. Rev. Anal. Chem.* **2022**, 1–18; h) A. K. Bagdi, S. Santra, K. Monir, A. Hajra, *Chem. Comm.* **2015**, *51*, 1555–1575.
[7] a) D. R. Mohbiya, N. Sekar, *ChemistrySelect* **2018**, *3*, 1635–1644; b) F. Yagishita, C. Nii, Y. Tezuka, A. Tabata, H. Nagamune, N. Uemura, Y. Yoshida, T. Mino, M. Sakamoto, Y. Kawamura, *Asian J. Org. Chem.* **2018**, *7*, 1614–1619; c) J. T. Hutt, J. Jo, A. Olasz, C.-H. Chen, D. Lee, Z. D. Aron, *Org. Lett.* **2012**, *14*, 3162–3165; d) Y. Ge, R. Ji, S. Shen, X. Cao, F. Li, *Sens. Actuators B Chem.* **2017**, *245*, 875–881; e) L. Wang, X. Han, G. Qu, Le Su, B. Zhao, J. Miao, *Stem. Cell Res. Ther.* **2018**, *9*, 343.
[8] G. Volpi, B. Lace, C. Garino, E. Priola, E. Artuso, P. Cerreia Vioglio, C. Barolo, A. Fin, A. Genre, C. Prandi, *Dyes Pigm.* **2018**, *157*, 298–304.
[9] a) F. Shibahara, R. Sugiura, E. Yamaguchi, A. Kitagawa, T. Murai, *J. Org. Chem.* **2009**, *74*, 3566–3568; b) G. Volpi, G. Magnano, I. Benesperi, D. Saccone, E. Priola, V. Gianotti, M. Milanesio, E. Conterosito, C. Barolo, G. Viscardi, *Dyes Pigm.* **2017**, *137*, 152–164; c) E. Yamaguchi, F. Shibahara, T. Murai, *J. Org. Chem.* **2011**, *76*, 6146–6158; d) M. Giordano, G. Volpi, C. Garino, F. Cardano, C. Barolo, G. Viscardi, A. Fin, *Dyes Pigm.* **2023**, *218*, 111482; e) G. Colombo, A. Cinco, G. A. Ardizzoia, S. Brenna, *Colorants* **2023**, *2*, 179–193; f) A. Marchesi, S. Brenna, G. A. Ardizzoia, *Dyes Pigm.* **2019**, *161*, 457–463.
[10] G. Volpi, C. Garino, E. Fresta, E. Casamassa, M. Giordano, C. Barolo, G. Viscardi, *Dyes Pigm.* **2021**, *192*, 109455.
[11] F. Shibahara, E. Yamaguchi, A. Kitagawa, A. Imai, T. Murai, *Tetrahedron* **2009**, *65*, 5062–5073.
[12] a) M. D. Weber, C. Garino, G. Volpi, E. Casamassa, M. Milanesio, C. Barolo, R. D. Costa, *Dalton Trans.* **2016**, *45*, 8984–8993; b) F. Yagishita, T.

Kinouchi, K. Hoshi, Y. Tezuka, Y. Jibu, T. Karatsu, N. Uemura, Y. Yoshida, T. Mino, M. Sakamoto, Y. Kawamura, *Tetrahedron* **2018**, *74*, 3728–3733; c) G. A. Ardizzoia, G. Colombo, B. Therrien, S. Brenna, *Ber. dtsch. Chem. Ges. A/B* **2019**, *2019*, 1825–1831; d) S. Durini, G. A. Ardizzoia, B. Therrien, S. Brenna, *New J. Chem.* **2017**, *41*, 3006–3014; e) C. Garino, T. Ruiu, L. Salassa, A. Albertino, G. Volpi, C. Nervi, R. Gobetto, K. I. Hardcastle, *Ber. dtsch. Chem. Ges. A/B* **2008**, *2008*, 3587–3591; f) L. Salassa, C. Garino, A. Albertino, G. Volpi, C. Nervi, R. Gobetto, K. I. Hardcastle, *Organometallics* **2008**, *27*, 1427–1435.

[13] G. Albrecht, C. Rössiger, J. M. Herr, H. Locke, H. Yanagi, R. Göttlich, D. Schlettwein, *Phys. Status Solidi B* **2020**, *257*, 1900677.

[14] G. Albrecht, C. Geis, J. M. Herr, J. Ruhl, R. Göttlich, D. Schlettwein, *Org. Electron.* **2019**, *65*, 321–326.

[15] N. Kulhanek, N. Martin, R. Göttlich, *Eur. J. Org. Chem.* **2024**, *27*, 10.1002/ejoc.202301007.

[16] a) K. C. Langry, *Org. Prep. Proced. Int.* **1994**, *26*, 429–438; b) M. Henze, *Ber. dtsch. Chem. Ges. A/B* **1936**, *69*, 1566–1568.

[17] G. Pelletier, A. B. Charette, *Org. Lett.* **2013**, *15*, 2290–2293.

[18] W. M. Boesveld, P. B. Hitchcock, M. F. Lappert, *J. Chem. Soc., Perkin Trans. 1* **2001**, *9*, 1103–1108.

[19] M. Marner, N. Kulhanek, J. Eichberg, K. Hardes, M. D. Molin, J. Rybniker, M. Kirchner, T. F. Schäberle, R. Göttlich, *RSC Med. Chem.* **2024**, 10.1039/D4MD00086B.

[20] D. F. Eaton, *Pure Appl. Chem.* **1988**, *60*, 1107–1114.

[21] A. M. Brouwer, *Pure Appl. Chem.* **2011**, *83*, 2213–2228.

[22] C.-X. Zhao, T. Liu, M. Xu, H. Lin, C.-J. Zhang, *Chin. Chem. Lett.* **2021**, *32*, 1925–1928.

[23] G. Volpi, E. Priola, C. Garino, A. Daolio, R. Rabezzana, P. Benzi, A. Giordana, E. Diana, R. Gobetto, *Inorganica Chim. Acta* **2020**, *509*, 119662.

[24] C. Rössiger, T. Oel, P. Schweitzer, O. Vasylets, M. Kirchner, A. Abdullahu, D. Schlettwein, R. Göttlich, *Eur. J. Org. Chem.* **2024**, *27*, e202400298.

[25] B. W. D´Andrade, S. Datta, S. R. Forrest, P. Djurovich, E. Polikarpov, M. E. Thompson, *Org. Electron.* **2005**, *6*, 11–20.

[26] J. C. Costa, R. J. Taveira, C. F. Lima, A. Mendes, L. M. Santos, *Opt. Mater.* **2016**, *58*, 51–60.

[27] a) C. Lee, W. Yang, R. G. Parr, *Phys. Rev. B* **1988**, *37*, 785–789; b) P. J. Stephens, F. J. Devlin, C. F. Chabalowski, M. J. Frisch, *J. Phys. Chem.* **1994**, *98*, 11623–11627; c) A. D. Becke, *J. Chem. Phys.* **1993**, *98*, 5648–5652.

[28] A. Schäfer, C. Huber, R. Ahlrichs, *J. Chem. Phys.* **1994**, *100*, 5829–5835.

[29] S. Grimme, J. Antony, S. Ehrlich, H. Krieg, *J. Chem. Phys.* **2010**, *132*, 154104.

[30] a) E. R. Johnson, A. D. Becke, *J. Chem. Phys.* **2006**, *124*, 174104; b) A. D. Becke, E. R. Johnson, *J. Chem. Phys.* **2005**, *123*, 154101.

[31] A. J. Garza, G. E. Scuseria, *J. Phys. Chem. Lett.* **2016**, *7*, 4165–4170.

[32] a) M. S. Wrighton, D. S. Ginley, D. L. Morse, *J. Phys. Chem.* **1974**, *78*, 2229–2233; b) A. E. Sedykh, M. Becker, M. T. Seuffert, D. Heuler, M. Maxeiner, D. G. Kurth, C. E. Housecroft, E. C. Constable, K. Müller-Buschbaum, *Chem. Photo. Chem.* **2023**, *7*, e202200244.

Manuscript received: July 12, 2024
Revised manuscript received: August 6, 2024
Accepted manuscript online: August 12, 2024
Version of record online: ■■, ■■

6.4 Further Co-Authored Publications

Reactivity of Copper(I) Complexes Containing Ligands Derived from (1S,3R)-Camphoric Acid with Dioxygen, F. Stöhr, N. Kulhanek, J. Becker, R. Göttlich, S. Schindler, *Eur. J. Inorg. Chem.*, 2021, **22**, 2079-2088. (DOI: 10.1002/ejic.202100187)

7. Acknowledgment

Above all, I would like to thank Prof. Dr. Richard Göttlich for giving me the opportunity and almost unlimited freedom to pursue my research. Without his advice and support, this would not have been possible. Additional acknowledgements go to Prof. Dr. Siegfried Schindler for writing the second report of this thesis and Prof. Dr. Bernd Smarsly for the participation in my dissertation examination. I am also grateful for the additional suggestions and assistance of all former and current members of the AG Göttlich.

On the part of the university, the smooth running of my doctorate would not have been possible without the support of Michaela Richter, Eike Santowski, Mario Dauber, Steffen Wagner, Anja Beneckenstein, Jana Küchenmeister, Inna Klein, Anja Platt, Anika Bernhardt and Edgar Reitz. In particular, I would like to thank Dr. Michael Marner and Prof. Dr. Till Friedrich Schäberle from the Fraunhofer IME Institute and all members of the Department I of Internal Medicine, University of Cologne, for the opportunities they gave me.

I am immensely grateful for the support of my family over the years and that they have always believed in me despite everything. In particular, the support of my girlfriend Olesia Vasylets is enormously valuable to me.